

RUSSIAN
JOURNAL
OF CYBERNETICS

УСПЕХИ КИБЕРНЕТИКИ

2020
Vol. 1. No. 1

**FEDERAL STATE INSTITUTION
“SCIENTIFIC RESEARCH INSTITUTE
FOR SYSTEM ANALYSIS
OF THE RUSSIAN ACADEMY OF SCIENCES”**

Russian Journal of Cybernetics

Успехи кибернетики

**Vol. 1
No. 1**

**Том 1
№ 1**

Moscow
2020

Founder and Publisher

Federal State Institution

Scientific Research Institute for System Analysis of the Russian Academy of Sciences (SRISA)

Russian Journal of Cybernetics is a peer-reviewed scholarly journal.

The journal publishes papers on physics, mathematics, and engineering. The key areas of interest are:

- system analysis, control, and information processing;
- simulation, numerical methods, and simulation software;
- solid-state electronics, electronic components, micro- and nanoelectronics, quantum effect devices.

The Journal's mission is to support the research disciplines development on asserted topic in Russia and abroad, relevant to the priority fields of science development, technologies and equipment in the Russian Federation and the list of critical technologies of the Russian Federation.

The objectives of the journal are: promotion of advanced ideas in physics, mathematics, engineering sciences, participating in the implementation of the objectives accomplishment worded by the President of the Russian Federation in the Decree from 01.12.2016 No. 642, on the scientific and technological development of the Russian Federation and also on the import substitution on the of strategic development priority areas of the country appropriate to the remit of the journal, ensuring the provision of publishing areas for qualified personnel, the quality improvement of dissertation researches in the areas through the development of mechanism for professional and public discussion of their research results, education of the younger generation of scientists.

The Journal accepts for publication original articles; translations of published articles from foreign journals (with the consent of the right holder for the translation and publication); reviews; essays; commentaries and event reports.

The publication is useful for the scientists working in the relevant fields of sciences, postgraduates and students.

Chief Editor

Prof. *Vladimir B. Betelin*, member of the Russian Academy of Sciences (RAS),
Doctor of Science (Phys&Math), Academic Director, SRISA, Moscow

Vice Chief Editor

Prof. *Valerii A. Galkin*, Doctor of Science (Phys&Math), Director, SRISA, Surgut Branch, Surgut

Editorial Board

- Prof. *Vladislav Ya. Panchenko*, member of the Russian Academy of Sciences (RAS), Doctor of Science (Phys&Math), Chairman of the Council, Russian Foundation for Basic Research, Chairperson of the Department of Medical Physics, Lomonosov Moscow State University, Moscow
- Prof. *Gennady I. Savin*, member of the Russian Academy of Sciences (RAS), Doctor of Science (Phys&Math),
Academic Director, Joint Supercomputer Center of the Russian Academy of Sciences – subdivision of SRISA, Moscow
- Prof. *Viktor A. Soifer*, member of the Russian Academy of Sciences (RAS), Doctor of Science (Engineering), President, Chief Researcher Scientific Research Laboratory of Automated Systems of Scientific Research, Korolev Samara National Research University, Academic Director, Institute of Image Processing Systems RAS, Samara
- Prof. *Vladimir N. Chubarikov*, Doctor of Science (Phys&Math), Chairperson of the Department of Mathematical and Computer Analysis Methods, Lomonosov Moscow State University, Moscow
- Prof. *Yuri A. Chaplygin*, member of the Russian Academy of Sciences (RAS), Doctor of Science (Engineering), President, National Research University of Electronic Technology, Moscow
- Prof. *Nikolay N. Smirnov*, Doctor of Science (Phys&Math), Deputy Dean of Faculty of Mechanics and Mathematics Lomonosov Moscow State University, Deputy Director for Strategic Information Technology, SRISA, Moscow
- Prof. *Vladimir F. Tishkin*, corresponding member of the Russian Academy of Sciences (RAS), Doctor of Science (Phys&Math), Professor of the Department of Computational Methods, Lomonosov Moscow State University, Moscow
- Prof. *Amir A. Gubaidullin*, Doctor of Science (Phys&Math), Director, Tyumen Division of the Khristianovich Institute of Theoretical and Applied Mechanics, Siberian Division of RAS, Tyumen
- Prof. *Mikhail V. Iakovovski*, corresponding member of the Russian Academy of Sciences (RAS), Doctor of Science (Phys&Math), Deputy Director for Science, Keldysh Institute of Applied Mathematics of RAS, Moscow
- Prof. *Rashit M. Shagaliyev*, Doctor of Science (Phys&Math)
- Prof. *Sergey O. Starkov*, Doctor of Science (Phys&Math), Head of Division of Intelligent Cybernetic Systems, Obninsk Institute of Atomic Energy, Obninsk
- Prof. *Valery M. Eskov*, Doctor of Science (Phys&Math), Doctor of Science (Biology), Head of Division, SRISA, Surgut Branch, Surgut
- Prof. *Mikhail M. Lavrentiev*, Doctor of Science (Phys&Math), Deputy Director for Science of the Institute of Automation and Electrometry of the Siberian Branch of the Russian Academy of Sciences, Novosibirsk
- Prof. *Sergey G. Pyatkov*, Doctor of Science (Phys&Math), Chairperson of the Department of Further Mathematics, Yugra State University, Khanty-Mansiysk
- Prof. *Valerii P. Il'in*, Doctor of Science (Phys&Math), Professor of the Department of Applied Mathematics, Novosibirsk State Technical University, Novosibirsk
- Prof. *Boris V. Kryzhanovskii*, corresponding member of the Russian Academy of Sciences (RAS), Doctor of Science (Phys&Math), Director, Opto-neural Technologies Center of Federal State Institution Scientific Research Institute for System Analysis of the Russian Academy of Sciences (SRISA), Moscow
- Prof. *Oleg V. Nagornov*, Doctor of Science (Phys&Math), First Vice-Rector, National Research Nuclear University MEPhI, Moscow
- Prof. *Vladimir V. Savchenko*, PhD (Theoretical Mechanics), Hosei University, Tokyo, Japan
- Prof. *Yasunari Zempo*, PhD (Physics), Hosei University, Tokyo, Japan
- Prof. *Athanase Papadopoulos*, Doctorat d'Etat (Habilitation), mathematics, University of Strasbourg, The French National Centre for Scientific Research, Strasbourg, France

Executive Editor

Taras V. Gavrilenko, PhD (Engineering)

Managing Editor

Anna P. Chalova, PhD (Linguistics)

Technical Editor

Dmitry A. Morgun, PhD (Phys&Math)

Editors

Alexander A. Egorov, PhD (Engineering)

Ivan N. Devitsyn

Erkin M. Kamilov

Cover Design

© Alexander S. Gorbunov

Published since 2020. 4 issues per year.

Editorial Board Address:

SRISA, Russia 117218, Moscow, Nakhimovsky pr., 36/1.

Tel.: +7 9226-54-57-88, fax: +7 (495) 719-76-81, e-mail: taras.gavrilenko@gmail.com. Web: jcyb.ru.

Учредитель и издатель

Федеральное государственное учреждение «Федеральный научный центр
Научно-исследовательский институт системных исследований Российской академии наук»
(ФГУ ФНЦ НИИСИ РАН)

«Успехи кибернетики» — это рецензируемый научный журнал, в котором публикуются научные статьи по следующим специальностям (физико-математические, технические науки):

05.13.01 – Системный анализ, управление и обработка информации;

05.13.18 – Математическое моделирование, численные методы и комплексы программ;

05.27.01 – Твердотельная электроника, радиоэлектронные компоненты, микро- и нанoeлектроника, приборы на квантовых эффектах.

Миссия журнала – развитие научных направлений по заявленной тематике в России и за рубежом, соответствующих приоритетным направлениям развития науки, технологий и техники в Российской Федерации, а также перечню критических технологий РФ.

Журнал ориентирован на пропаганду передовых идей в области физики, математики, технических наук, участие в реализации задач, сформулированных Президентом РФ в Указе от 01.12.2016 № 642, по научно-технологическому развитию РФ, а также импортозамещению по приоритетным направлениям стратегического развития страны, соответствующим тематике журнала, обеспечение печатными площадями высококвалифицированных кадров, повышение качества диссертационных исследований в данных отраслях путем развития механизма профессионального и общественного обсуждения их научных результатов, воспитание молодого поколения ученых.

Журнал принимает к публикации оригинальные статьи; переводы статей, опубликованных в зарубежных журналах (при согласии правообладателя на перевод и публикацию); обзоры; эссе; комментарии; другие информационные материалы.

Издание будет полезно ученым, работающим в соответствующих областях наук, а также аспирантам и студентам.

Главный редактор

Бетелин Владимир Борисович, академик РАН, д. ф.-м. н., профессор, научный руководитель, ФГУ ФНЦ НИИСИ РАН, Москва

Заместитель главного редактора

Галкин Валерий Алексеевич, д. ф.-м. н., профессор, директор, Сургутский филиал ФГУ ФНЦ НИИСИ РАН, Сургут

Члены редакционной коллегии

Власов Сергей Евгеньевич, д. т. н., директор, ФГУ ФНЦ НИИСИ РАН, Москва

Панченко Владислав Яковлевич, академик РАН, д. ф.-м. н., профессор, председатель Совета, Российский фонд фундаментальных исследований; заведующий кафедрой медицинской физики, Московский государственный университет им. М. В. Ломоносова, Москва

Савин Геннадий Иванович, академик РАН, д. ф.-м. н., профессор, научный руководитель, Межведомственный суперкомпьютерный центр РАН — филиал ФГУ ФНЦ НИИСИ РАН, Москва

Соифер Виктор Александрович, академик РАН, д. т. н., профессор, президент, главный научный сотрудник научно-исследовательской лаборатории автоматизированных систем научных исследований, Самарский национальный исследовательский университет им. ак. С. П. Королева, Институт систем обработки изображений РАН, Самара

Чубариков Владимир Николаевич, д. ф.-м. н., профессор, заведующий кафедрой математических и компьютерных методов анализа, Московский государственный университет им. М. В. Ломоносова, Москва

Чаплыгин Юрий Александрович, академик РАН, д. т. н., профессор, президент, Московский институт электронной техники, Москва

Смирнов Николай Николаевич, д. ф.-м. н., профессор, заместитель декана механико-математического факультета, Московский государственный университет им. М. В. Ломоносова, заместитель директора по стратегическим информационным технологиям, ФГУ ФНЦ НИИСИ РАН, Москва

Тишкин Владимир Федорович, член-корреспондент РАН, д. ф.-м. н., профессор, профессор кафедры вычислительных методов, Московский государственный университет им. М. В. Ломоносова, Москва

Губайдуллин Амир Анварович, д. ф.-м. н., профессор, директор, Тюменский филиал Института теоретической и прикладной механики им. С. А. Христиановича Сибирского отделения РАН, Тюмень

Яковлевский Михаил Владимирович, член-корреспондент РАН, д. ф.-м. н., профессор, заместитель директора по научной работе, Институт прикладной математики им. М. В. Келдыша РАН, Москва

Шагалиев Рашид Мирзагалиевич, д. ф.-м. н.

Старков Сергей Олегович, д. ф.-м. н., профессор, начальник отделения интеллектуальных кибернетических систем, Обнинский институт атомной энергетики, Обнинск

Есков Валерий Матвеевич, д. ф.-м. н., д. б. н., профессор, заведующий отделом, Сургутский филиал ФГУ ФНЦ НИИСИ РАН, Сургут

Лаврентьев Михаил Михайлович, д. ф.-м. н., профессор, заместитель директора по научной работе, Институт автоматизации и электротехники Сибирского отделения РАН, Новосибирск

Пятков Сергей Григорьевич, д. ф.-м. н., профессор, заведующий кафедрой высшей математики, Югорский государственный университет, Ханты-Мансийск

Ильин Валерий Павлович, д. ф.-м. н., профессор, профессор кафедры прикладной математики, Новосибирский государственный технический университет, Новосибирск

Крыжановский Борис Владимирович, член-корреспондент РАН, д. ф.-м. н., руководитель, Центр оптико-нейронных технологий ФГУ ФНЦ НИИСИ РАН, Москва

Нагорнов Олег Викторович, д. ф.-м. н., профессор, первый проректор, Национальный исследовательский ядерный университет «МИФИ», Москва

Савченко Владимир Васильевич, PhD (Theoretical Mechanics), Университет Хосэй, Токио, Япония

Земто Ясунари, PhD (Physics), Университет Хосэй, Токио, Япония

Пападопулос Атанас, Doctorat d'Etat (Habilitation), mathematics, Университет Страсбурга, Национальный центр научных исследований Франции, Страсбург, Франция

Ответственный секретарь

Гавриленко Тарас Владимирович, к. т. н.

Ответственный редактор

Чалова Анна Петровна, к. филол. н.

Технический редактор

Моргун Дмитрий Алексеевич, к. ф.-м. н.

Редакторы

Егоров Александр Алексеевич, к. т. н.

Девицын Иван Николаевич

Камилов Эркин Махмуджанович

Художественное оформление обложки

© Горбунов Александр Сергеевич

Издается с 2020 года. Выпускается 4 раза в год.

Адрес редакции:

ФГУ ФНЦ НИИСИ РАН, 117218, г. Москва, Нахимовский просп., дом 36, корпус 1.

Телефон: +7 9226-54-57-88, факс: +7 (495) 719-76-81, e-mail: taras.gavrilenko@gmail.com. Сайт: jcyb.ru.

CONTENTS

V. B. Betelin	
Welcome Address by V. B. Betelin, Member of the Russian Academy of Sciences	6
S. E. Vlasov, M. M. Godovitsyn, N. V. Starostin	
The Concept of Multistage Integrated Chip Routing with Virtual Channels	8
I. V. Afanaskin, P. V. Kryganov, A. A. Glushakov, P. V. Yalov	
CRM Well Interference Models for Evaluating Reservoir Filtration and Volumetric Properties from Production Data	16
G. E. Deev, S. V. Ermakov	
Automata-Based Model of DNA Replication	26
R. D. Gimranov, E. V. Gaydukova	
Organic Growth Strategy as the Foundation for an Agile Information System	31
A. Papadopoulos	
Map Drawing and Foliations of the Sphere	38
V. V. Savchenko, M. A. Savchenko	
A Computational Experiment of Simulating Light Propagation in a Fibre-Containing Profiled Structure	46
V. M. Eskov, V. F. Pyatin, Yu. V. Bashkatova	
Medical and Biological Cybernetics: Development Prospects	54
M. I. Zimin, O. A. Kumukova, M. M. Zimin	
Mathematical Model and Software for Avalanche Forecasting	63

СОДЕРЖАНИЕ

В. Б. Бетелин	
Приветственное слово	6
С. Е. Власов, М. М. Годовицын, Н. В. Старостин	
Концепция многоуровневой трассировки цепей интегральных схем с использованием виртуальных каналов	8
И. В. Афанаскин, П. В. Крыганов, А. А. Глушаков, П. В. Ялов	
Использование CRM-моделей интерференции скважин для оценки фильтрационно-емкостных свойств пласта по данным разработки	16
Г. Е. Деев, С. В. Ермаков	
Автоматная модель репликации молекулы ДНК	26
Р. Д. Гимранов, Е. В. Гайдукова	
Стратегия органического развития как фундамент гибкой ИС	31
А. Пападопулос	
Построение карт и развертка поверхности сферы	38
В. В. Савченко, М. А. Савченко	
Вычислительный эксперимент по моделированию распространения света в волокнистой профилированной структуре	46
В. М. Еськов, В. Ф. Пятин, Ю. В. Башкатова	
Медицинская и биологическая кибернетика: перспективы развития	54
М. И. Зимин, О. А. Кумукова, М. М. Зимин	
Математическое и программное обеспечение для прогнозирования возможности схода снежных лавин	63



Both in Russia and worldwide, 2020 is primarily associated with the coronavirus pandemic. IT has shown that the global economy of mass consumption is unable to confront such events; moreover, it significantly boosts the virus spreading. Indeed, the core of such an economy is the continuous shipping of multi-million international flows of humans within cities, regions, countries, and the entire planet. The flows of the infected and the healthy are mixed in the confined spaces of airports, terminals, aircraft, trains, hotels, restaurants, etc. providing perfect conditions for a planet-wide virus spreading.

The pandemic has also shown that a liberal civil society is unable to provide a unified national anti-virus strategy.

There are reasons to think that a more lethal virus in a global economy of mass consumption would result in a long-term global economic crisis with unpredictable social and political implications. It would also result in the crisis of the Russian economy of services that consumes the global economy products.

Indeed, the key goal of the global mass consumption economy is accelerating capital turnover. That is, increasing the investments and reducing time to ROI. The businesses want to return their investments as soon as they can, while a strict and long-term lockdown makes it impossible. It is also true for the Russian service-oriented SMBs.

The highest capital turnover today is in the digital industries such as text, image, and video messaging services. Such intangible services do not need to invest in product design, production planning, and manufacturing. Such services last as long as it takes to reach the consumer online.

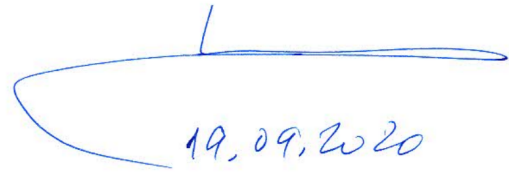
It is the essence of the so-called digital economy. Its stability depends on the solvency of the digital service users and the communication infrastructure maintenance costs. Quite obvious that a strict and long-term lockdown would reduce the actual demand and increase the communication infrastructure maintenance costs in Russia as well.

Our journal should discuss such issues of national importance. The problems can be used with cybernetics and IT, simulation, and high-performance computing.

The Editorial Board is concerned about the above aspects, but journal papers are not limited to them.

We receive submissions both from reputable and young researchers. The Journal is a discussion site for unconventional approaches and solutions, and new initiatives meeting the local and global needs.

We will try to share the most significant content with our readers. Together, we will make it!

A handwritten signature in blue ink, consisting of a long horizontal line with a small vertical tick at the top center and a curved line underneath that loops back to the left.

19, 09, 2020

DOI: 10.51790/2712-9942-2020-1-1-2

THE CONCEPT OF MULTISTAGE INTEGRATED CHIP ROUTING WITH VIRTUAL CHANNELS**Sergey E. Vlasov¹, Maksim M. Godovitsyn^{2,a}, Nikolay V. Starostin^{2,b}**¹ *Federal State Institution "Scientific Research Institute for System Analysis of the Russian Academy of Sciences", Moscow, Russian Federation, vlasov@niisi.ru*² *Lobachevsky State University of Nizhni Novgorod, Nizhniy Novgorod, Russian Federation*^a *maxim.godovicyn@gmail.com*, ^b *nvstar@mail.ru*

Abstract: the study solves the problem of circuit routing in ICs. We propose a multistage approach based on interconnection mesh reduction. It expands the chip interconnecting capability by introducing extra channels. The interconnection mesh reduction significantly accelerates the existing routing algorithms. The introduction of more channels makes it possible to reduce the routing problem in a complex interconnect space topology by removing the new routes from the extra (virtual) channels.

Keywords: circuit routing, integrated circuit, multistage method, virtual channels.

Cite this article: Vlasov S. E., Godovitsyn M. M., Starostin N. V. The Concept of Multistage Integrated Chip Routing with Virtual Channels. *Russian Journal of Cybernetics*. 2020;1(1):8–15. DOI: 10.51790/2712-9942-2020-1-1-2.

КОНЦЕПЦИЯ МНОГОУРОВНЕВОЙ ТРАССИРОВКИ ЦЕПЕЙ ИНТЕГРАЛЬНЫХ СХЕМ С ИСПОЛЬЗОВАНИЕМ ВИРТУАЛЬНЫХ КАНАЛОВ**С. Е. Власов¹, М. М. Годовицын^{2,a}, Н. В. Старостин^{2,b}**¹ *Федеральное государственное учреждение «Федеральный научный центр Научно-исследовательский институт системных исследований Российской академии наук»,**г. Москва, Российская Федерация, vlasov@niisi.ru*² *Нижегородский государственный университет, г. Нижний Новгород, Российская Федерация*^a *maxim.godovicyn@gmail.com*, ^b *nvstar@mail.ru*

Аннотация: рассматривается проблема трассировки цепей интегральной схемы. Предлагается многоуровневый метод, в основу которого положены идеи редукции сетки трассировки, а также расширения коммутационных ресурсов кристалла за счет введения дополнительных каналов. Редукция сетки трассировки обеспечивает существенное сокращение времени работы известных алгоритмов трассировки. Введение дополнительных каналов дает возможность свести задачи поиска трассы в сложной топологии коммутационного пространства к задаче вытеснения построенных трасс с дополнительных (виртуальных) каналов.

Ключевые слова: трассировки цепей, интегральная схема, многоуровневый метод, виртуальные каналы.

Для цитирования: Власов С. Е., Годовицын М. М., Старостин Н. В. Концепция многоуровневой трассировки цепей интегральных схем с использованием виртуальных каналов. *Успехи кибернетики*. 2020;1(1):8–15. DOI: 10.51790/2712-9942-2020-1-1-2.

Introduction

Circuit routing is an integrated part of the typical standard cell integrated circuit (IC) design process. Its purpose is the development of the conductive tracks topology. The tracks connect the contact pads of the circuit components. Each circuit is a continuous system of conductors, commonly referred to as a track. In any acceptable connection topology, no conductors belonging to different tracks may contact each other.

The key routing problems are high dimensionality and complexity of circuits, miniaturization of chip elements, which results in placing more items and the chip packing density increase. Considering the NP-completeness [1] of the routing problem and focusing on the signature large dimensionality of the actual problems, the requirements to applied routing algorithms increase. The situation is complicated by the fact that for submicron chips the interference of adjacent tracks should be taken into account. So, despite the

variety of available methods and tools for solving this class of problems, developing a fast and high-quality router tool is a relevant task.

This paper presents a multistage routing method. It uses not one but many interconnection meshes to reach the balance between the solution search performance and quality.

The Routing Problem

The input data for the routing problem are layers, horizontal and vertical tracks that form the interconnection mesh; no-metallization areas on the interconnection mesh including grounding and power supply circuits; contact pads of the chip components assigned to the interconnection mesh nodes; a list of the chip circuits indicating the contact pads; metallized tracks of some circuit subset. A track is a continuous system of metal conductors linking all the circuit contact pads. It passes only within the specified interconnection mesh avoiding the no-metallization areas and tracks of other circuits. The key routing task is developing the tracks of all circuits.

Exact and approximate routing algorithms are mostly of academic interest. They cannot be used in real life to solve practical problems because of the exponential growth of computational costs as the dimensionality increases.

The major useable heuristic routing algorithms can be divided into two classes. The first class consists of algorithms that search for solutions directly on the interconnection mesh. Such algorithms are channel routing, backbone routing [2, 3], Lee routing [4, 5], etc. The key issue with these algorithms is early track placement leading to deadlocks. As a result, it is not uncommon for a poorly located track to block the routing of other circuits.

The second class includes two-stage algorithms [6, 7]: first, tracks are placed on a continuous plane (making it possible to draw a third track between any pair of non-intersecting tracks.) Then they carry over the solution from continuous to discrete space of the interconnection mesh. In a sense, a circuit layout plan is developed in the first stage. Still, the basic routing deadlock problem at the second stage exists.

In real-life applications, algorithms of both classes often produce incomplete tracks. It is solved by repeatedly re-routing the tracks automatically (expert-assisted), either on the entire chip or in selected areas. Such solutions are costly and make the entire chip design process more expensive.

Fast Multistage Routing

To improve the algorithm performance, routing space is usually divided into large fragments (blocks, areas) and interconnect areas that connect the blocks with a mesh of macro discrete elements. At the global routing stage, only interconnect circuits linking elements from different blocks are implemented. At the detailed routing stage, local circuits are implemented within a single fragment. The key problem of such a two-level approach [8] is a progressive track placement. It greatly reduces the routing space available for placing subsequent tracks.

We propose to use the well-known multistage concept [9] for routing assuming that we can remove the negative aspects of the concept by manipulating the interconnection mesh, including its reduction and expansion.

With the multistage approach, we build a coarse interconnection mesh (interconnection mesh reduction.) It is generated by combining adjacent tracks (vertical or horizontal metallization tracks within the entire chip) into groups, with the same number of tracks in each (if possible.) Such groups form channels in the original interconnection mesh. The result is a new coarsened interconnection mesh, where each node and each edge corresponds to a certain fragment of the original interconnection mesh. Let us assign a potential number of tracks within the corresponding fragment to each edge of the mesh. We call this number “edge routing ability”. It is defined as the product of the number of tracks in the group and the number of metallization layers.

Similarly, we can perform a second reduction after the first one, and so on until the required number of reductions is reached. The result of the first stage is a system of interconnection mesh reductions described by graphs of different sizes and characterized by different levels of detail.

To route a single track, we propose to use a multistage Lee algorithm. First, it routes tracks on a coarse mesh without considering topological intersections of conductors from different circuits (pseudo routing) but taking into account the edge routing capacity. In this case, the resulting track, in terms of a

rough interconnection mesh, is a continuous fragment of the original interconnection mesh. Lee algorithm builds a track within it.

It is quite obvious that at some stage the algorithm will not be able to find a continuous track within the selected fragment. In this case, the fragment is expanded (in the extreme case it can cover all the elements of the given mesh) and the solution is generated beyond the mesh fragment represented by the track found on the coarse interconnection mesh.

As a result, the solution found on the original interconnection mesh is locked and the corresponding routing capabilities of the coarse versions of the interconnection mesh edges are adjusted.

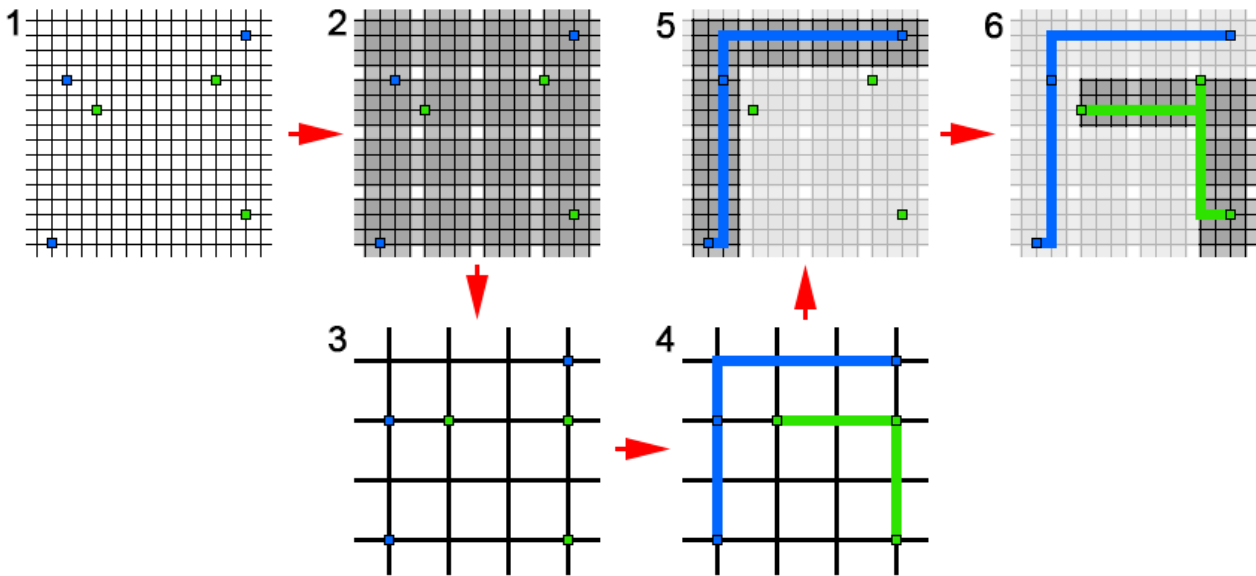


Figure 1. *Multistage Routing Steps*

The figure (refer to Fig. 1) is a chart of basic multistage routing stages (two levels are presented as an example.) The input data (stage 1) include the interconnection mesh, a list of circuits for each circuit, a list of contacts, and their location relative to the interconnection mesh tracks. Next (stage 2), the tracks of the original mesh are combined into groups (channels) and the interconnection mesh reductions are generated. The figure shows one reduction (stage 3.) In real life, there can be several, and their number is an input variable of the algorithm.

The reduced mesh is used for routing (stage 4.) At this stage, a general solution layout is generated. It is expressed as a system of tracks on the reduced mesh. At the same time, each such track describes a system of the original mesh fragments. With a high probability, the circuit would pass through these fragments. At this stage, the tracks can intersect, and their conflict-free configuration is produced as the reduced solution is carried over to the original mesh (stage 5.)

The general solution is progressively carried over to the original interconnection mesh (steps 5 and 6), then adjusted and optimized to meet the track topology requirements and to mitigate the interference of the adjacent conductors.

High-Quality Routing with Virtual Channels

The multistage approach described above accelerates routing. It uses the chip switching capacity uniformly. However, as noted above, the Lee algorithm in the multistage approach may fail to generate the desired track within a selected fragment on the original interconnection mesh. Let us focus on this problem.

We analyzed various solutions for the incomplete track problem and came to some conclusions as follows. First, rerouting on the original mesh is usually inefficient. Second, the application of topological rerouting methods in metric space involves the problem of mapping a continuous solution onto discrete space. However, the generation of circuits in continuous space is limited only by the topology of the circuit graph (hypergraph.) If a solution exists, then an efficient algorithm for finding it also exists. The reason is the continuous space properties: it is always possible to draw a third track between any pair of non-intersecting

tracks. We will use this feature to solve the re-routing problem.

To expand the switching capability it is proposed to introduce new tracks into the existing interconnection mesh. We will call them virtual channels. For this purpose, we will insert an additional virtual channel between each pair of adjacent existing tracks. The channel would to some extent represent the continuous space properties.

As a result, the rerouting procedure is as follows. In the first stage, virtual channels are added to the switching capacity and the partially generated tracks. In the second stage, an incomplete circuit is selected and its track is found. In the third stage, fragments of the tracks that coincide with the virtual channels are removed. The second and third stages are iterated over all the unsolved circuits. Let us consider all the proposed technology stages in detail.

Adding Virtual Channels to the Interconnection Mesh

To temporarily expand the chip switching capability we introduce extra (virtual) channels between each pair of adjacent existing tracks. Fig. 2 shows an interconnection mesh before (a) and after (b) the introduction of virtual channels.

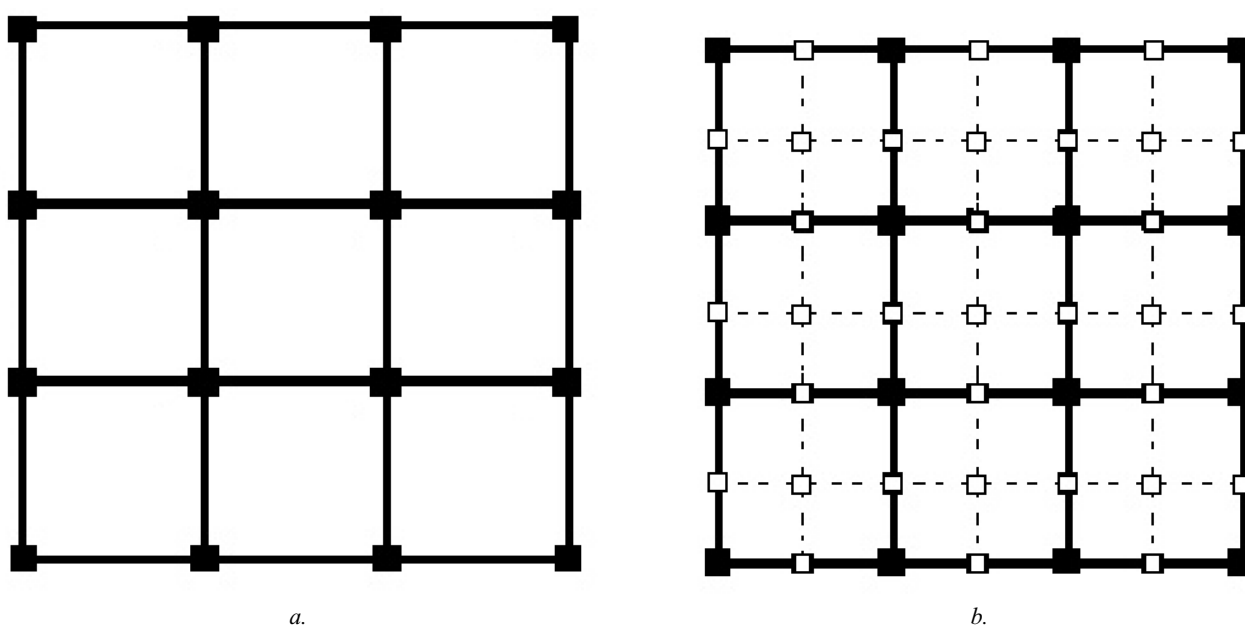


Figure 2. *Adding virtual channels to the interconnection mesh*

As a result, we get a new interconnection mesh (refer to Fig. 2) that has both real nodes (solid filled) and virtual ones (unfilled.) The latter is connected to the vertical and/or horizontal virtual channels. The interconnection mesh edges that are identical to the virtual nodes connected to two (vertical and horizontal) virtual channels are called “virtual” (dotted lines.)

Routing on a Mesh with Virtual Channels

It is proposed to apply the Lee algorithm to a single circuit routing on this mesh [5]. The algorithm is a BFS (breadth-first search) mesh pathfinding method. Given the nature of BFS, the Lee algorithm guarantees that its result has the min start-to-target path length. The Lee algorithm concept is simulating a wave coming from the source to target nodes, which are subsequently connected by a conductor.

A progressive multi-contact circuit routing is proposed. An initial contact pad is selected and permanently placed. Next, the wave routing algorithm is used to route tracks from all the non-metallized contacts to the metallized ones on this circuit. Each fragment found is added to the track. The last stage is repeated until all the contacts in the circuit are connected, or it is found to be impossible.

It is proposed to extend the classical Lee algorithm [8] to account for the weights of the interconnection mesh edges. The weights can be considered as “distances” between adjacent nodes. Let us limit the use of virtual channels by artificially increasing the weights of virtual edges on the interconnection mesh.

Removing Tracks from Virtual Channels

After successful routing on a mesh with virtual channels, it is required to remove the metallized tracks from all the virtual channels without violating the continuity of every generated track. For clarity, we will consider routing for single metallization layer chips.

Consider a special case when we want to remove metallization from a single node of the interconnection mesh while maintaining the integrity of the respective track. We will consider only track adjustment options when the metallization area is moved in a given direction from a given node to unoccupied adjustment nodes of the interconnection mesh. For the sake of certainty, at this stage, we will consider only 3 directions to move the metallization “up” (see Fig. 3.)

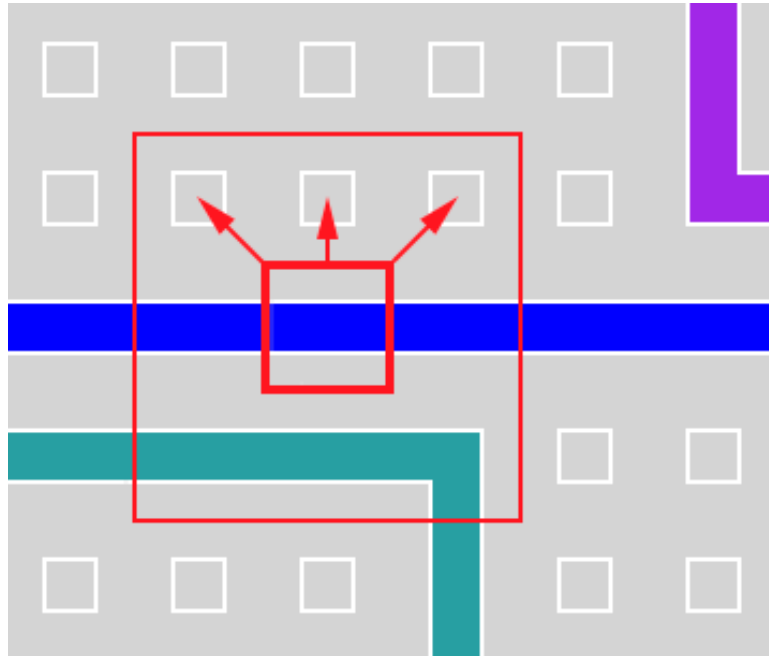


Figure 3. *A metallized mesh node and the directions of the metallization movement*

It is proposed to solve this particular problem with the NODE algorithm.

NODE Algorithm

1. Generate a new track configuration: the metallization is moved in the specified direction from the current node to all adjacent mesh nodes.
2. Check the track continuity. If the track is discontinuous, the partial problem has no solution. Restore the original track configuration exit with the "NO SOLUTION" result. If the track is continuous, go to Step 3.
3. Optimize the track removing excess metal as long as it does not affect the track continuity.
4. Check the new track for intersections with other tracks. If there are any intersections, the original track configuration is restored and the procedure is terminated with the "SOLUTION found" result indicating the list of conflicting mesh nodes.
5. The procedure is terminated with "SOLUTION FOUND" and a list of metallized mesh nodes is displayed.

NOTE. The NODE algorithm performance can be significantly optimized. We can build a database storing all possible track configuration options (256) and pre-configured solutions for each option. In this case, the algorithm is reduced to trivial retrieval of a pre-configured solution for a given configuration.

Consider a more general problem when we need to remove metallization for a single virtual channel of the interconnection mesh while maintaining the integrity of all tracks. To solve this problem, we will use the NODE algorithm for solving a specific problem. For clarity, let us assume that we need to remove metallization from a horizontal track. In this case, we should move the metallization from the virtual channel. It means that if the metallized mesh node is above the virtual channel, the metallization should be moved “up”, otherwise “down”.

TRACK Algorithm

1. Denote queue of nodes that require metallization movement as QUEUE. Add all metallized nodes adjacent to the metallization of the virtual channel to the QUEUE.
2. Check if metallization can be carried over from the virtual channels:
 - a. Check if it is possible to move the metallization “up”: the NODE algorithm is run for each metallized node of the virtual channel. If the result for each node is “SOLUTION FOUND”, then exit with the result “SOLUTION FOUND”.
 - b. Check the possibility of metallization carryover “down”: for each metallized node of the virtual channel, run the NODE algorithm. If the result for each node is “SOLUTION FOUND”, then exit with the result “SOLUTION FOUND”.
3. If the queue is empty, then exit the algorithm with the result “SOLUTION NOT FOUND”.
4. Retrieve a node from QUEUE. If the node has no metallization (it is possible), then go to step 3. Otherwise, go to step 5.
5. For a node, run the NODE algorithm. If the result is “NO SOLUTION”, go to step 3. If the result is “SOLUTION FOUND”, add the conflicting nodes to QUEUE and go to step 3. If the result is “SOLUTION FOUND”, go to step 6.
6. Generate a set of adjacent nodes extending from the found metallization nodes towards the virtual channel.
7. Add the set of adjacent nodes to QUEUE and go to step 2.

The finiteness of the TRACK algorithm is obvious: either all the metallized nodes of the virtual channel are removed (problem solved), or the node queue will eventually be empty (since the interconnection mesh is finite.) The proposed TRACK algorithm is easily transformed for handling vertical virtual channels.

The most general problem statement involves metallization removal from several interconnection mesh tracks while maintaining the continuity of each track. It is proposed to solve this problem by sequentially removing metallization from the virtual channels.

TRACKS Algorithm

1. No-metallization virtual channels are removed from the interconnection mesh.
2. Metallized virtual channels are checked one by one in some order. For each virtual channel:
 - a. The TRACK algorithm is run. If the result is “SOLUTION NOT FOUND”, then exit with the result “SOLUTION NOT FOUND”.
 - b. Remove the virtual channel from the interconnection mesh.
3. Exit with the result “SOLUTION FOUND”.

Computational Experiment

The algorithm described above was implemented in C#. A test application was developed to test the proposed multistage routing procedure.

Table 1 lists the results produced by the multistage routing algorithm with simulated test problems. The experiments were conducted on a PC with the following specifications: Intel i7 2 GHz / 16 GB, MS Windows 7x64.

Table

Test case				Run time (sec)	
Circuits	Contacts	Nodes per layer	Layers	Lee algorithm	Multistage algorithm
10^4	5×10^4	10^6	3	1,841	310
10^4	10^5	10^6	3	6099	855
10^4	5×10^4	10^7	3	2721	322
10^4	5×10^4	10^6	5	4155	582

Routing Algorithms Comparison

The multistage algorithm reduced the interconnection mesh once, reducing its size to 100x. As a result, the multistage algorithm is on average 700% faster than the classical Lee algorithm. It should be noted that the quality of the solutions produced by the presented algorithms differs slightly.

The screenshots below present an example of the routing algorithm with virtual channels.

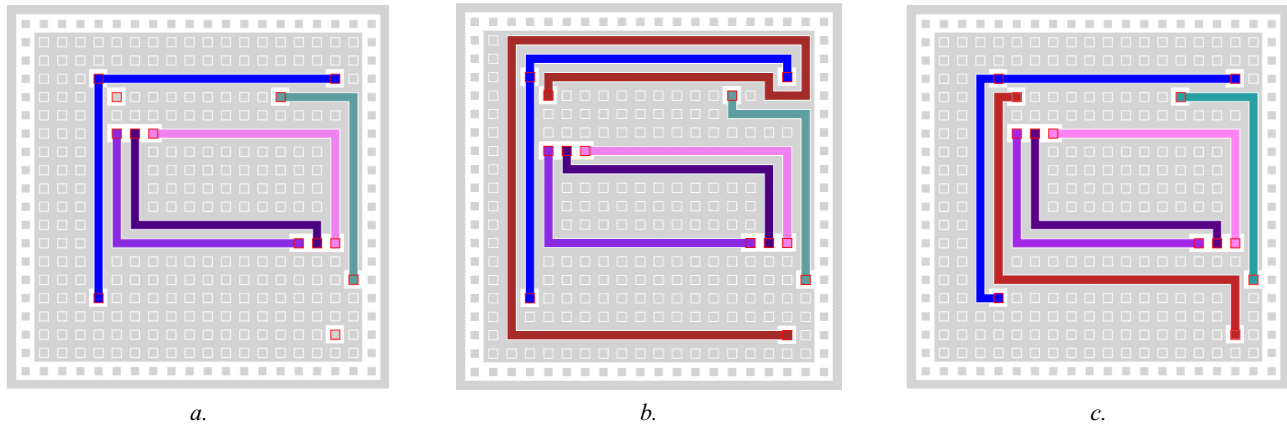


Figure 4. Routing with virtual channels

Fig. 4 shows an example produced by the routing algorithm with virtual channels. The image shows the initial data. Note that there is a no-route circuit for which the Lee algorithm fails to find a solution. Image b shows the result produced by the routing algorithm with virtual horizontal channels. Image c shows the result produced by the routing algorithm with the virtual vertical channels. In both cases, the circuit that was not routed by the Lee algorithm was successfully generated while maintaining the continuity of the originally routed tracks.

To summarize, we note that the experimental studies confirmed the assumption that the proposed multistage routing procedure is highly promising for real-life submicron IC design applications.

Conclusion

The study objective is improving the efficiency of IC circuit routing. We propose a multistage routing procedure that saves time and computational burden. The proposed multistage routing uses virtual channels and intended for better utilization of the available switching capacity. It is planned to test and fine-tune the presented algorithms as applied to solving real-life problems of submicron IC design.

REFERENCES

1. Garey M. R., Johnson D. S. *Computers and Intractability: A Guide to the Theory of NP-Completeness*. W. H. Freeman, 1979. 584 p.
2. Mikami K., Tabuchi K. A Computer Program for Optimal Routing of Printed Circuit Conductors. *Proc. IFIP Congress*. 1968:1475–1478.
3. Hightower D. W. A Solution to Line-Routing Problems on the Continuous Plane. *Proc. 6th Annual Design Automation Conference (DAC '69)*. 1969:1–24.
4. Hadlock F. O. A Shortest Path Algorithm for Grid Graphs. *Networks*. 1977; 7(4):323–334.
5. Lee C. Y. An Algorithm for Path Connections and Its Applications. *IRE Transactions on Electronic Computers*. 1961; EC-10 (3):346–365.
6. Hama T., Etoh H. Topological Routing Path Search Algorithm with Incremental Routability Test. *IEEE Transactions on Computer-Aided Design of Integrated Circuits and Systems*. 1999; Feb:142–150.
7. Starostin N. V., Balashov V. V. The Use of Hypergraphs for Solving the Problem of Orthogonal Routing of Large-Scale Integrated Circuits with an Irregular Structure. *Journal of Communications Technology and Electronics*. 2008;53(5):589–593. DOI: 10.1134/S1064226908050185.

8. Batishchev D. I., Starostin N. V., Filimonov A.V. Two-Level Evolutionary Genetic Tracing of Electrical Circuits on a Graph Model. *Problems of Advanced Micro- and Nanoelectronic Systems Development (MES)*. 2008;1:61–64. (In Russ.)
9. Batishchev D. I., Starostin N. V., Filimonov A. V. Multilevel Genetic Algorithm for Hypergraph K-way Partitioning. *Proceedings of Saint Petersburg Electrotechnical University Journal*. 2007;1:3–13. (In Russ.)

DOI: 10.51790/2712-9942-2020-1-1-3

CRM WELL INTERFERENCE MODELS FOR EVALUATING RESERVOIR FILTRATION AND VOLUMETRIC PROPERTIES FROM PRODUCTION DATA

Ivan V. Afanaskin, Pavel V. Kryganov, Alexey A. Glushakov, Pyotr V. Yalov

Federal State Institution "Scientific Research Institute for System Analysis of the Russian Academy of Sciences", Moscow, Russian Federation, ivan@afanaskin.ru, kryganov@mail.ru, stormwww@yandex.ru, petryalov@gmail.com

Abstract: the study proposes two CRM models that simulate well interference. The models combine the material balance equation and the inflow equation. The first model considers the reservoir pore volume common to all wells. The second model uses individual pore volumes to each well with interconnecting flows. The simulated examples show that the first model applies to infinite reservoirs while the second model gives the best results for limited reservoirs.

Keywords: CRM model, well interference.

Acknowledgements: this work was supported by RFBR grant 18-07-00677 A.

Cite this article: Afanaskin I. V., Kryganov P. V., Glushakov A. A., Yalov P. V. CRM Well Interference Models for Evaluating Reservoir Filtration and Volumetric Properties from Production Data. *Russian Journal of Cybernetics*. 2020;1(1):16–25. DOI: 10.51790/2712-9942-2020-1-1-3.

ИСПОЛЬЗОВАНИЕ CRM-МОДЕЛЕЙ ИНТЕРФЕРЕНЦИИ СКВАЖИН ДЛЯ ОЦЕНКИ ФИЛЬТРАЦИОННО-ЕМКОСТНЫХ СВОЙСТВ ПЛАСТА ПО ДАННЫМ РАЗРАБОТКИ

И. В. Афанаскин, П. В. Крыганов, А. А. Глушаков, П. В. Ялов

Федеральное государственное учреждение «Федеральный научный центр Научно-исследовательский институт системных исследований Российской академии наук», г. Москва, Российская Федерация, ivan@afanaskin.ru, kryganov@mail.ru, stormwww@yandex.ru, petryalov@gmail.com

Аннотация: в работе предложены две CRM-модели, описывающие интерференцию скважин. Модели получены путем комбинации уравнения материального баланса и уравнения притока. В первой модели рассматривается общий для всех скважин поровый объем пласта. Во второй модели все скважины имеют индивидуальные поровые объемы, между которыми происходят перетоки. На синтетических примерах показано, что для бесконечного пласта можно применять первую модель, а для ограниченного пласта лучшие результаты дает вторая модель.

Ключевые слова: CRM-модель, интерференция скважин.

Благодарности: работа выполнена при поддержке гранта РФФИ 18-07-00677 А.

Для цитирования: Афанаскин И. В., Крыганов П. В., Глушаков П. В., Ялов П. В. Использование CRM-моделей интерференции скважин для оценки фильтрационно-емкостных свойств пласта по данным разработки. *Успехи кибернетики*. 2020;1(1):16–25. DOI: 10.51790/2712-9942-2020-1-1-3.

Introduction

A capacitance resistive model (CRM) [1] describes the operation of several wells draining the same formation. The model is a combination of the material balance equation (the formation fluid flow continuity equation) and the well inflow equation [1]. There are many modifications of CRM models taking into account the various effects.

Most publications consider analytical (or semi-analytical) solutions of the ordinary differential equation for downhole pressure or fluid flow rate obtained through a CRM model development [1–3]. This paper deals with a numerical solution.

The advantage of CRM models is that the reservoir pressure value is not required as it changes during the extraction, and its field measurements are rare and often irregular.

As a rule, such models are used to estimate the drained volumes of production wells and optimize the reservoir pressure maintenance system [1–3]. They are also used for short-term forecasting of production metrics.

The purpose of this work is developing CRM models that evaluate reservoir filtration and capacitive properties (including permeability) around the wells and in the inter-well space from the production logging data. The production data, in this case, are fluid flow rate, injected water flow rate, and bottom hole pressure. The fluid flow rate and the injected water flow rate are logged at all production and injection wells. Most production wells are equipped with submersible electric submersible pumps (ESPs) with telemetry units (TMUs) comprising of a pressure sensor at the pump suction line. Such units can measure downhole pressure in production wells. The downhole pressure in injection wells is measured with dedicated downhole pressure gauges (either stand-alone or plugged to a cable), or estimate from the wellhead pressure with Bernoulli's equation.

We will consider two CRM models of well interference as applied to the interference of a production well and an injection well.

A Single Volume Model

Consider a single volume CRM model for the production-injection wells interference. The model is a single volume since only the common pore volume served by both wells is considered. The system of equations describing the production well operation under such conditions is as follows:

$$c_t V_p \frac{dP}{dt} = q_{iw}(t) - q_l(t), \quad (1)$$

$$q_l(t) = PI [P(t) - P_w(t)] + \frac{PI}{K} q_{iw}(t), \quad (2)$$

where (1) is the material balance equation (fluid flow continuity equation) in a drained volume; (2) is the production well inflow equation (obtained by applying the potential theory to solving the planar steady-state filtration problem [4]), c_t is the total compressibility of the formation and the fluids saturating it; V_p is the pore volume; $P(t)$ is the reservoir pressure, $q_{iw}(t)$ is the injected water flow rate, $q_l(t)$ is the production fluid flow rate, t is time, PI is the productivity factor of the producing well; K is the injection-to-production well interference factor, $P_w(t)$ is the production well bottom-hole pressure. The equations are expressed through the reservoir variables.

Let us express the reservoir pressure from the inflow equation (2):

$$P(t) = P_w(t) + q_l(t)/PI - q_{iw}(t)/K. \quad (3)$$

By substituting (3) into (1), we obtain:

$$c_t V_p \left(\frac{dP_w}{dt} + \frac{1}{PI} \frac{dq_l}{dt} - \frac{1}{K} \frac{dq_{iw}}{dt} \right) = q_{iw}(t) - q_l(t). \quad (4)$$

Expressing the downhole pressure derivative from (4), we obtain a first-order ordinary differential equation with respect to P_w :

$$\frac{dP_w}{dt} = \frac{1}{c_t V_p} [q_{iw}(t) - q_l(t)] - \frac{1}{PI} \frac{dq_l}{dt} + \frac{1}{K} \frac{dq_{iw}}{dt}. \quad (5)$$

Let us apply the first-order Runge-Kutta method to equation (5):

$$P_w(t + \Delta t) = P_w(t) + \frac{\Delta t}{c_t V_p} [q_{iw}(t) - q_l(t)] - \frac{1}{PI} [q_l(t + \Delta t) - q_l(t)] + \frac{1}{K} [q_{iw}(t + \Delta t) - q_{iw}(t)] \quad (6)$$

where Δt is the time increment.

As indicated in[4], the productivity and interference factors can be expressed as:

$$PI = \frac{2\pi k_1 h_1}{\mu} \cdot \frac{1}{\ln\left(\frac{R_c}{r_w} + S\right)}, \quad (7)$$

$$K = \frac{2\pi k_{12} h_{12}}{\mu} \cdot \frac{1}{\ln\left(\frac{R_c}{r_{12}}\right)}, \quad (8)$$

where k_1 is the reservoir permeability at the production well location; h_1 is the reservoir thickness at the production well location; μ is the fluid dynamic viscosity; R_c is the external reservoir boundary radius; r_w is the production wellbore radius; S is the production well skin factor; k_{12} is the reservoir permeability in the inter-well area; h_{12} is the reservoir thickness in the inter-well area; r_{12} is the production to injection well distance.

Provided that other variables are known, equations (7) and (8) give the k_1 reservoir permeability at the production well and the k_{12} reservoir permeability in the inter-well area. If the skin factor for a particular well is unknown (it is a typical situation in real life), we can use an empirical skin factor vs. permeability relation obtained from the results of hydrodynamic studies in other wells in the same reservoir [5]. The fluid viscosity should generally be estimated taking into account the relative phase permeabilities.

To account for the stationary inflow as the well operation mode changes, the following correction factors are applied to the productivity and interference factors [3]:

$$PI(t) = \frac{PI}{1 + b_1 \ln(t/t_1)}, \quad (9)$$

$$K(t) = \frac{K}{1 + b_{12} \ln(t/t_{12})}, \quad (10)$$

where b_1 and b_{12} are constant factors; t_1 and t_{12} are the periods of relaxation.

For an infinite reservoir (in real life, a very large value of the V_p pore volume when no reservoir pressure drop occurs), the external reservoir boundary radius is estimated by the Pisman equation [6]. In this particular case it can be reduced to:

$$R_c = 0,12\sqrt{2F}, \quad (11)$$

$$F = \frac{V_p}{mh_{12}}, \quad (12)$$

where F is the drainage area, m is the reservoir porosity.

For a limited reservoir (relatively small V_p pore volume), the drainage zone shape can be represented as an ellipse with the well at its focal points. Then we can use Borisov's equation [7] to approximate the external reservoir boundary radius:

$$R_c = 2a + \sqrt{4a^2 - r_{12}^2}, \quad (13)$$

$$a = \sqrt{\frac{\pi^2 r_{12}^2 / 4 + \sqrt{\pi^4 r_{12}^4 / 16 + 4\pi^2 F^2}}{2\pi^2}}, \quad (14)$$

where a is the major semi-axis of the ellipse.

If the production well downhole pressure, fluid flow rate and water injection volume values are available, we can estimate the reservoir parameters by adapting the downhole pressure model (6). For this, the following optimization problem is to be solved:

$$F(X) = \sum_t \left[P_w^c(t) - P_w^f(t) \right]^2 \rightarrow 0, \quad (15)$$

where F is the function to be minimized; X is a vector of variables; the c and f superscripts indicate the estimated and actual values, respectively. We add the values for each moment t when the actual downhole pressure value is available.

The optimization problem variables are:

- 1) V_p : porous volume
- 2) PI : production well productivity factor
- 3) K : production-to-injection well interference factor
- 4) b_1 and b_{12} factors
- 5) t_1 and t_{12} relaxation periods.

If PI and K are known, we can estimate k_1 and k_{12} provided that other variables are also available. The above model can be easily generalized for a larger number of wells.

A Multivolume Model

Let us consider a multivolume CRM model of well interference. The model is multivolume since the number of pore volumes considered is equal to the number of wells. Each well operates in its dedicated pore volume. There are inter-flows between the porous volumes of the wells. The system of equations describing the production and injection wells operation under such conditions is as follows:

$$c_{t,1}V_{p,1}\frac{dP_1}{dt} = q_{21}(t) - q_l(t), \quad (16)$$

$$c_{t,2}V_{p,2}\frac{dP_2}{dt} = q_{iw}(t) - q_{21}(t), \quad (17)$$

$$q_l(t) = PI_1 [P_1(t) - P_{w,1}(t)], \quad (18)$$

$$q_{iw}(t) = PI_2 [P_{w,2}(t) - P_2(t)], \quad (19)$$

$$q_{21}(t) = PI_{21} [P_2(t) - P_1(t)], \quad (20)$$

where (16) and (17) are material balance equations (fluid continuity equations) for the porous volumes of the production and injection wells, respectively; (18) and (19) are the production well inflow and injection well outflow equations, respectively; (20) is the porous volume-to-porous volume inter-flow equation; subscript “1” indicate the production well porous volume; superscript “2” indicate the injection well porous volume; $c_{t,1}$ and $c_{t,2}$ are the total compressibility of the reservoir and the fluids saturating it; $V_{p,1}$ and $V_{p,2}$ are the porous volumes; $P_1(t)$ and $P_2(t)$ are the reservoir pressures; $q_{iw}(t)$ is the injection water rate; $q_l(t)$ is the production well flow rate; q_{21} is the second-to-first porous volume inter-flow; t is time; PI_1 is the production well productivity factor; PI_2 is the injectivity factor of the injection well; PI_{21} is the porous volume-to-porous volume inter-flow factor; $P_{w,1}(t)$ and $P_{w,2}(t)$ are the downhole pressures of the production and injection wells, respectively. The equations are expressed through the reservoir variables.

Let us express reservoir pressures from (18) and (19):

$$P_1(t) = P_{w,1}(t) + q_l(t)/PI_1, \quad (21)$$

$$P_2(t) = P_{w,2}(t) - q_{iw}(t)/PI_2, \quad (22)$$

By substituting (21) and (22) into (16) and (17), respectively, we obtain:

$$c_{t,1}V_{p,1}\left(\frac{dP_{w,1}}{dt} + \frac{1}{PI_1}\frac{dq_l}{dt}\right) = q_{21}(t) - q_l(t), \quad (23)$$

$$c_{t,2}V_{p,2}\left(\frac{dP_{w,2}}{dt} - \frac{1}{PI_2}\frac{dq_{iw}}{dt}\right) = q_{iw}(t) - q_{21}(t). \quad (24)$$

Expressing the downhole pressure derivatives from (23) and (24), we obtain a first-order ordinary differential equation with respect to $P_{w,1}$ and $P_{w,2}$:

$$\frac{dP_{w,1}}{dt} = \frac{1}{c_{t,1}V_{p,1}} [q_{21}(t) - q_l(t)] - \frac{1}{PI_1} \frac{dq_l}{dt}. \quad (25)$$

$$\frac{dP_{w,2}}{dt} = \frac{1}{c_{t,2}V_{p,2}} [q_{iw}(t) - q_{21}(t)] + \frac{1}{PI_2} \frac{dq_{iw}}{dt}. \quad (26)$$

Let us apply the first-order Runge-Kutta method to equations (25) and (26):

$$P_{w,1}(t + \Delta t) = P_{w,1}(t) + \frac{\Delta t}{c_{t,1}V_{p,1}} [q_{21}(t) - q_l(t)] - \frac{1}{PI_1} [q_l(t + \Delta t) - q_l(t)] \quad (27)$$

$$P_{w,2}(t + \Delta t) = P_{w,2}(t) + \frac{\Delta t}{c_{t,2}V_{p,2}} [q_{iw}(t) - q_{21}(t)] + \frac{1}{PI_2} [q_{iw}(t + \Delta t) - q_{iw}(t)], \quad (28)$$

where

$$q_{21}(t) = PI_{21} [P_{w,2}(t) - P_{w,1}(t) - q_l(t)/PI_1 - q_{iw}(t)/PI_2], \quad (29)$$

Δt is the time increment.

Productivity (injectivity) and inter-flow factors can be defined as follows:

$$PI_i = \frac{2\pi k_i h_i}{\mu} \cdot \frac{1}{\ln\left(\frac{R_{c,i}}{r_{w,i}} + S_i\right)}, \quad i = 1, 2 \quad (30)$$

$$PI_{21} = \frac{k_{21}}{\mu} \cdot \frac{A_{21} h_{21}}{r_{21}}, \quad (31)$$

where k_1 and k_2 are the reservoir permeability at the production and injection wells, respectively; h_1 and h_2 are the reservoir thicknesses at the production and injection wells, respectively; μ is the fluid dynamic viscosity; $R_{c,1}$ and $R_{c,2}$ are the external reservoir boundary radii; $r_{w,1}$ and $r_{w,2}$ are the bore well diameters; S_1 and S_2 are the well skin factors; k_{21} is the reservoir permeability in the inter-well area; h_{21} is the reservoir thickness in the inter-well area; r_{21} is the production-to-injection well distance; A_{21} is the length of the wells porous volume interface where the fluid inter-flows occur.

Provided that other variables are known, equations (30) and (31) give the k_1 , k_2 reservoir permeability at the well location and the k_{21} reservoir permeability in the inter-well area.

To account for the stationary inflow as the well operation mode changes, we can introduce correction factors to the productivity and interference factors similar to (9).

The external reservoir boundary radius can be determined with Pisman equation [6]. In this particular case it can be reduced to:

$$R_{c,i} = 0,12\sqrt{2F_i}, \quad i = 1, 2, \quad (32)$$

$$F_i = \frac{V_{p,i}}{m_i h_i}, \quad i = 1, 2, \quad (33)$$

where F_1 and F_2 are draining (injection) areas; m_1 and m_2 are the porosities.

The shape of the total drainage (injection) area of the two wells can be represented as an ellipse with the wells located at its focal points. Then, the ellipse geometry equations can be used to estimate the length of the interface between the well pore volumes through which the fluid flows:

$$A = 2b, \quad (34)$$

$$b = \sqrt{a^2 - r_{21}^2/4}, \quad (35)$$

$$a = \sqrt{\frac{\pi^2 r_{12}^2/4 + \sqrt{\pi^4 r_{12}^4/16 + 4\pi^2 F^2}}{2\pi^2}}, \quad (36)$$

where a and b are the major and minor ellipse semi-axes.

If the production well downhole pressure, fluid flow rate and water injection volume values are available, we can estimate the reservoir parameters by adapting the downhole pressure model (27) and (28). For this, the following optimization problem is to be solved:

$$F(X) = \sum_t \left\{ \left[P_{w,1}^c(t) - P_{w,1}^f(t) \right]^2 + \left[P_{w,2}^c(t) - P_{w,2}^f(t) \right]^2 \right\} \rightarrow 0, \quad (37)$$

where F is the function to be minimized; X is a vector of variables; the c and f superscripts indicate the estimated and actual values, respectively. We add the values for each moment t when the actual downhole pressure value is available. The injection well downhole pressure can easily be estimated from the wellhead pressure using Bernoulli's equation.

The optimization problem variables are:

- 1) $V_{p,1}$ and $V_{p,2}$ porous volumes
- 2) PI_1 and PI_2 productivity and injectivity factors
- 3) PI_{21} : fluid inter-flow factor

- 4) b_1 and b_2 factors account for the stationary inflow as the well operation modes change
- 5) t_1 and t_2 : relaxation periods

If PI_1 , PI_2 and PI_{21} are known, we can estimate k_1 , k_2 and k_{21} provided that other variables are also available.

The above model can be easily generalized for a larger number of wells.

Optimization Problem Solution

In this paper, we use Newton's method to solve optimization problems. Let us consider its principles.

Suppose we need to find the minimum of the $f(X)$ multi-argument function, where $X=(x_1, x_2, x_3, \dots, x_n)$. This problem is equivalent to the problem of finding the X values at which the gradient of the function $f(X)$ is zero:

$$\text{grad}(f(X)) = 0. \quad (38)$$

Let us apply Newton's method to (38):

$$\text{grad}(f(X^j)) + H(X^j)(X^{j+1} - X^j) = 0, \quad (39)$$

where $j=1,2,3,\dots, m$ is the iteration number, $H(X)$ is a hessian of the function $f(X)$.

Note that the Hessian of a function is a symmetrical quadratic form that describes the behavior of the function in the second order:

$$H(X) = \sum_{i=1}^n \sum_{j=1}^n a_{ij} x_i x_j, \quad (40)$$

where $a_{ij} = \partial^2 f / \partial x_i \partial x_j$, $f(X)$ is defined over an n -dimensional space of real numbers.

For convenience, equation (40) can be represented as:

$$X^{j+1} = X^j - H^{-1}(X^j) \text{grad}(f(X^j)). \quad (41)$$

Models Testing with Simulated Examples

Problem No. 1

Consider a two-well (production and injection) interference problem in a homogeneous infinite reservoir as the well operation is variable. In general, Laplace images are used to obtain the exact solution to such a problem. We used the Saphir software from Kappa Engineering to plot the production well downhole pressure vs. time curve. The flow is single-phase. The initial data are as follows:

- 1) well radius: 0.1 m
- 2) reservoir thickness: 9.1 m
- 3) reservoir porosity factor: 0.1 dec.qty
- 4) well-to-well distance: 300 m
- 5) volume factor: 1 m³/m³
- 6) dynamic fluid viscosity: 1 cps
- 7) total compressibility of the reservoir-fluid system: 4.267·10⁻⁵ 1/bar
- 8) dimensionless well skin factor: 0
- 9) initial reservoir pressure: 350 bar
- 10) reservoir permeability: 50 mD.

Refer to Fig. 1 for the variable fluid flow rate and injected water flow rate.

We interpreted the flow rate and downhole pressure measurements using the single-volume CRM model presented in Section 1. The downhole pressure curves are shown in Fig. 1. A satisfactory matching of the downhole pressure curves was obtained. The results are as follows:

- 1) reservoir porous volume: 6.0·10¹⁰ m³
- 2) production well productivity factor: 2.0 m³/day/bar
- 3) production-to-injection well interference factor: 6.2 m³/day/bar
- 4) reservoir permeability at the production well: 78.6 mD
- 5) reservoir permeability in the inter-well area: 59.6 mD.

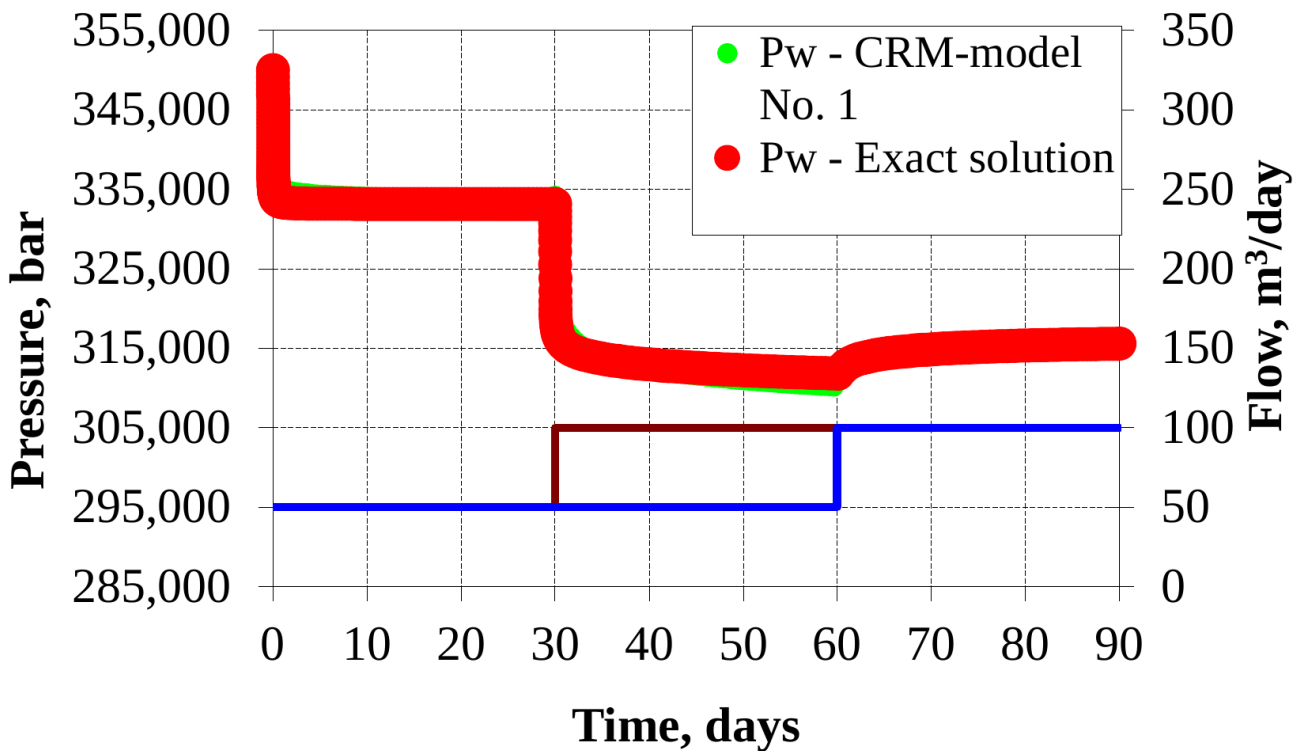


Figure 1. Well performance for a homogeneous infinite reservoir. CRM model No. 1

The resulted permeability values are in satisfactory agreement with the initial data.

Problem No. 2

Consider a two-well (production and injection) interference problem in a heterogeneous (in terms of permeability) limited square-shaped reservoir. The wells operate in a variable mode. There is no exact solution to such a problem. We used a simulation model developed with the Saphir software from Kappa Engineering to plot the production well downhole pressure vs. time curve (refer to Fig. 2.) The flow is single-phase. The piezoconductivity problem is solved. The Voronoi grid is used. The initial data are as follows:

- 1) XY plane area size: 848x848 m
- 2) permeability at the production well: 50 mD
- 3) permeability at the injection well: 100 mD.

We used linear interpolation of the inter-well area permeability. The rest of the data are similar to those used in Problem No. 1.

The fluid flow rate and the injected water flow rate are variable, refer to Fig. 3.

We used two approaches to interpret the flow rate and downhole pressure measurements.

The first one is using the single-volume CRM model described in section 1. The downhole pressure curves are shown in Fig. 3. Good matching of the downhole pressure curves was obtained. The results are as follows:

- 1) reservoir porous volume: $6.3 \cdot 10^5 \text{ m}^3$
- 2) production well productivity factor: $3.6 \text{ m}^3/\text{day}/\text{bar}$
- 3) production-to-injection well interference factor: $40.2 \text{ m}^3/\text{day}/\text{bar}$
- 4) reservoir permeability at the production well: 50.4 mD
- 5) formation permeability in the inter-well area - 105.7 mD.

The resulted permeability values are in satisfactory agreement with the initial data. The reservoir permeability at the production agrees well with the target value. The reservoir permeability in the inter-well area poorly agrees with the “actual” value that can be estimated from the initial permeability at the wells using the average harmonic equation as 66.7 mD. This is probably due to imprecise external reservoir boundary radius estimation as the drained volume is elliptical.

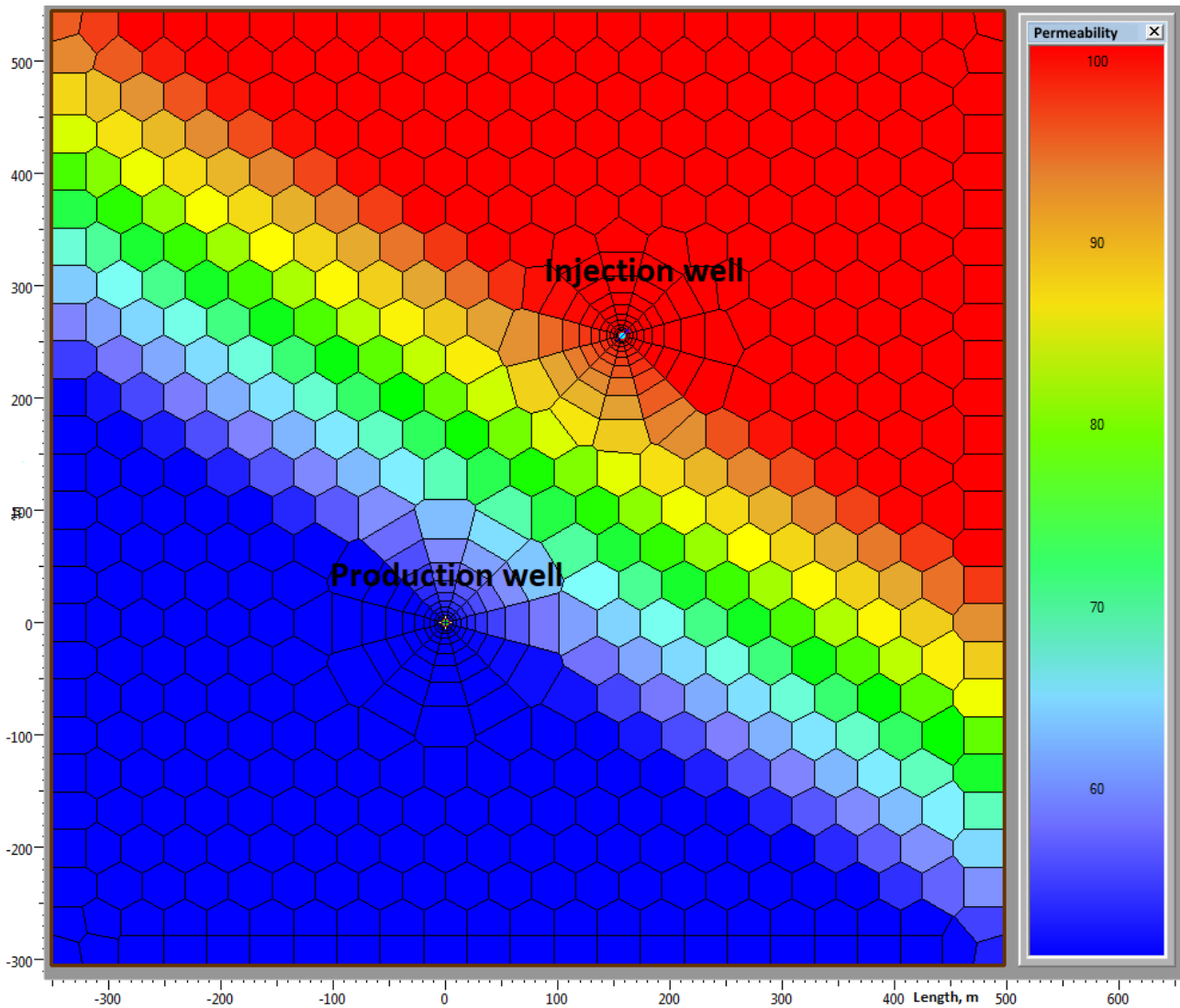


Figure 2. Permeability distribution over the grid (Saphir software)

The second approach is using the multivolume CRM model described in Section 2. The downhole pressure curves are shown in Fig. 4. Good matching of the downhole pressure curves was obtained.

The results are as follows:

- 1) reservoir porous volume at the production well: $3.19 \cdot 10^5 \text{ m}^3$
- 2) reservoir porous volume at the injection well: $3.21 \cdot 10^5 \text{ m}^3$
- 3) production well productivity factor: $3.7 \text{ m}^3/\text{day}/\text{bar}$
- 4) injection well injectivity factor: $7.15 \text{ m}^3/\text{day}/\text{bar}$
- 5) inter-flow factor: $12.5 \text{ m}^3/\text{day}/\text{bar}$
- 6) reservoir permeability at the production well: 50.1 mD
- 7) reservoir permeability at the injection well: 96.2 mD
- 8) reservoir permeability in the inter-well area: 52.9 mD.

In general, the resulted permeability values are in good agreement with the initial data. The reservoir permeability at the production and injection wells agrees well with the target values. The reservoir permeability in the inter-well area satisfactory agrees with the “actual” value that can be estimated from the initial permeability at the wells using the average harmonic equation as 66.7 mD.

Conclusion

This paper proposes two CRM models of production-injection well interference used to estimate the reservoir filtration and volumetric properties based on the production data. The production data, in this case, are fluid flow rate, injected water flow rate, and bottom hole pressure. CRM models are a combination of

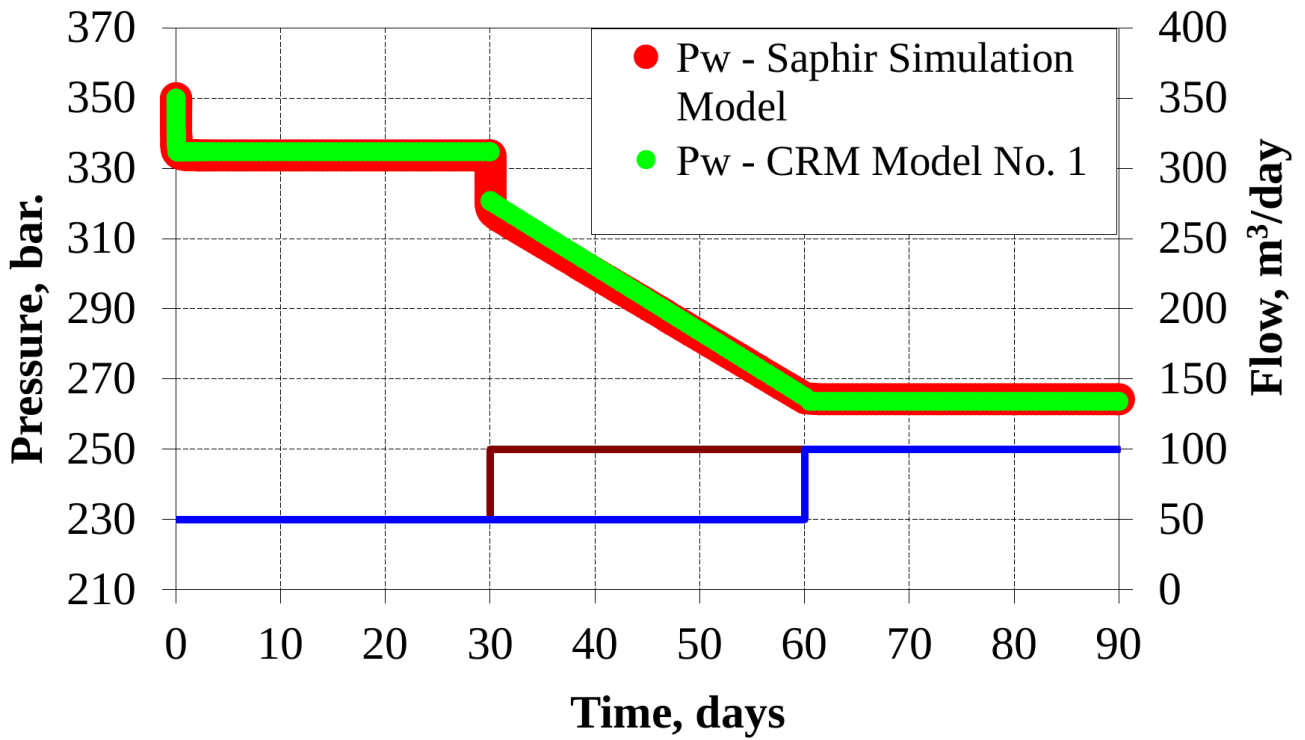


Figure 3. Well performance in a heterogeneous (in terms of permeability) square-shaped limited reservoir. CRM model No. 1

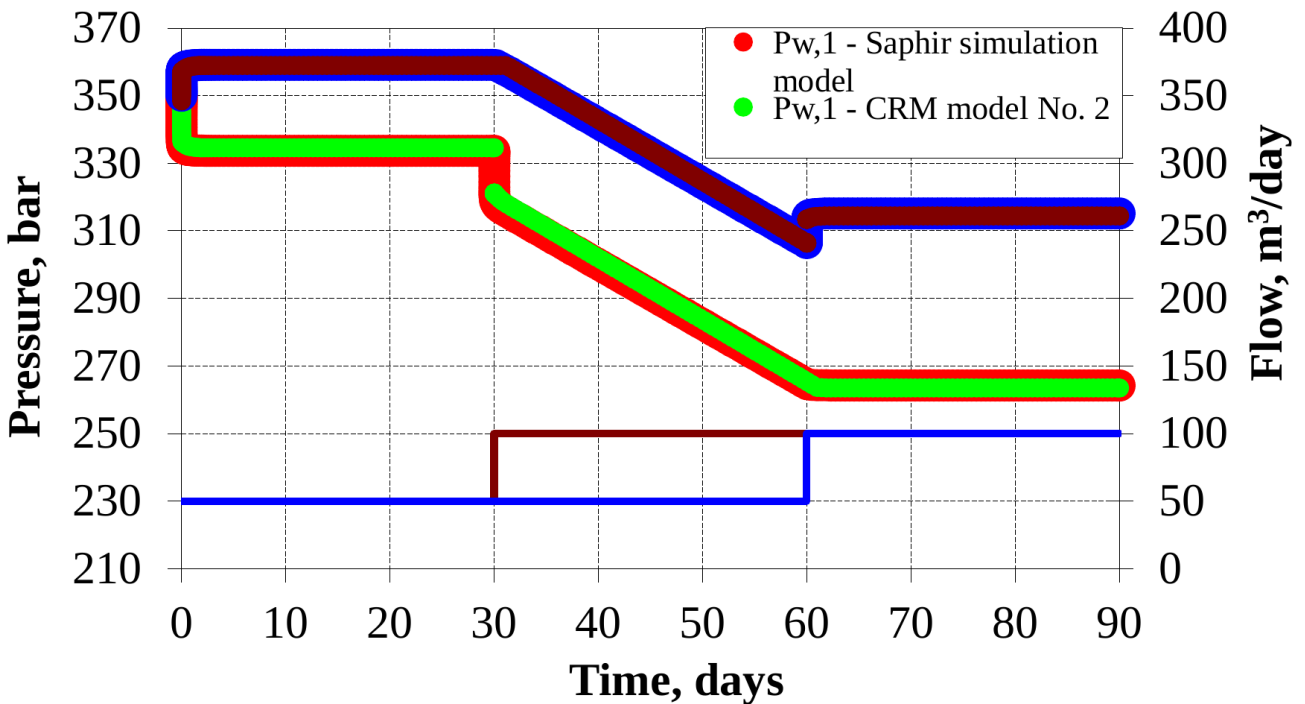


Figure 4. Well performance in a heterogeneous (in terms of permeability) square-shaped limited reservoir. CRM model No. 2

the material balance equation (the formation fluid flow continuity equation) and the well inflow equation. The advantage of all CRM models is that the reservoir pressure value is not required as it changes during the extraction, and its field measurements are rare and often irregular.

The first proposed model is single-volume because only one, common pore volume served by both wells is considered.

The second proposed model is multivolume since the number of pore volumes considered is equal

to the number of wells. Each well operates in its dedicated pore volume. There are inter-flows between the porous volumes of the wells.

The models were applied to a two-well case: a production well and an injection well. However, the models can be easily generalized for a larger number of wells.

This paper proposes to solve inverse subsoil hydrodynamics problems with CRM models by combining estimated and actual downhole pressure values. The filtration and capacitive reservoir properties, including its permeability in various regions, are evaluated in this way. The inverse problem is solved by Newton's method.

The models were tested with simulated examples generated by Kappa Engineering's Saphir software. It is shown that for an infinite reservoir (in real life, a very large porous volume value at which no reservoir pressure drop occurs), the simpler first CRM model can be applied, while for a limited reservoir, the second CRM model provides better results. In general, with the right choice of the proposed CRM models, it is possible to determine the filtration and capacitive parameters with accuracy sufficient for practical purposes.

REFERENCES

1. Danko M. Yu., Brilliant L. S., Zavyalov A. S. Application of Dynamic Material Balance Method and CRM Method (Capacitance-Resistive Models) for Reserves Assessment in Achimov and Bazhenov Reservoirs. *Nedropolzovanie XXI Vek*. 2019;4:76-85. (In Russ.)
2. Ruchkin A. A., Stepanov S. V., Knyazev A. V., Stepanov A. V., Korytov A. V., Avsyanko I. N. Applying CRM Model to Study Well Interference. *Tyumen State University Herald. Physical and Mathematical Modeling. Oil, Gas, Energy*. 2018;4(4):148-168. DOI: 10.21684/2411-7978-2018-4-4-148-168. (In Russ.)
3. Khatmullin I. F., Tsanda A. P., Andrianova A. M., Budenny S. A., Margarit A. S., Lushpeev V. A., Simonov M. V., Perets D. S. Semi-Analytical Models for Calculating Well Interference: Limitations and Applications. *Neftyanoe khozyaystvo – Oil Industry*. 2018;12:38-41. DOI: 10.24887/0028-2448-2018-12-38-41. (In Russ.)
4. Basniev K. S., Kochina I. N., Maksimov V. M. *Underground Hydromechanics*. M.: Nedra; 1993. 416 p. (In Russ.)
5. Volpin S. G., Svalov A. V., Shteynberg Yu. M., Volpin A. S. Monitoring of Producing Well Deliverability. *Neftyanoe khozyaystvo – Oil Industry*. 2005;6:116-119. (In Russ.)
6. Kanevskaya R. D. *Simulation of Hydrodynamic Processes for Hydrocarbon Field Development*. M.–Izhevsk: Institute for Computer Studies; 2002. 140 p. (In Russ.)
7. Borisov Yu. P., Pilatovsky V.P., Tabakov V. P. *Oil Fields Development with Horizontal and Multibranch Wells*. M.: Nedra; 1964. 155 p. (In Russ.)

DOI: 10.51790/2712-9942-2020-1-1-4

AUTOMATA-BASED MODEL OF DNA REPLICATION**Georgiy E. Deev, Sergey V. Ermakov***Obninsk Nuclear Energy Institute, National Research Nuclear University MEPhI,
Obninsk, Russian Federation, georgdeo@mail.ru, ermakov@iate.obninsk.ru*

Abstract: it is shown that DNA replication can be simulated as computation by the simplest abstract single-state automata: the permutation automata.

Keywords: abstract automaton, B-scheme, DNA (deoxyribonucleic acid), replication, complementarity.

Acknowledgements: this study is supported by RFBR, project No. 20-07-00862.

Cite this article: Deev G. E., Ermakov S. V. Automata-Based Model of DNA Replication. *Russian Journal of Cybernetics*. 2020;1(1):26–30. DOI: 10.51790/2712-9942-2020-1-1-4.

АВТОМАТНАЯ МОДЕЛЬ РЕПЛИКАЦИИ МОЛЕКУЛЫ ДНК**Г. Е. Деев, С. В. Ермаков***Обнинский институт атомной энергетики, Национальный исследовательский ядерный университет «МИФИ», г. Обнинск, Российская Федерация, georgdeo@mail.ru, ermakov@iate.obninsk.ru*

Аннотация: показано, что репликация молекулы ДНК может быть промоделирована как вычисление, проводимое простейшими абстрактными автоматами с одним состоянием — перестановочными автоматами.

Ключевые слова: абстрактный автомат, В-схема, ДНК — дезоксирибонуклеиновая кислота, репликация, комплементарность.

Благодарности: работа выполнена за счет гранта РФФИ (проект № 20-07-00862).

Для цитирования: Деев Г. Е., Ермаков С. В. Автоматная модель репликации молекулы ДНК. *Успехи кибернетики*. 2020;1(1):26–30. DOI: 10.51790/2712-9942-2020-1-1-4.

Abstract Automata

The definition of the automaton is comprehensive. An automaton is a compound object that includes the following components:

1. The set $Z_k = \{0, 1, \dots, k-1\}$ is the input alphabet of the automaton. It consists of k digits of the base- k number system. The last digit “ $k-1$ ” should be considered as a single character, although it seems to consist of three separate characters: “ k ”, “-”, “1”. This is because we do not know how users of the k -base number system may agree on the symbol for the last digit.

2. The set $Z_l = \{0, 1, \dots, l-1\}$ is the output alphabet of the automaton. It consists of l digits of the l -base number system. The same observation as for the digit “ $k-1$ ” is true for the digit “ $l-1$ ”

The input and output alphabets of the automaton can be different.

3. The set $Q = \{q_1, q_2, \dots, q_n\}$ — is the set of the automaton states. The states can be denoted by any symbols. The states designations (and their hardware implementation) do not affect the automaton operation.

4. The transition function $q' = \theta(q, x)$ defines the movement of an automaton from one state q to another q' for a specific input symbol x .

5. The output function $y = \sigma(q, x)$ returns the output signal of the automaton in the state q for the input signal x .

Everywhere above ($q', q \in Q$, $x \in Z_k$, $y \in Z_l$).

For brevity, to specify the components of automaton A , we write:

$$A = A(Z_k, Z_l, Q, \theta(q, x), \sigma(q, x)).$$

Usually, automata with finite sets Z_k , Z_l , Q are considered. Such automata are called *finite automata*.

Just listing the automaton components is not sufficient to define an automaton. The automation operation is to be defined.

The automaton operates in discrete time. We will mark time moments with integers without limiting generality. At an integer point in time, the automaton “comes to life” for a moment, operates and then “freezes” until the next integer point in time comes. In this case, it is governed by the *operating equations* of the following type:

$$A: \begin{cases} q(t + 1) = \theta(q(t), x(t)), \\ y(t) = \sigma(q(t), x(t)). \end{cases} \quad (t \in Z = \{\dots - 2, - 1, 0, + 1, + 2, \dots\}). \quad (1)$$

Other types of the operating equation are also possible.

When an automaton is set to one or another state as the initial state, it will represent a certain mapping.

The effect of the automaton A being in its initial state q , on the object \bar{x} is expressed as $\bar{y} = A\bar{x}|q$.

If all states of an automaton are non-equivalent, then the automaton can represent as many different mappings as many states it has. The range of available representations governs the capabilities of the automation.

Single-State Permutation Automata

We only need single-state permutation automata. A permutation automaton is an automaton with its output function performing a permutation of the output alphabet characters. The number of single-state permutation automata for the quaternary number system Z_4 is $4! = 24$.

Single-state permutation automata are defined by type 1 tables.

Table 1

$x \backslash q$	0
0	$0, y_0$
1	$0, y_1$
2	$0, y_2$
3	$0, y_3$

In Table 1 $y_i \in Z_4$ are different. Among such automata, there is an automaton defined by Table 2.

Table 2

$x \backslash q$	0
0	$0, 0$
1	$0, 1$
2	$0, 2$
3	$0, 3$

This automaton implements an identity mapping (identity computation)

$$x_r \dots x_2 x_1 x_0 \rightarrow x_r \dots x_2 x_1 x_0,$$

i.e. any number $x_r \dots x_2 x_1 x_0$ translates into itself. In terms of substitutions, it implements an identical substitution

$$\begin{pmatrix} 3 & 2 & 1 & 0 \\ 3 & 2 & 1 & 0 \end{pmatrix}.$$

An arbitrary automaton defined by Table 1, implements an arbitrary substitution

$$\begin{pmatrix} 3 & 2 & 1 & 0 \\ y_3 & y_2 & y_1 & y_0 \end{pmatrix}.$$

It is known how content-rich the algebraic theory of substitution is. As we see, all the facts from the permutation theory can be represented in terms of single-state permutation automata.

Biological Interpretation of the Permutation Automata Operation

In genetics, single-state permutation automata are extensively represented.

The genetics information we used is borrowed from [1].

According to the Watson-Crick model, the DNA molecule as a carrier of hereditary information is two stranded helical nucleotide sequences (double helix) of four types: adenine (A), guanine (G), thymine (T), and cytosine (C). The nucleotides sequence along the molecule is arbitrary [1, p. 22]. The number of nucleotides along the helix is high. The arbitrariness of the nucleotides sequence and their number in the molecule implies a huge number of hereditary information combinations [6, p. 237]. Although the sequence of nucleotides along one helix is arbitrary, the sequence of nucleotides in the parallel helix associated with it cannot be arbitrary and is determined by the distribution of nucleotides in the first helix. This dependent arrangement of nucleotides along the parallel helix is determined by the *complementarity law*: there must be a one-to-one match between nucleotides:

$$A \leftrightarrow T, \qquad G \leftrightarrow C. \qquad (2)$$

In the DNA environment, the DNA helices may diverge. Then the lost nucleotides are built on each of them according to the principle of complementarity. As a result, the separated spirals are reconstructed identical to the one that split, and instead of one DNA molecule, we get two identical DNA molecules (not different from the original DNA molecule either.) This process of doubling the DNA molecule is called *replication*, and it (and similar ones that differ in detail, but not in principle) is the foundation of the organism growth.

This is illustrated in Figs. 1 and 2. The captions are taken from [1].

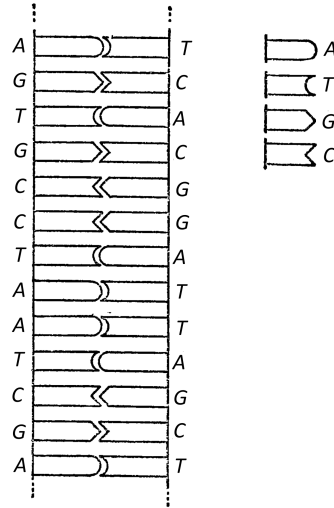


Figure 1. The DNA molecule looks like a rope ladder consisting of two types of steps: A-T and G-C nucleotide pairs

The described process of DNA molecule replication can be simulated with the considered single-state permutation automata.

Indeed, both in replication and in other processes that can be interpreted as information retrieval, a certain object moves along the molecule. The object perceives the input information, reacts to it, and produces its output information used to build a molecule.

If we translate this into B-schemes, it can be presented as the diagram in Fig. 3.

The law of complementarity is represented by the links within the rectangle. The dots on the left represent a possible nucleotide sequence. The sequence of dots on the left if read from top to bottom, means that this DNA section has a guanine nucleotide (1) at the top, a thymine nucleotide (2) at the bottom, an

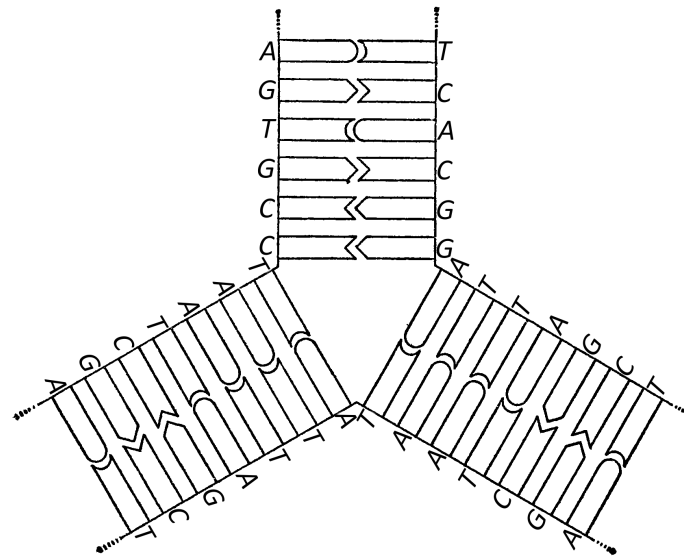


Figure 2. According to Watson and Crick, the DNA is replicated. As a result, two identical molecules emerge from the original molecule shown in Fig. 1

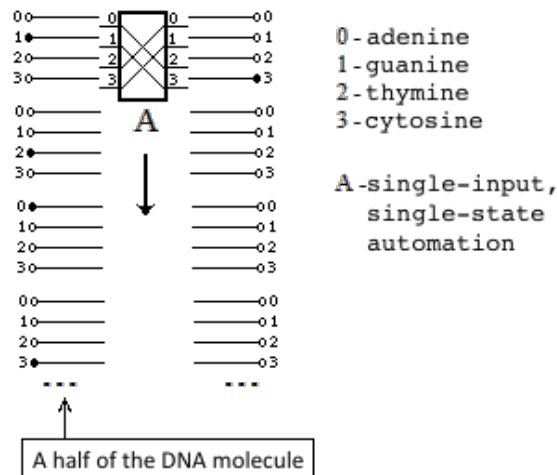


Figure 3. Automated model of the DNA replication process

adenine nucleotide (0) further down, and then a cytosine nucleotide (3). On the right almost all points are empty. It means that there is no complementary construction yet.

Automaton *A*, moving along the left half of the DNA molecule, with its left input perceives the input information and uses it to produce an output signal that is complementary to the input. Fig. 3 shows the situation when the automaton already completed the generation of one complementary output, i.e., one complementary nucleotide. Specifically, passing the upper left nucleotide, it perceived the input information through its left input at line 1, “recognized” the guanine nucleotide number 1, and, according to the connections within the automaton (see Fig. 3 and Fig. 4), developed a reaction as the signal 3/. In terms of genetics it means the addition of cytosine nucleotide, complementary to guanine nucleotide, to the DNA molecule. A single-input automaton for complementary overlapping can be represented as an ordinary single-input automaton with a typical *B*-scheme containing four & elements. This is the *A*₁₀ automation (Fig. 4) (The *A*₁₀ automaton is borrowed from the general theory of permutation automata given in [4].)

The field structure of the molecules on the left (Fig. 4), interacting with the field structure of the “rectangle” molecules, creates a new field structure. By the principle of variation, it attracts only one of the four possible nucleotides: the one complementary to the left nucleotide. After attraction, a new field structure is created. It pushes out the molecular formation represented by the rectangle and forces

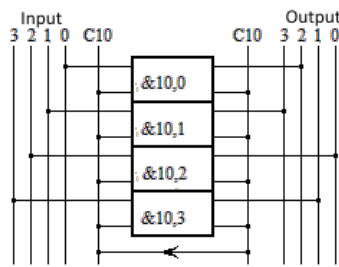


Figure 4. A_{10} automaton for complimentary overlapping

it to move further along the DNA molecule. After pushing out, the complementary nucleotides are glued together, and the “rectangle” moves on to the next position. There it performs a subsequent interaction with the nucleotide on the left and the process repeats. It should be noted that the field structure of the “left nucleotide-rectangle-right nucleotide” formation is such that the rectangle is always pushed out to one side and grabbed by the next left nucleotide in the molecule. This ensures the directional movement of the rectangle along the molecule. In principle, all these field structures can be estimated. The pushing out effect (always in one direction) can also be found by calculation. It is possible to calculate the process duration and estimate the performance of such a biological computer. As we can see, the simplest, single-state biological automaton does exist. It governs all our life with its incredible complexity. It should be noted that at this elementary abstract level the laws of mathematics allow for various variations such as not 4- but 6-nucleotide formations. However, they are not found on Earth. The question arises: for what reason? Are the principles of variation really to blame?

Be that as it may, biological processes of cybernetic nature can be *directly* simulated by B-computers, as shown above, without any software support, unlike existing computers requiring special software for such simulation.

Conclusion

It is shown that life processes at the DNA molecule level can be modeled by abstract automata represented by B-schemes. The four-letter B-schemes best suit the variational principle of optimization existing in nature.

REFERENCES

1. Frank-Kamenetskii M. *The Live Cell Queen*. M.: AST-PRESS; 2010. 272 p. (In Russ.)
2. Shrodinger Eh. *What Is Life?* AST; 2018. 288 p. (In Russ.)
3. Deev G. E. *Abstract Computers*. M.: Ehnergoatomizdat; 2007. 332 p. (In Russ.)
4. Deev G. E. *The Theory of Computers*. P. 1. Lecture notes. Obninsk; 2009. (In Russ.)
5. De Robertis E. D. P., Nowinski W. W., Saez F. A. *Cell Biology*. 1970.
6. Watson J. *Molecular Biology of the Gene*. M.: Mir; 1978. 720 p. (In Russ.)
7. Kolmogorov A. N. *Automata and Life. Matematika – nauka i professiya*. M.: Nauka; 1988. Pp. 43–62. (In Russ.)

DOI: 10.51790/2712-9942-2020-1-1-5

ORGANIC GROWTH STRATEGY AS THE FOUNDATION FOR AN AGILE INFORMATION SYSTEM

Rinat D. Gimranov, Elena V. Gaydukova

PJSC “Surgutneftegas”, Surgut, Russian Federation, gimranov_rd@surgutneftegas.ru

Abstract: the paper proposes an executive approach to the digitalization of business processes by bimodal separation into a business level and an IT level. These levels are served by separate teams to enable the business analysts and the process owners to develop business applications with a low-code platform in real-time to support an organic growth strategy. The IT level is involved only to develop the platform by conventional methods.

Keywords: high availability management systems, low-code digital platforms, Comindware business application platform, ontology platforms, organic growth strategy, digitalization of business processes.

Cite this article: Gimranov R. D., Gaydukova E. V. Organic Growth Strategy as the Foundation for an Agile Information System. *Russian Journal of Cybernetics*. 2020;1(1):31–37. DOI: 10.51790/2712-9942-2020-1-1-5.

СТРАТЕГИЯ ОРГАНИЧЕСКОГО РАЗВИТИЯ КАК ФУНДАМЕНТ ГИБКОЙ ИС

Р. Д. Гимранов, Е. В. Гайдукова

ПАО «Сургутнефтегаз», г. Сургут, Российская Федерация, gimranov_rd@surgutneftegas.ru

Аннотация: в статье предлагается организационный подход к цифровизации бизнес-процессов би-модальным разделением на уровень бизнеса и на уровень ИТ, которые не объединяются в единые команды, а, напротив, разделяются с целью дать возможность бизнес-аналитикам и владельцам процессов развивать бизнес-приложения с помощью лоукод платформы в режиме реального времени и в стратегии органического роста. Уровень ИТ подключается только для развития платформы путём классических подходов.

Ключевые слова: системы управления высокой степени готовности, лоукод цифровые платформы, Comindware business application platform, онтологические платформы, стратегия органического роста, цифровизация бизнес-процессов.

Для цитирования: Гимранов Р. Д., Гайдукова Е. В. Стратегия органического развития как фундамент гибкой ИС. *Успехи кибернетики*. 2020;1(1):31–37. DOI: 10.51790/2712-9942-2020-1-1-5.

Introduction

The complexity of existing corporate information systems (InfSys) requires to reconsider their development strategy and the conventional approach to IT management [1].

A hierarchical structure is at the heart of each approach to IT management (e.g., ITSM, IT4IT or Prince2.) It defines all the IT deployment project management models, their agility, and prioritization.

This paper presents an original approach to InfSys development by implementing a 2-tier IT management model. Its concept was proposed by the Gartner analytical agency in 2014 [11] and matured to a ready-to-use level based on the IT management experience in a large oil company.

Conventional Approach to InfSys Development Management

Large corporate information systems over the past decades of intensive development reached a high level of complexity. It leads to a range of problems that require special solutions [2]. Started as a set of simple computational programs, information systems evolved into a complex multi-component system. As part of such a system, every medium or large company runs many servers and other hardware components, a large number of databases and DB management systems, numerous applications integrated with end-to-end business processes, business process monitoring, analysis, and management tools [3].

Conventionally, the cascade approach is used to manage complex InfSys development. The development process is a flow consistently passing through such phases as requirements analysis and approval, design, coding, testing, integration, and support.

The established InfSys project management practices may seem to enable the control of budgets, deadlines, resources, to assure predictable project results. At the same time, these practices have several drawbacks [4]:

- It is impossible to verify if the solution meets the business goal before a pilot operation
- Specification freeze for the duration of the project
- high efforts when making adjustments to the already approved specification
- The solution shall be detail designed as early as at the planning stage
- The high level of detail leads to huge documentation volumes and high upgrade efforts.

Such an inflexible approach to InfSys project management often slows down the attempts to keep up with emerging technologies and results in more business problems. The key problems are:

- low InfSys adaptability to external changes: as the corporate business environment changes continuously, the actual requirements for information processing often go beyond the InfSys functionality [5]
- internal InfSys rigidity: not all emerging needs of the InfSys users can be satisfied within the conventional architecture [6], which often covers individual corporate functions, while the processes are supported through e-mail, Excel files, paper stickers, regulations, and document flows (paper or electronic.) In this situation, it is not always possible to retrieve the information the user needs, even if it is available in the system. In can happen, for example, for non-trivial composite queries [7]
- poor software usability: the developers do not always pay proper attention to ergonomics and UX; the user interface is often overloaded with graphics. Therefore, each time it takes a lot of time for the user to learn the software and get used to it. This factor reduces productivity leading to irritation and fatigue
- high labor intensity and low development rate: requirements management practices and a multi-step approval process enable to control budgets, deadlines, and resources, but widen the gap between business and technology, and significantly slow down the development process. The deceleration varies directly with the number of affected systems [8].

The problems listed above are more evident in the digitalization environment. Gartner gives this definition: “Digitalization is the use of digital technologies to change a business model and provide new revenue and value-producing opportunities; it is the process of moving to a digital business” [9].

Today, a large company urgently needs a new approach to InfSys development to solve its pressing business problems and support its digital transformation and operations in a fluid economic reality [10]. Below we propose an original approach to managing InfSys development with a 2-tier IT management model. The concept was proposed by Gartner [11] and matured to a ready-to-use level based on the IT management experience in a large oil company.

InfSys Organic Growth Strategy

InfSys Organic Growth Strategy Concept Compared to the Conventional Step-by-Step Growth

What is the conventional approach to creating corporate management InfSys? A description or model of business processes is compiled, appropriate software components are selected (often together with consultants and integrators.) The components are delivered to a private data center or made available on the “cloud” with a set of pre-configured “best practices”. They are subsequently adapted to the needs of a particular company and supplemented with program code to implement the features not initially available [12].

The step-by-step process of developing such a system includes programming, purchasing new modules and systems supporting new “best practices” and implementation of applications managed with a cascade model. Creating new IT solutions and making changes, even the smallest ones, to existing solutions is done by programmers assisted by IT experts. The IT expert converts a request into a product specification, the programmer converts the request into a language that the system understands. After “translating” the request from the business language to the IT language it often turns out that the final solution only approximately meets the original request [13].

To fix the low InfSys adaptability, intrinsic rigidity, and improve UX there shall be a direct interaction between the InfSys and the business people The InfSys should “understand” humans in any intuitive interaction format, for example, through customized process flowcharts [14].

In any case, there is some intermediary (non-human) between the human-understandable representation and the machine code. On the one hand, it operates with concepts (entities, properties and relations),

while on the other hand, with machine language commands. Ontology can serve as a universal interface language¹. An ontology engine can be used as an intermediary. In the current context, we can skip the implementation details of such a digital intermediary and focus on the fact that the modern approach to InfSys development requires a direct interaction between InfSys and business people.

If the InfSys “understands” a business person, then to create an applied IT solution we need only the first step of the conventional approach: representing the solution in terms understandable to both the InfSys and the business people (an ontological model). The description added to the InfSys immediately reveals the required IT solution. It is a foundation for further organic growth when InfSys is developed together with the corporate processes.

For example, when designing a simple maintenance request management process, the business user initially generated a simple process and commissioned it (Fig. 1). During the implementation, the process became more complicated through successive iterations and now it looks much more complex (Fig. 2).

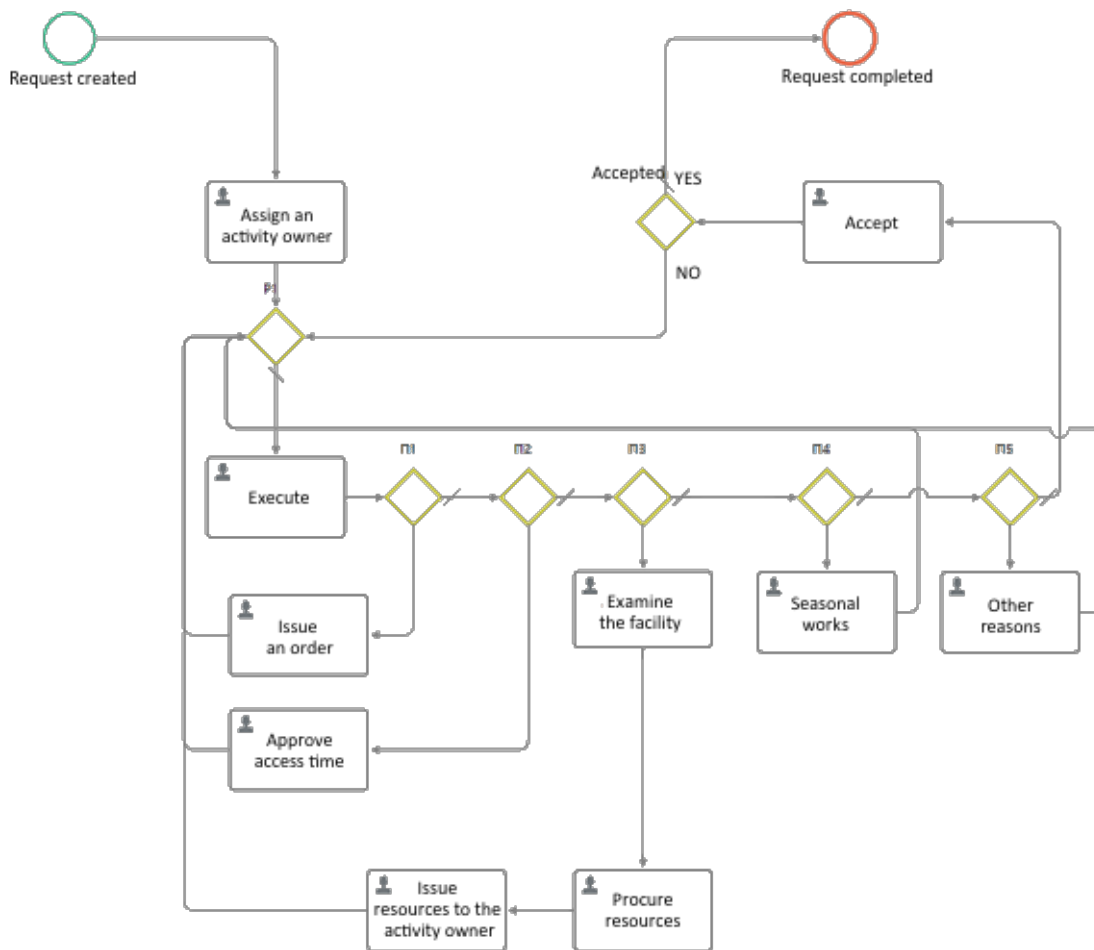


Figure 1. A simple process, initially generated by the business user

Further optimization, reengineering will be required: not of the programs and applications, but the ontological models and solutions based on them. You still can not do without coding, but the efforts sharing between business analysts and programmers will be changed, and the IT management model will be transformed to meet the corporate approach to implementing an organic IT growth strategy.

Two-tier IT as an Approach to Implementing an Organic InfSys Development Strategy

Two-tier IT is a management model used to create both sustainable and predictable IT systems and

¹ Ontology is a formal specification of a shared conceptual model, where “conceptual model” means an abstract model of a subject area describing its system of concepts, “shareable” means an agreed understanding of the conceptual model by a certain community (group of people), “specification” means an explicit description of the system of concepts, “formal” means that the conceptual model is defined in a formal language [16].

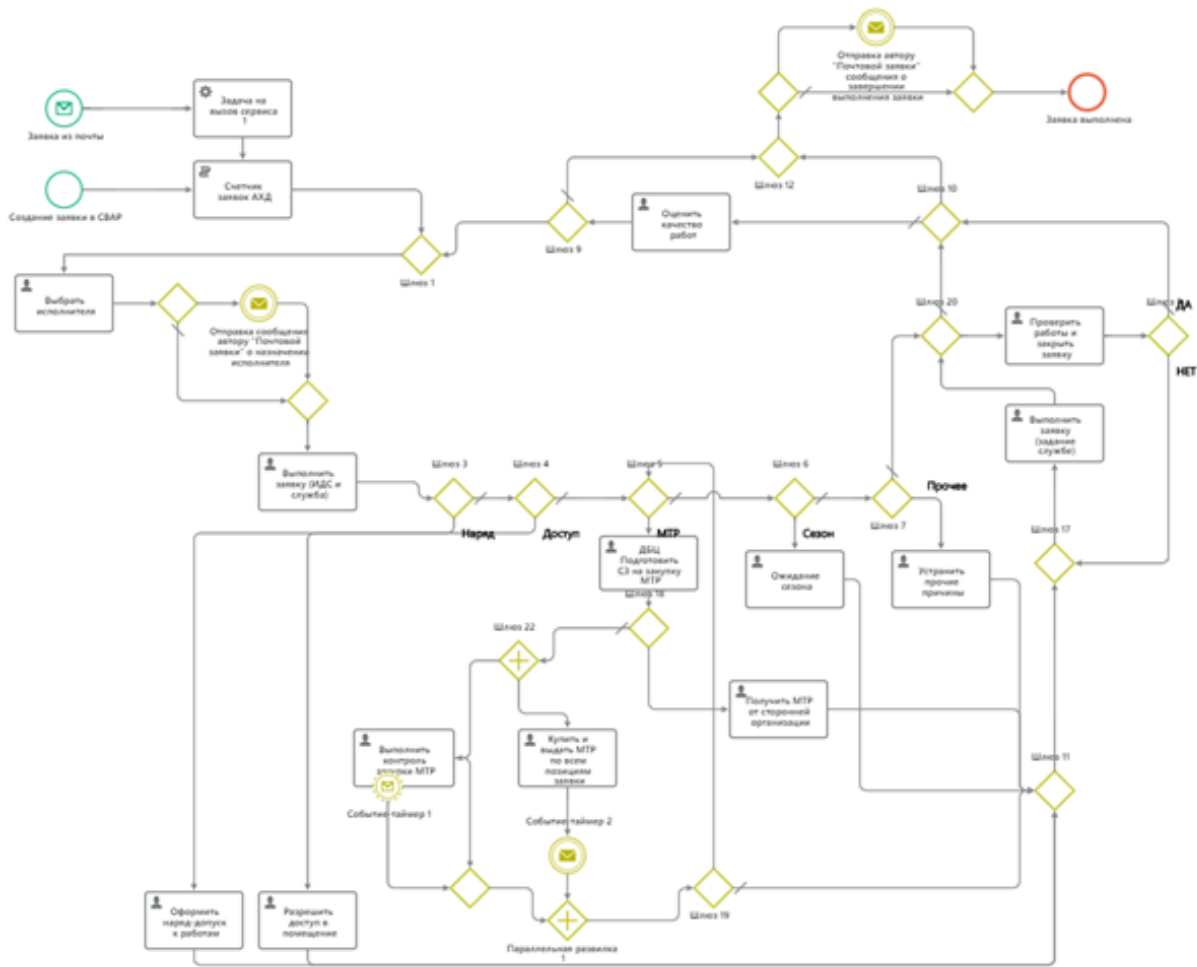


Figure 2. During the implementation, the process became more complicated

point IT solutions to quickly solve urgent business problems. Gartner defines the two tiers of IT management as follows: “Tier 1 is conventional and consistent, ensuring safety and accuracy. Tier 2 is research and non-linear, providing agility and speed” [9]. This combination of consistency and non-linearity supports basic business processes and encourages continuous optimization of all corporate business processes.

This IT management model is already used by Russian and international companies. In some companies, this idea was transformed into a two-speed model with a “rapid response team” within the existing IT department. Such a group focuses on one or two most significant business areas. Sharp focusing enables to quickly transform the InfSys in the most significant areas, and then apply the results to the other IT applications.

The second IT tier is organizational. It does not require a physical or administrative resource reallocation. Any of the tiers can be enhanced by outsourcing, contracting integrators or vendors at any stage of the solution development.

The approach used by a major oil company is an illustrative example of a two-tier IT management model to implement the InfSys organic growth strategy.

Case Study: InfSys Organic Growth Strategy at Surgutneftegas, PAO

The IT/InfSys solutions development process is divided into 2 tiers:

- second tier. The tier includes business analysts and business users. A fast evolutionary development methodology (agile) with frequent releases is used. Creating an IT solution at this tier follows the Deming-Shewhart cycle and generally looks like this:

- a graphical business process model is developed by iterative edits to make a minimal viable product (MVP) based on a self-documenting software platform that “understands” business people.



Figure 3. Case Study: InfSys Organic Growth Strategy at Surgutneftegas, PAO

- MVP is launched and improved on the fly, taking into account the real practice with specific business processes and the interactions between them.

- first tier. The programmers work at this tier. They receive requests from the second tier when there is a need to develop specific business logic, data processing, and integration with other systems. conventional ITSM methodologies, change management and a corporate release strategy are used.

For the successful application of organic InfSys growth strategy with a two-tier IT model, the right choice of the platform is paramount. Business process management systems created with a configurable platform (hereinafter called a High Readiness Enterprise Management System, or HREMS) should enable a human to describe the required solutions in an intuitive format and automatically convert such descriptions into machine code [16].

We tested the above two-tier IT model at Surgutneftegas enabled by Comindware Business Application Platform, a commercially available HREMS platform closest in its concept and functionality to the InfSys organic growth concept and can operate as an ontological engine [17].

The key criteria to evaluate Comindware Business Application Platform as a product suitable for building an HREMS were [18]:

- The versatility of the platform enables the building of any function-oriented corporate IT solutions using built-in tools. For second-tier development, there are low-code tools for building ontology models of business applications and user interfaces. For first-tier development, there are general-purpose coding tools in common programming languages

- The adaptability of the digital platform and its IT solutions to continuous changes in subject areas. This means that the solution model can be created, verified for compliance with the business problem and approved on the second tier. As early as at this stage the requirements are adjusted to the solution and the business logic taking into account the system user feedback. The requirements are not frozen at the high tier, and the requests passed to the first tier are verified and do not require adjustments.

- Highly flexible data processing. The platform enables the user to perform any unstructured and non-standard information processing. This is achieved with a graph database and the platform's ability to handle the semantics (meaning) of user queries in a given context supported by the ontology. The platform can find the necessary concepts and relationships in the ontology, create a set of them that meets the query, and perform the operations that yield the result (answer) [19].

- Excellent UX. The user interfaces and forms are created and adapted to the needs of users in the second tier. In this way, the UX is continually improved to lower the IT solution learning curve.

For the above model of InfSys development can be recommended as the key enterprise-wide strategy, we had to prove its feasibility for both technically complex projects, and projects with relatively simple business logic.

A technically complex pilot project was creating a new petroleum products customer relations management system (CRM) to replace a legacy solution. This project includes a customer web site, digitalization of end-to-end business processes from requisition to shipment, integration, analytical reporting and much more. As one could expect, implementing such functionality took a lot of first-tier resources. We managed to significantly reduce the IT department efforts, reach a sustainable short release cycle and reduce the total cost of creating and aftersales support. As a result, we proved the viability of the proposed management model and platform for large projects, and the developed CRM system has been successfully growing and developing to meet the business needs since 2016.

To test the proposed approach for smaller-scale IT solutions without using the first-tier resources, we launched the projects to develop solutions for business processes and IT projects portfolio management. These IT solutions were successfully implemented by the business analysts and are in commercial operation.

The proposed approach to managing the InfSys organic growth was implemented, yields a tangible economic effect, and can be recommended for large companies.

Conclusion

The application of the organic growth strategy to the InfSys development with two-tier IT management is a modern approach to solving the problem of InfSys complexity in large companies. It enables fast response to business needs. The technology behind the InfSys organic growth strategy and the modern approach to simplifying large corporate InfSys is a high-availability enterprise management system. A significant part of the HREMS activities is at the level of individual experts and business unit managers. It increases the IT projects efficiency, reducing project costs and total system ownership costs through the ability to develop IT solutions code-free and documentation-free, minimizing approval procedures, as well as making changes to the applications without adjusting the infrastructure. It is the key to the organic and dynamic development of a corporate InfSys.

REFERENCES

1. Ananyin V. I., Zimin K. V., Lugachev M. I., Gimranov R. D., Skriprin K. G. Digital Organization: Transformation into the New Reality. *Business Informatics*. 2018;2:45-54. DOI: 10.17323/1998-0663.2018.2.45.54. (In Russ.)
2. Gimranov R. D., Lugachev M. I. Introducing a Digital Enterprise with Emergent Stratification of Information Systems. *Proceedings in Cybernetics*. 2016;2:166-169. (In Russ.)
3. Belaichuk A. *DBM Evolution in 1990-2020. Infographic*. Available at: <https://www.comindware.com/ru/blog-%D0%B8%D0%BD%D1%84%D0%BE%D0%B3%D1%80%D0%B0%D1%84%D0%B8%D0%BA%D0%B0-%D1%8D%D0%B2%D0%BE%D0%BB%D1%8E%D1%86%D0%B8%D1%8F-bpm-1990-2020/>. (In Russ.)
4. Belaichuk A. *The Second Coming of DBM*. Available at: <https://www.itweek.ru/management/article/detail.php?ID=200028>. (In Russ.)
5. Hiatt J. M., Creasey T. J. *Change Management. The People Side of Change*. Loveland: Prosci Research; 2003.
6. Anan'ev V., Chernov A. *The Architecture Difference between Automation and Digitalization*. Available at: https://www.cnews.ru/articles/2019-06-03_chem_otlichayutsya_arhitekturnye_podhody_pri_avtomatizatsii_i_tsifrovizatsii. (In Russ.)
7. Kemsli S. *Conway's Law and End-To-End Business Processes*. Available at: <http://bpms.ru/post/20200426-conway-law>.
8. Aldzhanov V. *IT Architecture. A to Z Practical Guide*. 2018. 1380 p. (In Russ.)
9. How to Revitalize a Stalled Digital Transformation. Available at: <https://www.gartner.com/smarterwithgartner/how-to-revitalize-a-stalled-digital-transformation>.
10. Andersson H., Tuddenham Ph. *Reinventing IT To Support Digitization*. Available at: <https://www.mckinsey.com/business-functions/mckinsey-digital/our-insights/reinventing-it-to-support-digitization#>.

11. Gartner Says CIOs Need Bimodal IT to Succeed in Digital Business. Available at: <https://www.gartner.com/en/newsroom/press-releases/2014-11-10-gartner-says-cios-need-bimodal-it-to-succeed-in-digital-business>.
12. Rybal'chenko M. V. *IT Systems Architecture*. University Textbook. M.: Yurait; 2018. 91 p. (In Russ.)
13. Mikhailov A. *IT Strategy: Best Russian and International Practices*. M.: Konsalting po upravleniyu IT; 2018. 450 p. (In Russ.)
14. Lewis B. *IT-as-a-business is Dead. Long Live BusOps*. Available at: <https://www.cio.com/article/3445899/it-as-a-business-is-dead-long-live-busops.html>.
15. Gavrilova T. A., Kudryavtsev D. V., Muromtsev D. I. *Knowledge Engineering Models and Methods: Textbook*. SPb.: Lan'; 2016. 324 p. (In Russ.)
16. Belaichuk A. *Fast Software Development in the Digital Age*. Available at: <http://mainthing.ru/ru/item/795>. (In Russ.)
17. Gimranov R. D., Kholkin I. N. *Inventing the Information Systems of the Future. Theories and Applications*. Surgut, 2017. 192 p. (In Russ.)
18. *Low-Code in Action*. Available at: <https://www.comindware.com/ru/low-code-development-platform>. (In Russ.)
19. *DBM for Rednecks: What Real Low-Code Is*. Available at: <https://www.comindware.com/ru/blog-what-is-true-low-code>. (In Russ.)

DOI: 10.51790/2712-9942-2020-1-1-6

MAP DRAWING AND FOLIATIONS OF THE SPHERE**Athanase Papadopoulos***University of Strasbourg, The French National Centre for Scientific Research, Strasbourg, France,
papadop@math.unistra.fr*

Abstract: I consider some questions related to Euler’s work on cartography and its consequences, in which the foliations of the sphere by meridians and parallels play important roles.

Keywords: mathematical geography, map drawing, history of cartography, perfect map, Leonhard Euler, Joseph-Nicolas Delisle, foliation.

Acknowledgements: this paper is based on a talk I gave in Obninsk, on May 14, 2019, at a conference commemorating Pafnouti Chebyshev. I would like to thank the organizer, Valerii Galkin, for inviting me to that conference. I would also like to thank Alena Zhukova for her corrections on a preliminary version of this paper.

Cite this article: Papadopoulos A. Map Drawing and Foliations of the Sphere. *Russian Journal of Cybernetics*. 2020;1(1):38–45. DOI: 10.51790/2712-9942-2020-1-1-6.

ПОСТРОЕНИЕ КАРТ И РАЗВЕРТКА ПОВЕРХНОСТИ СФЕРЫ**А. Пападопулос***Университет Страсбурга, Национальный центр научных исследований Франции, Страсбург,
Франция, papadop@math.unistra.fr*

Аннотация: в статье рассматриваются вопросы, касающиеся работ Эйлера в области картографии, и их последствия, в которых важную роль играют развёртки поверхности сферы по меридианам и параллелям.

Ключевые слова: математическая география, построение карт, история картографии, идеальная карта, Леонард Эйлер, Жозеф-Никола Делиль, развертки.

Благодарности: эта статья основана на моём выступлении на конференции в Обнинске 14 мая 2019 года, посвящённой Пафнутию Львовичу Чебышёву. Я бы хотел поблагодарить организатора конференции Валерия Галкина за приглашение. Также хочу выразить благодарность Алёне Жуковой за помощь в работе над черновиком статьи.

Для цитирования: Пападопулос А. Построение карт и развертка поверхности сферы. *Успехи кибернетики*. 2020;1(1):38–45. DOI: 10.51790/2712-9942-2020-1-1-6.

Introduction

I will consider some questions related to Euler’s work on the drawing of geographical maps and its ramifications, in which the foliations of the sphere by meridians and parallels play important roles. This article can be regarded as a sequel to my article [1] in which I talked about the works of Euler and Chebyshev on geography. It is also the occasion to straighten out a statement often made in the literature concerning Euler’s contribution to cartography.

On Euler’s “perfect” maps

I will start with a few remarks on Euler’s memoir *De repraesentatione superficiei sphaericae super plano* (On the representation of spherical surfaces on a plane) [2], presented to the Saint Petersburg Academy of Sciences on September 4, 1775, and published in the 1777 volume of the *Acta Academiae Scientiarum Imperialis Petropolitinae*.

This memoir is very poorly quoted in the literature. On the one hand, it is referred to for a result which is attributed to Euler, although this result was known since Greek antiquity, and its proof follows immediately from results in spherical geometry that were known in that period. On the other hand, there are interesting results that Euler proved in this memoir which, to my knowledge, are never mentioned in the papers or books on mathematical cartography.

The result that is usually attributed to Euler in relation with the paper [2] says that there is no “perfect” map from a subset of the sphere to the Euclidean plane. A confusion is entertained by the fact that the word “perfect” was used by Euler in his paper without a proper definition. In the (relatively large number of) papers in which Euler’s memoir is quoted, it is said that Euler proved in this memoir that there is no map from a subset of the sphere onto the Euclidean plane that preserves distances up to scale, which is surely not what Euler proved. The reason for this situation is that, as it often happens in “historical” papers, authors get their information from papers written by other authors on the subject without bothering to look into the original sources and try to understand them. Let us give a few examples of such quotes.

T. Feeman, in his book *Portraits of the Earth: A Mathematician Looks at Maps* [3], discusses the existence of a map from a portion of the sphere onto the plane which has a fixed scale, that is, as the author puts it, a map such that the quantity

$$\frac{\text{distance between two points on the globe}}{\text{distance between their images}}$$

is constant, i.e. independent of the chosen pair of points. The author writes: “Over the years various attempts by cartographers to solve this problem resulted in some ingenious, if flawed, maps. Finally, in 1775, Leonhard Euler (1707–1783), the leading mathematician of his day and one of the most important mathematical figures of all time, presented to the St. Petersburg Academy of Sciences a paper entitled *On representations of a spherical surface on the plane* in which he proved conclusively that such a map could not exist” [3, p. 25].

In the article *Dallo spazio come contenitore allo spazio come rete*, C. Corrales Rodriganez writes [4, p. 125]: “The mathematician Leonhard Euler, in his article *De repraesentatione superficiei sphaericae super plano*, published in the eighteenth century, proved that no part of the Earth can be reproduced over a plane surface without deformation. Euler’s theorem says that the perfect map does not exist”¹. Incidentally, the author adds that “Euler’s theorem has pushed the mathematical cartographers to study spherical geometry and trigonometry as a subject in itself, independent of Euclidean geometry.”². It is not clear to what mathematical cartographers the author is referring to, but Euler himself was a cartographer, and he had published several works on spherical geometry and spherical trigonometry several decades before he wrote this memoir.³ Furthermore, long before Euler, Ptolemy (2nd c.A.D.), one of the most famous mathematical cartographers of all times, was also thoroughly involved in spherical geometry and spherical trigonometry. As a matter of fact, the field of spherical geometry remains poorly known to historians of mathematics. In the book *Portraits of the Earth: A Mathematician Looks at Maps* which we already mentioned, the author claims [3, p. 25] that spherical geometry can be developed axiomatically as a Euclidean geometry in which Euclid’s fifth postulate is replaced by a postulate saying that any two lines intersect (in two points). This statement is not correct. The confusion is probably caused by the fact that the axioms of hyperbolic geometry (which, together with Euclidean and spherical geometry forms the three “classical” geometries, or the geometries of constant curvature) are precisely those of Euclidean geometry with the fifth postulate replaced by its negation. Spherical geometry may be developed axiomatically, but such a set of axioms cannot be so simply obtained from those of Euclidean geometry.

Let us continue with our citations of Euler’s result.

R. Osserman, in his paper *Mathematical mapping from Mercator to the millennium* [6, p. 234] (2004) attributes the following theorem to Euler: *It is impossible to make an exact scale map of any part of a spherical surface*. By an “exact scale map”, Osserman means a map that preserves distances up to scale, and he refers again to Euler’s paper [2].

P. Robinson, in a paper titled *The sphere is not flat* [7] (2006), writes the following: “The theorem of our title asserts that there is no isometric (that is, distance-preserving) function from the sphere (or indeed from any of its nonempty open subsets) to the Euclidean plane; more generally, there is no isometry to any Euclidean space. This theorem may be traced back to Euler, in his *De repraesentatione superficiei sphaericae super plano* of 1778”.

¹ [Il matematico Leonard Euler] nel suo articolo *De repraesentatione superficiei sphaericae super plano*, pubblicato nel Settecento, ha provato che nessuna parte della Terra pu’o essere riprodotta su una superficie piana senza deformazione. Il teorema di Eulero dice che la carta perfetta non esiste.

² Il teorema di Eulero ha spunto i cartografi matematici a studiare la geometria sferica e la trigonometria come materie a s’e, indipendenti dalla geometria euclidea.

³ An edition of Euler’s and his collaborators on spherical geometry will appear in the book [5].

The same poor attribution to Euler occurs in the chapter titled *Curvature and the notion of space* in the book *Mathematical Masterpieces: Further Chronicles by the Explorers* (2007) by A. Knoebel, J. Lodder, R. Laubenbacher and D. Pengelley [8, p. 163], where the authors write: “In the paper presented to the St. Petersburg Academy of Science in 1775, *De repraesentatione superficiei sphaericae super plano*, Euler proved what cartographers had long suspected, namely, the impossibility of constructing a flat map of the round world so that all distances on the globe are proportional (by the same constant of proportionality) to the corresponding distances on the map”.

J. Gray, in his book *Simply Riemann, Simply Charly* [9] which appeared in 2020, says the following, about Euler’s work on cartography: “Euler used all his analysis to prove that every cartographer suspected: that there could be no map of the Earth’s surface onto a plane that is accurate in every respect. Some maps send curves of shortest length on the sphere to straight lines in the plane; there are maps that send equal angles to equal angles, and there are maps that scale all areas by the same amount. But there can be no map that does all of these at once”.

Naturally, popular science authors get their information from mathematicians’ writings when they understand them: In the Spanish daily newspaper *La Vanguardia*, on 26 March 2017, in an article titled *Un mundo, tres mapas*, the author, A. Molins Renter, writes: “Passing from a spherical geometric form to a plane support, two-dimensional and usually of rectangular shape, results in the fact that something is always lost in the translation, as the Swiss mathematician and physicist Leonhard Euler already demonstrated in 1778, in his work *De repraesentatione superficiei sphaericae super plano*”⁴.

One could give are many other examples.

In fact, the statement attributed by all these authors to Euler was obviously known to him, but it does not convey the slightest idea of the results obtained in the memoir quoted, which are much stronger and much more interesting than what all these authors claim. Furthermore, as I suggested, the result that they quote was known since the 1st-2nd century A.D., since it follows as a corollary from several results contained in Menelaus’ *Spherics* on the geometry of spherical triangles. For instance, it is an immediate consequence of the result saying that the angle sum in a spherical triangle is always greater than 2 right angles (this is Proposition 12 in [10]), or from the comparison result saying that in any spherical triangle ABC , if D and E denote the midpoints of AB and AC respectively and if DE is the shortest arc joining them. Then $DE > AC/2$ (Proposition 27 in [10]). A local isometry between an open region of the sphere and an open region of the Euclidean plane would preserve the two properties of triangles, and obviously neither of them is satisfied by a Euclidean triangle.

At the end of Section 9 of his paper, Euler writes: “It is proved through computation that a perfect mapping of the Sphere onto the plane is not possible.” But since he did not give the definition of a *perfect map*, the meaning of this sentence should be understood in context, that is, by following the arguments that lead to it.

Recently, C. Charitos and I. Papadoperakis wrote a paper titled *On the non-existence of a perfect map from the 2-sphere to the Euclidean plane* [11] in which they give a precise statement of Euler’s result and provide a detailed proof of it.

To state Euler’s result correctly, we call a map f from a region S of the 2-sphere to the Euclidean plane *perfect* if every point in the domain has a neighborhood on which the following two conditions hold:

- (1) f sends meridians and parallels to two fields of lines that make mutually the same angles;
- (2) f preserves distances infinitesimally along the meridians and the parallels.

Thus, a perfect map sends the meridians and parallels to two line fields that are orthogonal. Furthermore, a perfect map preserves globally the length element along the meridians and the parallels. One should note here that on the spherical globe, the meridians are geodesics but the parallels are not. The fact that distances are preserved infinitesimally along the meridians implies immediately that the distances between points on these lines are preserved. It also follows, although not so immediately, that distances between points on parallels is preserved by a perfect map.

The idea of Euler’s proof was to translate these geometrical conditions into a system of partial differential equations and to show that this system has no solution.

Furthermore, Euler, in his paper, after showing the non-existence of a perfect map, proves several other results. He declares that since perfect maps do not exist, one has to look for best approximations. He

⁴ Pasar de una forma geométrica esférica a un soporte plano, bidimensional y normalmente con forma rectangular provoca que algo se pierda siempre en la translación, como ya demostró el matemático Leonhard Euler en 1778, en su obra *De repraesentatione superficiei sphaericae super plano*.

writes: “We are led to consider representations which are not similar, so that the spherical figure differs in some manner from its image in the plane.” He then examines several particular projections of the sphere, searching systematically for the partial differential equations that they satisfy. He considers several classes of maps: conformal maps (which he calls “similitudes on the small scale”), area-preserving maps, and maps where the images of all the meridians are perpendicular to a given axis while those of all parallels are parallel to it. He gives examples of maps satisfying each of the above three properties and in each case he studies their distance and angle distortion.

On the action of a geographical map on the foliations by parallels and meridians

An important feature of Euler’s memoir [2] and of the other memoirs that we shall consider below is that most of the properties of the geographical maps that are requested are formulated in terms of how these maps transform the two geographically most famous foliations of the sphere, namely, the foliations by parallels and by meridians.

Let us recall that when the surface of the Earth is considered to be a sphere, the *parallels* are the family of circles that are equidistant from the equator. The latter is the great circle that is perpendicular to the rotation axis of the Earth, the one that separates the Northern hemisphere from Southern one. In the geometry of the sphere, the parallels are geometric circles, that is, equidistant points from a center, which is either the North or the South pole (a circle on the sphere has two centers). Furthermore, the parallels are small circles, that is, intersections of the sphere with planes that do not pass through the center, except the equator itself, which is also considered as a parallel (at zero distance from itself) and which is a great circle, the intersection of the sphere with a plane passing through the center. The difference is important because on the sphere great circles are geodesics whereas small circles are not. This foliation has two singular points, situated at the North and South poles.

The second foliation that is used in the paper [2] is the foliation by *meridians*, whose leaves are the great circles perpendicular to the equator, or, equivalently, the great circles that pass through the North and South poles. Unlike the parallels, the meridians are all great circles, and therefore geodesics. It has two singular points, situated at the North and South poles.

Since the time of ancient Greek geography, the foliations by parallels and meridians play an important role in map drawing, for representing regions of the Earth, but also for maps of the celestial sphere. Figure 1 is a reproduction of a representation of a celestial globe dating from the 1st century A.D. on which the foliations by parallels and meridians are drawn. The same picture could serve for the representation of the Earth.

The properties of the images of the meridians and parallels are important factors in several known projections. For instance, under a stereographic projection centered at the North pole, the parallels are sent to concentric circles centered at the image of the South pole, while the meridians are sent to straight lines meeting at the North pole. The projection from the center of the sphere to a plane tangent to the South pole, known as the gnomonic projection, and which was used since the times of Thales, has a similar property: parallels are sent to circles centered at the South pole and meridians are sent to straight lines passing through this pole.

The foliations by parallels and by meridians are perpendicular. Their images by a geographical map are usually drawn on the map, see e.g. Fig. 1.

Two other memoirs by Euler on geography were published the same year as his memoir *De repraesentatione superficiei sphaericae super plano*, namely, *De proiectione geographica superficiei sphaericae* [12] and *De proiectione geographica Deslisiana in mappa generali imperii russici usitata* [13]. I would like to make a few comments on the latter.

The memoir [13] is concerned with a projection from the sphere that was used by Joseph-Nicolas Delisle who, during several years, was the main geographer and the director of the astronomical department of the Saint Petersburg Academy of Sciences. He was in charge of drawing new and precise maps of the Russian Empire. From 1735 to 1740, Euler assisted Delisle in this work until he became himself the head of the geography department of the Academy, after a conflict emerged between Delisle and the Academy’s administration, in relation with the so-called *Atlas Russicus* (the “Russian Atlas”), a project initiated by Peter the Great and of which Delisle was in charge, and which he kept postponing. In 1740, the responsibility of the Russian Atlas was taken away from him and given to Euler.

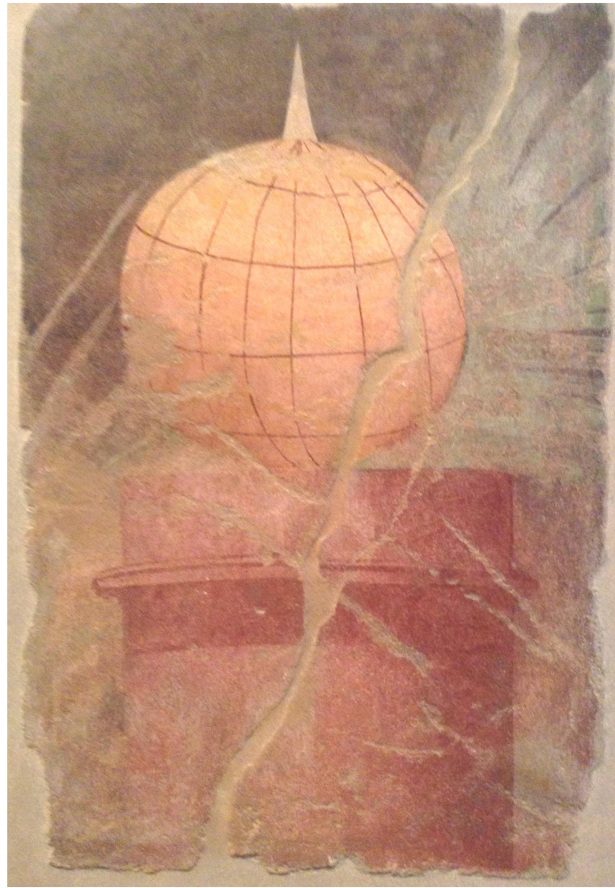


Figure 1. *A celestial globe with its two perpendicular foliations by parallels and meridians. Wall painting fragment from the first century A.D. Metropolitan Museum of Art, New York, Department of Greek and Roman Art. (Photo A. Papadopoulos.)*

In his memoir, Euler starts by reviewing the main properties of a stereographic projection used by the geographer Johann Matthias Hadius. The latter had published in Nuremberg, in 1739, a map of Russia known under the name “Imperii Russici et Tatariae universae tam majoris et asiaticae quam minoris et europaeae tabula” (Geographical map of the Russian Empire and of Tataria, both large and small, in Europe and Asia). Euler mentions properties of the images of the two foliations by parallels and meridians, in particular that these images intersect at right angles (in fact, the map is conformal, that is, it is angle-preserving). Euler then reviews the inconveniences of this projection: length is highly distorted in the large, especially for maps that represent large regions of the Earth and the images of the meridians are not evenly curved on the geographical map, even though these lines are circles. In particular, the province of Kamchatka is distorted by a factor of four, compared to another region at the center of the map.

In §5, of his memoir, Euler states the following four properties that are required from an ideal geographical map: (i) the images of the meridians are straight lines; (ii) the degrees of latitudes do not change along meridians; (iii) the images of the parallels meet the images of the meridians at right angles; (iv) at each point of the map, the ratio of the degree on the parallel to the degree on the meridian is the same as on the sphere. He then declares that since this cannot be achieved one may request, instead of the last condition, that the deviation of the degree of latitude to the degree of longitude at each point from the true ratio be as small as possible (ideally, this error should not be noticeable).

He then recalls the construction of Delisle’s map.

In this map, one first chooses two outer parallels that contain the region that is to be represented. In the case of the Russian Empire, these outermost parallels are chosen to be those at 40° and 70° of latitude. Then, one chooses two other special parallels on which the ratios of the degrees of latitude to the degrees of longitude will be represented by their exact values. Euler writes that the question becomes that of choosing these two new parallels in such a way that the maximum deviation of the ratios of the degrees of latitude and

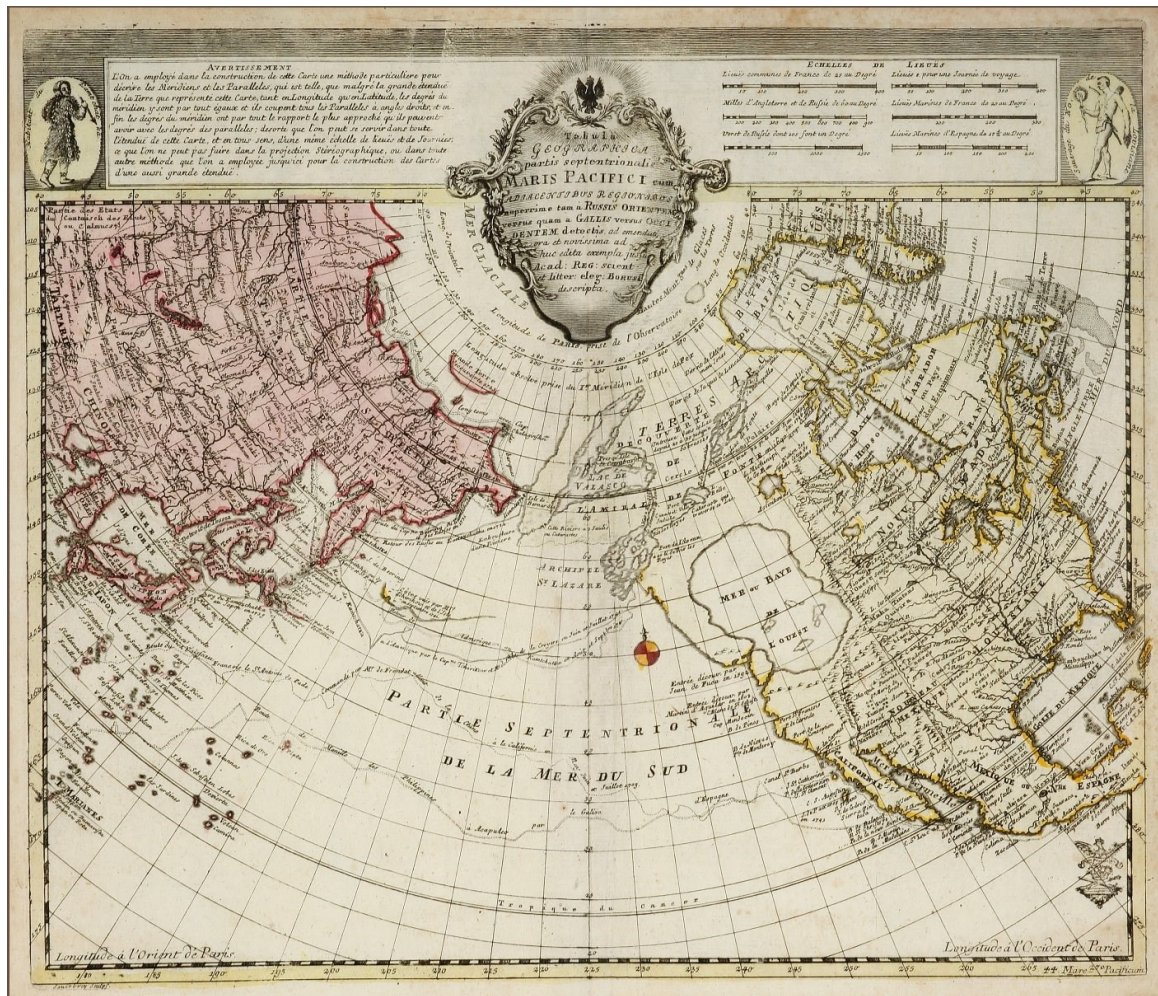


Figure 2. A map of the Northern Pacific, with the Eastern part of Asia and the Northern part of America, from Euler's *Atlas Geographicus* (Berlin, 1753)

longitude over the entire map is minimized. He writes that Delisle found that the optimal choice of these parallels is to take them equidistant from the central parallel of the map and from the outermost parallels chosen. Besides, distances should be preserved on all meridians, and the maximum of a certain deviation over the entire map must be minimized. Figure 3 reproduces a map drawn by Delisle using his method.

Starting in §7, Euler presents a mathematical construction of a family of straight lines representing meridians which are at distance one degree from each other. He notes that one advantage of Delisle's projection is that while meridians are represented by straight lines, the images of the other great circles do not deviate considerably from straight lines (§22 of [13]), and he gives some precise estimates of this deviation (§23ff).

In §10–16 of his memoir, Euler gives the mathematical details that show the difference between this representation and the real situation at the extreme points he started with, and in §17–23, he makes the actual computations in the special case where the map is that of the Russian Empire. In the last sections of his memoir, he studies the images of great circles on the sphere and he shows that the difference between these images and circular arcs is not noticeable. He computes the radius of such an arc, which he finds to be very large and he concludes that the shortest lines on the map do not differ sensibly from straight lines.

In conclusion, let us stress once again that in Euler's treatment of Delisle's projection, like in the theorem we stated above on perfect maps, the important requirements concern the behavior of the images of the two foliations defined by the parallels and the meridians.

Besides the memoir [13] in which he described Delisle's method of drawing geographical maps, Euler explained the same method in the *Atlas Geographicus omnes orbis terrarum regiones in XLI tabulis exhibens* [15] that was published by the *Académie Royale des Sciences et Belles Lettres de Prusse*, in the year 1753, in Berlin, where he worked for 25 years, between his two stays in Saint Petersburg. The atlas



Figure 3. *A map of the Russian Empire by Joseph-Nicolas Delisle (Saint Petersburg, 1745) [14]*

contains 45 maps, and was edited under the direction of Euler who also wrote its preface, which is dated May 13, 1753. Several projections are used in this atlas, which is concerned only with large parts of the Earth. In all these projections, the meridians are perpendicular to the parallels.

The map in Figure 2 is extracted from this atlas. It is the last one in the series, and it is drawn using Delisle's method. Euler, in the preface, comments on this method. He writes that Delisle's method seems to him the most appropriate for a proper representation of these Northern regions of the terrestrial globe. He recalls that in this representation, the meridians are straight lines and all their degrees are equal: the images of two meridians that are distant apart by one degree converge in such a manner that at two latitudes that are chosen in advance, the ratio of the degrees of longitude to the degrees of latitude are the same ratio as in reality. This is the property that he presents in his memoir [13] that we noted above. For the Russian Empire, after the choice of the two outer parallels at 40° and 70° , the two parallels which are at the same elevation from the extremities of the region that is represented as well as from its center are those at $47^\circ 30'$ and $62^\circ 30'$. Under these two latitudes, the ratios between the degrees of longitude and latitude are accurate on the map. At the other locations, they are almost accurate (the difference is not noticeable). Besides, in this representation, all the meridians (which are straight lines) merge at a point, although this point is not the North pole; it is at a distance which would correspond to 7 degrees farther than this pole. From this point as center, the images of the parallels are circles. Euler writes that one should not regard as a shortage of this map the fact that the center in which all the meridians intersect is so far from the pole, nor the fact that on this map the parallels, which form semi-circles, do not occupy 180° in longitude, but much more, sometimes even up to 250° .

Lagrange, whose name is associated to the one Euler in several respects, already stressed in his paper on the construction of geographical maps the fact that the only thing we have to do in drawing a geographical map is to specify the images of meridians and parallels according to a certain rule (see [16, p. 640]). This simple remark was at the basis of the the development of modern mathematical cartography. We have tried to convey this idea by mentioning examples from the works of Euler and Delisle, but others may be found in works of Lambert, Gauss, Bonnet and others. The forthcoming book [5] contains a section on cartography at the epoch of Euler.

REFERENCES

1. Papadopoulos A. *Euler and Chebyshev: From the Sphere to the Plane and Backwards*. 2016. hal-01352229.
2. Euler L. De repraesentatione superficiei sphaericae super plano. *Acta Academiae Scientiarum Imperialis Petropolitinae*. 1777, p. 107–132. *Opera Omnia*. Series 1, Volume 28, pp. 248–275.
3. Feeman T. G. *Portraits of the Earth: A Mathematician Looks at Maps*. AMS, Providence, RA; 2002.
4. Corrales Rodriganez C. Dallo spazio come contenitore allo spazio come rete. In: *Matematica e cultura 2000*. Papers from the conference held at the Università Ca' Foscari di Venezia, Venice, March 26–27, 1999. Ed. M. Emmer. Collana Matematica e Cultura. Milan: Springer-Verlag Italia; 2000.
5. Caddeo R., Papadopoulos A., Zhukova A. *Spherical Geometry in the Eighteenth Century*, book to appear.
6. Osserman R. Mathematical Mapping from Mercator to the Millennium. *Mathematical Adventures for Students and Amateurs* / Ed. D. F. Hayes and T. Shubin. Mathematical Association of America; 2004. P. 233–257.
7. Robinson P. L. The Sphere is not Flat. *The American Mathematical Monthly*. 2006;113(2):171–173.
8. Knoebel A., Lodder J., Laubenbacher R., Pengelley D. *Mathematical Masterpieces: Further Chronicles by the Explorers*. Springer Verlag; 2007.
9. Gray J. *Simply Riemann, Simply Charly*. New York; 2020.
10. Rashed R., Papadopoulos A. *Menelaus' Spherics: Early Translation and al-Māhānī/al-Harawī's Version (Critical edition of Menelaus' Spherics from the Arabic manuscripts, with historical and mathematical commentaries)*. De Gruyter, Series: Scientia Graeco-Arabica, 21, 2017. 890 p.
11. Charitos C., Papadoperakis I. On the Non-existence of a Perfect Map from the 2-sphere to the Euclidean Plane. *Eighteen Essays in Non-Euclidean Geometry*. Ed. V. Alberge and A. Papadopoulos. Zürich: Eur. Math. Soc.; 2019. P. 125–134.
12. Euler L. De proiectione geographica superficiei sphaericae. *Acta Academiae Scientiarum Imperialis Petropolitinae*. 1777, p. 133–142. *Opera Omnia*. Series 1, Volume 28, pp. 276–287.
13. Euler L. De proiectione geographica Deslisiana in mappa generali imperii russici usitata. *Acta Academiae Scientiarum Imperialis Petropolitinae*. 1777, p. 143–153. *Opera Omnia*. Series 1, Volume 28.
14. Delisle J.-N. *A Proposal for the Measurement of the Earth in Russia*, Read at a Meeting of the Academy of Sciences of St. Petersburg, Jan. 21. 1737. by Mr Jos. Nic. de L'Isle, First Professor of Astronomy, and F. R. S., Translated from the French, Printed at St. Petersburgh, Phil. Trans. R. Soc. Lond. 40, 27–49 (1737).
15. Euler L. Preface of the *Atlas Geographicus omnes orbis terrarum regiones in XLI tabulis exhibens*, Académie Royale des Sciences et Belles Lettres de Prusse, Berlin, 1753. *Opera Omnia*. Series 3, Volume 2, p. 305–317.
16. De Lagrange J.-L. Sur la construction des cartes géographiques. Nouveaux mémoires de l'Académie royale des sciences et belles-lettres de Berlin, année 1779, Premier mémoire, *Œuvres complètes*, tome 4, 637–664. Second mémoire *Œuvres complètes*, tome 4, 664–692.

DOI: 10.51790/2712-9942-2020-1-1-7

A COMPUTATIONAL EXPERIMENT OF SIMULATING LIGHT PROPAGATION IN A FIBRE-CONTAINING PROFILED STRUCTURE

Vladimir V. Savchenko¹, Maria A. Savchenko²

¹ Faculty of Computer and Information Sciences, Hosei University, Tokyo, Japan, vsavchen@hosei.ac.jp

² Meiji Institute for Advanced Study of Mathematical Sciences, Meiji University, Tokyo, Japan, savchenko_maria@yahoo.com

Abstract: many studies show that profiled structures are the source of attaining desired system characteristics in industrial or other applications. In this short note, we continue considering proposed recently by us the profiled structure such as a beach umbrella based on the principles of origami design. To demonstrate the optical properties of the given model, a developed recursive ray tracing algorithm is used to simulate the propagation of light rays through the modelled paper fiber sample. In this paper, modeling light propagation through a porous structure using ray tracing technique is presented and results of modeling light propagation in a profiled structure with respect to simulated light propagation in fiber structure are discussed.

Keywords: fiber structure, ray tracing technique, bending energy.

Acknowledgements: we would like to take this opportunity to thank Professor N. J. Suematsu (Meiji University, Tokyo, Japan) for preparing microscopic images of washi-paper structure. We thank Professor V.A. Galkin, (Scientific Research Institute of System Development RAS, Moscow, Russia) for his constructive suggesting during the development of this research work.

Cite this article: Savchenko V. V., Savchenko M. A. A Computational Experiment of Simulating Light Propagation in a Fibre-Containing Profiled Structure. *Russian Journal of Cybernetics*. 2020;1(1):46–53. DOI: 10.51790/2712-9942-2020-1-1-7.

ВЫЧИСЛИТЕЛЬНЫЙ ЭКСПЕРИМЕНТ ПО МОДЕЛИРОВАНИЮ РАСПРОСТРАНЕНИЯ СВЕТА В ВОЛОКНИСТОЙ ПРОФИЛИРОВАННОЙ СТРУКТУРЕ

В. В. Савченко¹, М. А. Савченко²

¹ Факультет вычислительной техники и информатики, Университет Хосэй, Токио, Япония, vsavchen@hosei.ac.jp

² Институт современной математики Мэйдзи, Университет Мэйдзи, Токио, Япония, savchenko_maria@yahoo.com

Аннотация: в ряде исследований показано, что профилированные структуры позволяют получать требуемые характеристики систем в промышленных и других областях применения. В настоящей краткой статье мы продолжаем рассмотрение недавно предложенных нами профилированных структур — таких, как пляжный зонтик, — основанных на принципе оригами. Для демонстрации оптических свойств данной модели был разработан рекурсивный алгоритм трассировки лучей, выполняющий моделирование распространения световых лучей через модель образца из бумажных волокон. В настоящей статье представлено моделирование прохождения света через пористую структуру методом трассировки лучей, а также обсуждаются результаты моделирования прохождения света в профилированной структуре по сравнению с моделированием прохождения света в волокнистой структуре.

Ключевые слова: волокнистая структура, метод трассировки лучей, энергия деформационного колебания.

Благодарности: авторы выражают благодарность проф. Н. Дж. Суэмацу (N. J. Suematsu) (Университет Мэйдзи, Токио, Япония) за подготовку микроскопических снимков структуры бумаги васи. Мы также благодарим проф. В.А. Галкина (Научно-исследовательский институт системных исследований РАН, Сургутский филиал, Сургут, Россия) за его конструктивные предложения, полученные в ходе проведения исследования.

Для цитирования: Савченко В. В., Савченко М. А. Вычислительный эксперимент по моделированию распространения света в волокнистой профилированной структуре. *Успехи кибернетики*. 2020;1(1):46–53. DOI: 10.51790/2712-9942-2020-1-1-7.

Introduction

Decreasing harmful effects on human health is important topic for the investigations, see for instance [1], and references therein. Widely used umbrellas and shade structures, which can be made from dense fabrics of cotton, flax, hemp, and natural silk fabrics, provide limited sun radiation. In [2] it was observed that wool knitted fabric with the optimized parameters such as fibre diameter, yarn linear density, yarn twist, cover factor setting can provide high ultraviolet protection to human body.

A wedge-shaped structure is a potentially promising periodic structure for sun light protection that, in fact, was shown in [1]. Washi-paper is widely used in Japan as a material for producing various goods such as lampshades, umbrellas, and etc., see, for instance [3]. The article [1] is devoted to the study of an origami-like screen for protection from sunlight which might reduce the harmful effects of solar radiation on humans. The purpose of the simulation was to show the effectiveness of the profiled structure to redirect light rays in comparison with the non-profiled structure. When light is incident on a material surface, the light wave will either be reflected, transmitted, or absorbed. However, light propagation simulation through a profiled paper structure is based on widely used in various application Kubelka – Munk (K-M) model, see [4], [5], where the light propagation model is considered as a continuum to describe the forward and backward scattering of light.

Due to the short wavelengths of light compared to the geometrical parameters of the desired structure, the problem of light propagation can be solved by means of geometric optics. In [1] an analysis of the Fresnel formulas [6] shows that the reflection coefficient r increases markedly with increasing the angle of incident φ . Such a correlation between parameters r and φ can be used to create structures with high reflectance. The article implements the idea of using the profiled structures based on origami principles to increase the number of reflections with increasing the angle of incident φ on the flat faces. Problem of optimization of initial or basic structure has been also studied.

Nevertheless, exploring the possibility of applying the profiled structure to create a sun-protection screens made from paper or fabrics shown in Fig. 1(a) is in its early phases. Also there is an obvious problem to design a fabric or paper structure satisfying some conditions, see, for instance [7].

Unfortunately, the K-M paper model does not consider any change in orientation in the angular distribution of light fluxes that can introduce some intrinsic errors. This question is discussed, for instance in [8], where Henyey-Greenstein phase function commonly used to describe light fluxes in turbid media such as human tissues is used. Investigating orientation effects to prove correctness or validity of implementing the K-M theory used in [1] for profiled structures is the main objective of this short note. Another one is the extension of previously developed by us the recursive ray tracing algorithm (RRT) allowing simulating light propagation in porous structures. As an application of the developed software algorithm we mimic and examine the properties of reflection/refraction of the fibre structure such as a washi-paper, which we call washi-like paper. The RRT algorithm is implemented using the C++ programming language and is designed to study the light propagation through the fibres presented by polygons.

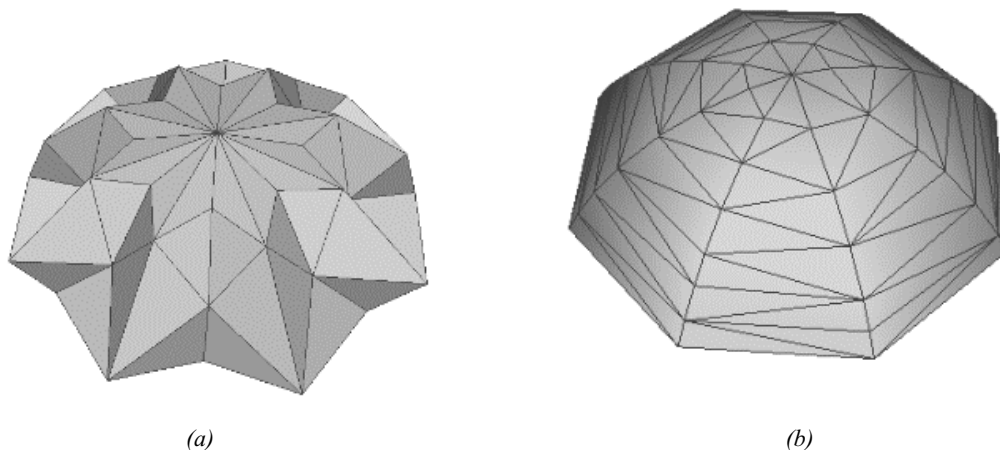


Figure 1. Geometry models [1]. (a) The profiled polygonal model. (b) The non-profiled polygonal model

Related works

Myriads of articles related to the questions of paper industry were published recently, among them [9-13]. A lot of *applicable* information such as size of fibres, fibre lumens, length, diameter, and others like illustrations of crimped sections of fibres can be found on the web site of Pekka Komulainen.

The main objective of the recent study [7] is the stress analysis of paper, nevertheless, in some way results shown can be used for study of light propagation. Authors investigate the effect of extreme tensile performance of individual softwood fibres. In a particular, simulated networks were generated using a random deposition model that mimics the handsheet filtration. Wall thickness, diameter, length and curl of the fibres, grammage, and density profile of the network are the control parameters in the deposition model. An example of a deposited fibre network is presented in Fig. 2 [7].

The review article [14] highlights progress in understanding the optical properties such as opacity, brightness, color, fluorescent properties, gloss of paper.

Transparent wood (TW) is now considered as building material of the future. In many applications, the total light transmittance is an important property. The [15] discusses potential applications of TW and presents optical, mechanical performance, and functionalization routes for realization of advanced applications. In the paper [16] authors note that better understanding of optical properties of TW is essential for further development of this class of optically functional materials. Light transmittance through a TW is highly influenced by light scattering. The paper studies the light diffusion in media with both absorption and scattering. Diffusion equation for photon transport in a scattering material was modified – two different diffusion coefficients were considered: D_{xy} (in the plane perpendicular to the fiber direction) and D_z (along the fiber direction). It is found that the angle-integrated total light transmittance of TW has an exponentially decaying dependence on sample thickness.

In geometric optics, an assumption is made that in uniform media, light travels in a straight-line path, which can be approximated by a ray, where the ray is a straight line perpendicular to the wave fronts. When the light wavelength is much less than the feature size of the medium, Maxwell's equations reduce to the eikonal equation, which is the basis of geometric optics [17] or the ray tracing method. In computer graphics, ray tracing is used for rendering the 3D objects by recursively following the path that the incident light takes or by using so called Monte-Carlo method.

A model based on Monte-Carlo ray tracing for simulating scattering and linear polarization by particles with arbitrary shapes and size is presented in [18]. Authors examine absorption and scattering behaviour of single irregular particles. Particle shapes, size, and optical constants are taken into account for exploring the relationship between actual physical properties and of large particles and the single-particle parameters. In [19] authors demonstrate that the values of the reflection and transmission through the optical medium consisting of air, cell sap, chloroplast, and cell wall of a leaf found from ray tracing agree closely with experimental results.

The paper [20] presents an approach which describes the behavior of light in matter as a special kind of random walk. The paper presents a Markov chain modelling the K-M-like scattering process and studies its combinatorial properties.

The paper [21] introduces an open source Monte-Carlo simulation tool for the modelling of light scattering in paper and prints. Surface scattering is treated as a combination of two effects. The long-range topographic structure, called the surface waviness, deflects incident wave packets according to Snell's law and the Fresnel equations. In addition, the short-range topographic structure, called the microroughness, scatters the light diffusely in a Lambertian manner. Within a homogenous turbid medium representing a fibre wall, the scattering process is controlled by three parameters, the scattering and absorption coefficients, and the asymmetry factor which is used to compute the new direction of the wave packet. Each sheet was modelled as a statistical layer bounded by two surfaces, simulating a sheet with constant thickness. Fibres were modelled as rough hollow cylinders, stretched out into an elliptic shape and a homogeneously distributed along the thickness direction of the sheet, and isotropically oriented in the plane of the paper. The only contribution to light scattering came from light reflections at fibre and layer boundaries. The refractive index of the layer and fibre wall was set to 1.5. The applicability of the simulation tool was demonstrated by modelling the effect of a structure modification on the light scattering.

Let us emphasize or repeat mentioned above that our intention is to estimate possible relations between intensity values of falling light fluxes on a sheet of simulated paper material and values of transmitted light fluxes.

Paper model and simulating light intensity by ray tracing

Paper's ability to scatter and absorb visible light is highly dependent on many factors including paper structure and its chemical composition. A geometry model of the sample of paper, the image of which is shown in Fig.2 (produced by our algorithm), is considered to simulate light propagation as it is described below.

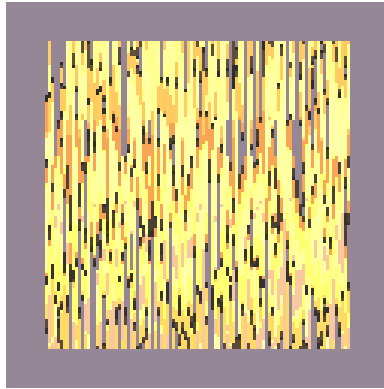


Figure 2. Image of simulated fibre structure generated by ray tracing

For estimation of light propagation characteristics of a simulated paper model we use the idea of voxel visualization [22] to demonstrate the distribution of light rays in the areas inside and below the structures under consideration. A cubic (voxel) volume represents the area of reception of each ray location. Following this concept, we define the 3D volume with cells as identical sub-cubes, where we store the input and output data such as the simulated light intensity data.

There are many effective algorithms for spatial partitioning of 3D space to reduce vast amount of calculations arising in ray tracing algorithms, see, for instance, [23] and references therein. In our application, a developed by us 3D chained list (a series of records) is composed of input data to store geometry data or other. Such list allows easily to store also the contribution of each individual ray to the resulting output data like the electric field strength amplitude, phase, and polarization for each position on an arbitrary ray at a specified distance from the source.

The light is scattered but it is being transmitted through the gaps between the paper fibres. The fibres are not absolutely opaque as it can be seen in Fig. 3. In this study, one record of input data contains coordinates x,y,z of the fibre centre and 3 coefficients of essential matrix defining space orientation of single fibres, modelled as hollow cylinders, stretched out into an elliptic shape by a scaling factor. Fibres were modelled as hollow cylinders with a fibre wall thickness $d = 3.1\mu\text{m}$, stretched out from initially almost circular cross-sectional shape with radius $17\mu\text{m}$ into an elliptic shape and non isotropically oriented in the plane of the paper. Slight angular deviation in y (vertical in our system of coordinates) direction is also produced. Fibres contact and intersection were taken into account by allowing formation of pores what can be observed in the Fig 2. Length of the fibre is about 3.2 mm. The mentioned above modelling parameters approximately correspond to parameters of the modelled washi-like paper.

Thus, for simulating light propagation through the sample of washi-like paper where the two sides of the base are of length approximately 3.1 mm and 3.2 mm respectively, and the height (thickness) of the sample is 0.1 mm, a cubic volume with $8 \times 3 \times 128$ cells size is used in x,y,z directions, respectively.

The simplest (Lambertian) reflection model is applied as a model for diffuse reflection. It is known that the intensity of light should decrease exponentially with the distance d that it enters an absorbing medium. According to Bouguer's experiment, an exponential relationship $T_\lambda = t_\lambda \text{pow}(d)$ was found between the thickness and the spectral transmittance. T_λ and t_λ are the spectral transmittance of a transparent object and spectral transmittance according to the unit thickness, respectively. A 0.9 transmittance for the unit thickness was used in our experiment. Refraction is calculated in accordance with a quantity of the refraction indices by using Snell's law for a given pair of media air and fibre. This process of reflection/refractions continues iteratively.

Traditionally for modelling reflectance and transmittance of particle structures spherical or cylindrical parametrically defined objects are used. In our application polygonal model of fibres is used. Total number

of polygons is 31720.

In our implementation of recursive ray tracing discussed in [1], a set of refraction/reflection events is considered as n -layered material obtained using the adding method, see [5]. In the adding method n is treated with respect to the number of ray intersections with modelled walls.

As we mentioned above, the K-M model does not consider any change in orientation in the angular distribution of light fluxes. For realization of modelling propagation of the paper sample dependence outlined above in investigation of propagating light in the profiled and non-profiled structures we have to take into account orientations in the angular distribution of the paper sample. For that, we precalculate and store light intensity of transparent light in an analogy of look up table, an array that replaces runtime computation. In the table we store direction vectors of the incident light rays and values reflected and transmitted light intensities. Each ray is continued until it ended up as reflection or transmission from the considered paper sample. To reduce the time and efforts required in ray tracing some of the rays are discontinued after 5 levels of recursion.



Figure 3. Microscopic image of washi-paper structure (the top view)

Results of simulations

Results of simulating light propagation in the sample of the washi-like paper structure are shown in Fig 4.

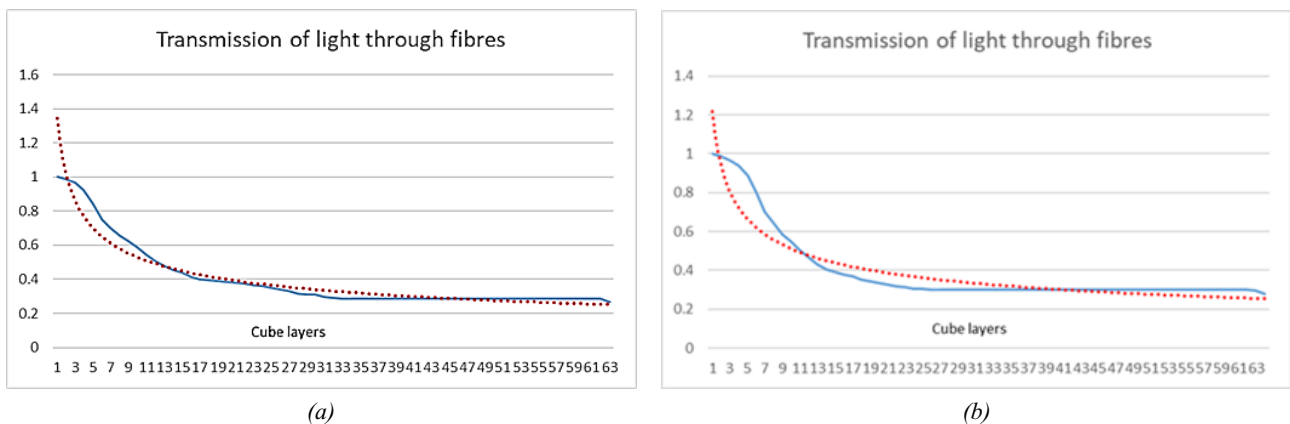


Figure 4. The ray tracing simulation of light propagation in the modelled sample of washi-like paper. (a) Graph of the normalized light intensity (in blue) and power fit of the data (red dots). (b) graph of the normalized intensity of linearly polarized light (in blue) and power fit of the data (red dots)

For simulating light propagation in profiled and non-profiled models (Fig.1), they are embedded in the cube of cells size $128 \times 128 \times 128$. Tracing rays of light with wavelength of 400 nm with correspondent reflection/refraction indices 1 and 1.5 is produced to calculate the integral value of the photon energy E for each sub-cube.

Each ray is continued until it ended up as reflection or transmission from the cube. To reduce

the time and efforts required in ray tracing some of the rays are discontinued after 5 levels of recursion in analogy to ray tracing of the paper sample. The same level of recursion is used to calculate light propagation in the paper sample.

In the RRT algorithm, we consider light intensity as the rate at which light energy is delivered to a sub-cube. We consider an optimal design of the given geometry model that is optimal with respect to the basic designed profile model. Coordinates of vertices of the 3D polygonal model are modified and the resulting warped shape is evaluated with the help of the RRT algorithm, which allows us to take into account a collection of light intensities of refracted and reflected rays stored in the area under the profiled structure. The combination of ray tracing and the optimization techniques based on Genetic Algorithms (GA) for the modification of the model shape is used. Resulting light distribution for profiled model after 331 steps of GA is shown in Fig.5. Our experiments show that with the evolutionary optimization of the geometry of the profiled model, we can improve the shading effect with respect to the basic design. Fig. 5 also illustrates that profiled structures with using paper as a material can provide reasonable decreasing light intensity in the area under the structures.

We may note that with the evolutionary optimization of the profiled model we can improve the shading effect with respect to the basic design by about 2%, it is shown in (Fig. 6 a).

In our own experience, we have found that important problems in computer simulation, surface reconstruction, animation, and geometry processing, can be solved by involving the methods related to a bending energy quantity $\mathbf{h}^t \mathbf{A}^{-1} \mathbf{h}$. \mathbf{A}^{-1} is the bending energy matrix, \mathbf{h} is a vector of so called heights. Questions related to definition matrix \mathbf{A} based on using radial basis functions are discussed remarkably well in [24]. So-called heights \mathbf{h} , in our case, are space transformations defined by the initial and final (destination) points engaged in the process of the model shape modification by implementation of GA optimization. Fig.6 exposes stimulating for further investigation of the relationship between bending energy and light propagation through the profiled structure.

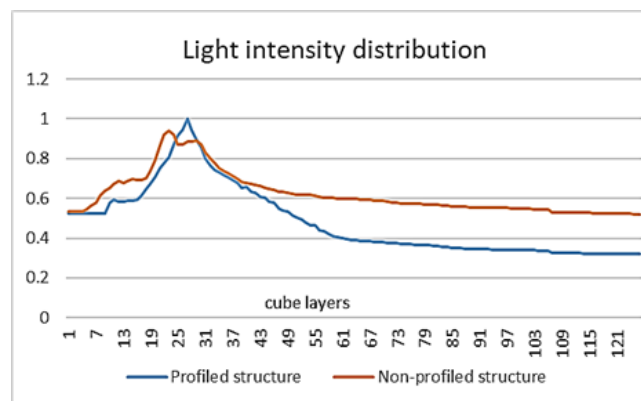


Figure 5. The ray tracing simulation: graphs of the resulting data in the layers of the cube. The light intensities normalised according to values of the profile model are shown on the vertical axis. The area between the layers 4 and 28 represents the region of the model inside the cube

Conclusion remarks

One of the directions of using the RRT algorithm discussed in this note might be the development of models of light reflection/refraction/absorption phenomena in various types of paper structures based on the analysis of their microscopic images. But processing time (the time it takes to complete one calculating step) for the considered modelled sample of paper is about approximately 29 sec on Intel Pentium 2.50 GHz processor. It is obvious that parallel or distributed processing is necessary for such applications.

This study actually supports our idea or even prove that the given structures with using paper as a material can provide reasonable decreasing light intensity in the area under the structures.

According to the simulation results of the modelled paper sample, we also considered an optimal design of the given geometry model that is optimal with respect to the basic designed profiled model. The criterion for the distribution of light intensity using geometric field tracing is implemented in the form of the RRT algorithm. We do not present here results of shape improving with respect to the simulated

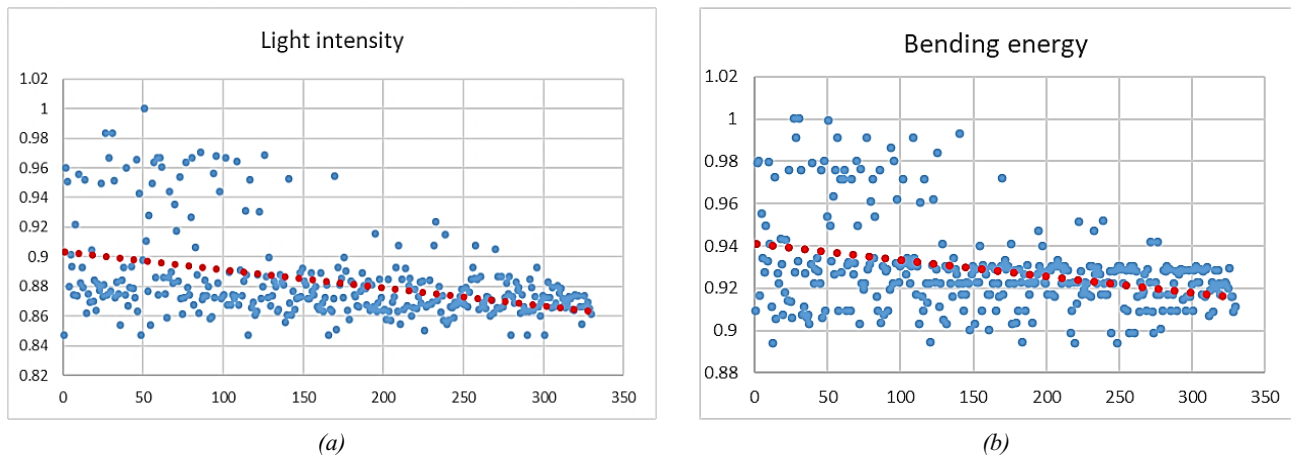


Figure 6. (a) Illustration of light intensity distribution during GA iteration steps. (b) Bending energy values. In both plots, red dots illustrate a linear dependency

light propagation characteristic. Let us notice that there is no distinct difference between the improved model attained by using the K-M light propagation model [1] and discussed in this paper. Nevertheless, to prove applicability developed paper model we have to show agreement between modelled light propagation data and measurements that is seen as our urgent future task. There is an interesting question of defining a fitness function for optimization of profiled models. Polarized light is produced by the interactions of unpolarized light with materials, particles, and surfaces. So, we can define a fitness function as a result of all propagated lights through a media or as a flux of polarized light. This is an open question which requires future consideration. There is also intriguing question of obvious correlation between bending energy of the profiled models and light scattering distribution.

Naturally, to confirm the results obtained in this study, more experiments would need to be conducted. Nevertheless, our numerical simulation of light propagation through a fibre like structure shows almost exponentially decaying dependence on the thickness of the paper sample.

REFERENCES

1. Savchenko M., Savchenko V., Abe A., Hagiwara I., Thai P. T. A Study on an Origami-Based Structure for Use as a Sun Umbrella. *SN Applied Sciences*. 2020;2(7):1278. DOI: <https://doi.org/10.1007/s42452-020-3018-3>.
2. Yu Y. *UV Interactions with Fibres and Fibrous Structures*. Dissertation, Deakin University, Australia. 2015. Available at: <http://hdl.handle.net/10536/DRO/DU:30084236>.
3. *Paper Umbrellas*. Available at: <https://www.pinterest.com/dharamayavat/paper-umbrellas>.
4. Kubelka P. New Contributions to the Optics of Intensely Light-Scattering Materials. Part I. *Journal of the Optical Society of America*. 1948; 38(5):448-457. DOI: <https://doi.org/10.1364/JOSA.38.000448>.
5. Kubelka P. New Contributions to the Optics of Intensely Light-Scattering Materials. Part II. *Journal of the Optical Society of America*. 1954; 44(4):330-335. DOI: <https://doi.org/10.1364/JOSA.44.000330>.
6. Lvovsky A. I. Fresnel Equations. *Encyclopedia of Optical and Photonic Engineering*. New York; 2013. Pp. 1-6.
7. Kouko J., Turpeinen T., Kulachenko A., Hirn U., Retulainen E. Understanding Extensibility of Paper: Role of Fibre Elongation and Fibre Bonding. *Tappi Journal*. 2020;19(March):125-135. DOI: [10.32964/TJ19.3.125](https://doi.org/10.32964/TJ19.3.125).
8. Granberg H., Béland M.-C. Modelling the Angle-Dependent Light Scattering from Sheets of Pulp Fibre Fragments. *Nordic Pulp and Paper Research Journal*. 2004;19(3):354-359. DOI: [10.3183/NPPRJ-2004-19-03-p354-359](https://doi.org/10.3183/NPPRJ-2004-19-03-p354-359).
9. Carlsson J., Persson W., Hellentin P., Malmqvist L. The Propagation of Light in Paper: Modelling and Monte-Carlo Simulations. *Proceedings of the International Paper Physics Conference*. 1995;83-86.

10. Bjuggren M., Quinteros T., Béland M.-C., Krummenacher L., Mattsson L. Light and Paper: Progress Report 1995-96. *Institute of Optical Research Technical Report*. 1997;316.
11. Hainzl R., Berglind R., Bjuggren M., Beland M.-C., Quinteros T., Granberg H., Mattsson L. A New Light Scattering Model for Simulating the Interaction between Light and Paper. *Proceedings of the TAPPI International Printing and Graphic Arts Conference*. 2000;9–17.
12. Raunio J.-P. *Quality Characterization of Tissue and Newsprint paper based on Image Measurements; Possibilities of On-line Imaging*. Dissertation, Tampere University of Technology, Publication 1270. 2014. ISBN 978-952-15-3416-4, ISSN 1459-2045.
13. Krölinga H., Endresb A., Nubboc N., Fleckensteinc J., Miletzkyb A., Schabel S. Anisotropy of Paper and Paper Based Composites and the Modelling Thereof. *ECCM16 – 16th European Conf. on Composite Materials*, Seville, Spain, 22-26 June 2014.
14. Hubbe M., Pawlak J., Koukoulas A. Paper's Appearance: A Review. *Bioresources*. 2008;3(2). DOI: 10.15376/biores.3.2.627-665.
15. Li Y., Fu Q., Yang X., Berglund L. Transparent Wood for Functional and Structural Applications. *Phil. Trans. R. Soc. A*. 2018;376:20170182. DOI: <http://dx.doi.org/10.1098/rsta.2017.0182>.
16. Chen H., Baitenov A., Li Y., Vasileva E., Popov S., Sychugov I., Yan M., Berglund L. Thickness Dependence of Optical Transmittance of Transparent Wood: Chemical Modification Effects. *ACS Appl. Mater. Interfaces*. 2019;11(38):35451–35457. DOI: <https://doi.org/10.1021/acsami.9b11816>.
17. Born M., Wolf E. *Principles of Optics*. Sixth Corrected ed., Pergamon, Oxford; 1989.
18. Grundy W. M., Doute S., Shmitt B. A Monte Carlo Ray-Tracing Model for Scattering and Polarization by Large Particles with Complex Shapes. *Journal of Geophysical Research*. 2000;105(E12):29291-29314. DOI: <https://doi.org/10.1029/2000JE001276>.
19. Kumar L., Silva L. Light Ray Tracing trough a Leaf Cross Section. *LARS Technical Reports*. 1972;16. Available at: <http://docs.lib.purdue.edu/larstech/16>.
20. Simon K., Trachsler B. A Random Walk Approach for Light Scattering in Material. *Discrete Mathematics and Theoretical Computer Science AC*. 2003;289–300.
21. Gustafsson Coppel L., Edström P. Open Source Monte Carlo Simulation Platform for Particle Level Simulation of Light Scattering from Generated Paper Structures. *Papermaking Research Symposium* [Internet]. 2009. Available at: <http://urn.kb.se/resolve?urn=urn:nbn:se:miun:diva-9122>.
22. Elvins T. T. A Survey of Algorithms for Volume Visualization. *Computer Graphics*. 1992;26(3):194-201.
23. Havran V., Sixta F. Comparison of Hierarchical Grids. *Ray Tracing News*. 1999;12(1). Available at: <http://jedi.ks.uiuc.edu/~johns/raytracer/rtn/rtnv12n1.html#art3>.
24. Vasilenko V. A. *Spline-functions: Theory, Algorithms, Programs*. Novosibirsk: Nauka Publishers; 1983.

DOI: 10.51790/2712-9942-2020-1-1-8

MEDICAL AND BIOLOGICAL CYBERNETICS: DEVELOPMENT PROSPECTS**Valery M. Eskov¹, Vasiliy F. Pyatin², Yuliya V. Bashkatova**¹ *Surgut Branch of Federal State Institute "Scientific Research Institute for System Analysis of the Russian Academy of Sciences", Surgut, Russian Federation, firing.squad@mail.ru*² *Samara State Medical University, Samara, Russian Federation*

Abstract: life sciences advanced greatly in molecular and cell research for the last 40-50 years. However, the system-oriented approach lags behind. Since the times of N. Wiener, cybernetics switched to specific problems and ceased to be the primary science for studying complex systems. We believe the reason for this is the general crisis of deterministic and stochastic approaches to living systems. The revival of medical and biological cybernetics as a science of control in biological systems is possible only through a new understanding of the regulation and operation principles of any complex biosystems. Such a new understanding should be based on new principles of biosystem regulation, as chaos and repetitive processes shall prevail over deterministic certainty or stochastic uncertainty. A special role in this revival of interest in cybernetics is given to the new chaos-self-organization theory, which is now being developed by several teams in Moscow, Tula, Samara, and Surgut. This new area of research is based on the Eskov-Zinchenko effect (lack of statistical robustness of any human body properties) and new models of the biosystem state vector behavior $x=x(t)=(x_{12}, x_{21}, \dots, x_m)^T$ in the phase state space.

Keywords: stochastics, chaos, self-organization, Eskov-Zinchenko effect.

Cite this article: Eskov V. M., Pyatin V. F., Bashkatova Yu. V. Medical and Biological Cybernetics: Development Prospects. *Russian Journal of Cybernetics*. 2020;1(1):54–62. DOI: 10.51790/2712-9942-2020-1-1-8.

МЕДИЦИНСКАЯ И БИОЛОГИЧЕСКАЯ КИБЕРНЕТИКА: ПЕРСПЕКТИВЫ РАЗВИТИЯ**В. М. Еськов¹, В. Ф. Пятин², Ю. В. Башкатова**¹ *Сургутский филиал Федерального государственного учреждения «Федеральный научный центр Научно-исследовательский институт системных исследований Российской академии наук»,**г. Сургут, Российская Федерация, firing.squad@mail.ru*² *Самарский государственный медицинский университет, г. Самара, Российская Федерация*

Аннотация: за последние 40–50 лет биологические науки сделали существенный прорыв в области молекулярно-клеточных исследований. При этом системный уровень за этот период претерпел существенное отставание. Со времен Н. Винера кибернетика перешла к решению частных задач, уйдя из области главных наук в изучении сложных систем. На наш взгляд, такая ситуация обусловлена общим кризисом детерминистского и стохастического подходов в изучении живых систем. Возрождение медицинской и биологической кибернетики как науки об управлении в биологических системах возможно только в связи с новым пониманием принципов регуляции и функционирования любых сложных биосистем (*complexity*). Это новое понимание должно базироваться на новых принципах регуляции биосистем, в которых хаос и многократные повторения одних и тех же процессов должны превалировать над детерминистской определенностью или стохастической неопределенностью. В этом возрождении интереса ко всей кибернетике особую роль должна сыграть новая теория хаоса-самоорганизации, которая сейчас разрабатывается несколькими научными школами Москвы, Тулы, Самары и Сургута. В основе этого нового научного направления лежит эффект Еськова–Зинченко (отсутствие статистической устойчивости любых параметров организма человека) и новые модели поведения вектора состояния биосистемы $x = x(t) = (x_{12}, x_{21}, \dots, x_m)^T$ в фазовом пространстве состояний.

Ключевые слова: стохастика, хаос, самоорганизация, эффект Еськова–Зинченко.

Для цитирования: Еськов В. М., Пятин В. Ф., Башкатова Ю. В. Медицинская и биологическая кибернетика: перспективы развития. *Успехи кибернетики*. 2020;1(1):54–62. DOI: 10.51790/2712-9942-2020-1-1-8.

Introduction

Two outstanding scientists who contributed greatly to the rapid development of cybernetics (as a science of control in animate and inanimate nature) in the mid-20th century are P. K. Anokhin [1] and N. Wiener. We should emphasize that P. K. Anokhin introduced the concept of acceptors of action results applied to the work of any functional system of the human organism (FSO.) The purpose of the FSO functioning in P. K. Anokhin's theory is gaining benefits for the body. He introduced the concept of feedback that adjusts the activities of any FSO. However, till today a strict mathematical definition of the "utility" concept and of the action acceptor functioning is not available; the latter and little studied.

N. Wiener praised P. K. Anokhin's works, but for 70-80 years, biocybernetics in its development followed deterministic and stochastic models. Now we can claim that some slowing down the cybernetics progress are caused by the efforts of deterministic-stochastic approach (DSA) advocates when describing processes in living systems. However, as far back as 1948 *W. Weaver* [2] categorized living systems as a separate class of type III systems (3TS.) Following the logic of *W. Weaver*, such 3TSs would have to be modeled within some other (not DSA) approach [2]. However, for more than 70 years nothing new was created to build a mathematical theory for describing the 3TS-complexity [3–11]. During this period, no one attempted to study the properties of 3TS; living systems were studied with DSA [3–6].

Such a delay with the development of biocybernetics is precisely due to the global limitations of DSA methods in describing living systems. Still, the compartmental-cluster theory of biosystems (CCTBS) [12–13] was created in the last 25-30 years, and the theory of chaos-self-organization (CSO) is in the making. The emergence of CCTBS and CSO significantly changes our understanding of the regulation and control principles in biosystems [14]. It is now becoming apparent that the DSA cannot describe the real properties of living systems (3TS according to *W. Weaver*.) We expect that CSO will open new perspectives in the development of biocybernetics and cybernetics [15–17].

Prerequisites for the Development of CSO and New Biocybernetics

Originally, in the 1930-50s, P. K. Anokhin proposed the basic operation principles of various regulatory systems in human and animal organisms. P. Anokhin criticized I. Pavlov's theory of reflexes, emphasizing the linearity of any reflex [1]. P. K. Anokhin introduced the concept of the acceptor of action results, i.e., he was the first to emphasize the importance of feedback for any regulatory system. With such feedbacks, an action acceptor eventually corrects the activity of both the FSO and the organism as a whole [15–16].

P. K. Anokhin highlighted that the human body is supported by the operation of its various functional systems (FSO.) These FSOs are expected to give some benefits through their activities. The action result acceptor should support a steady-state of the organism under various (and chaotic) environmental changes or by changing the FSO itself. The FSO should support not only homeostasis but also various types of life activities (including thinking.) P. K. Anokhin emphasized the presence of feedbacks in living nature, and this was appreciated by N. Wiener as he developed the foundations of cybernetics.

We emphasize that cybernetics of the 20th century paid special attention to reverse feedbacks. However, as early as the end of the 19th century, A. A. Bogdanov emphasized the importance of positive feedback in living systems. at the turn of the 19th and 20th centuries, in his *Tectology*, A. A. Bogdanov tried to develop a generalized systems theory where both types of feedbacks were equally applied. *H. Haken* (1969) noted positive feedbacks as he tried to develop synergy as a complement and extension of cybernetics [18]. However, synergy was not properly developed, either [3, 8, 15]. After a certain surge at the end of the 20th century, now we see some decline in the interest in synergy [4, 8, 11, 15].

What is the reason for such a decline in the development of cybernetics as a control theory in complex systems and synergy in the 21st century? Is this natural, or are there any subjective reasons to blame? We should note that as early as *I. R. Prigogine* (as a final result of his entire career) talked about the end of the deterministic approach to living systems [19]. In his final work *The end of Certainty*, *I. R. Prigogine* wrote that all processes in living systems are irreversible. Living systems are far from equilibrium, so for such systems, he developed thermodynamics of nonequilibrium systems (TNS.)

Note that TNS is a linear theory, while all living systems (it was also emphasized by *H. Haken* in his *Synergy* [18]) are nonlinear. The concept of non-linearity in mathematics is associated with the presence of non-linear elements on the right side of differential equations describing the behavior of systems in

animate and inanimate nature. A typical example of such models is the Verhulst-Pearl equation, with reverse feedback. The equation itself contains a quadratic term on the right-hand side (this equation has a historical value since it was created almost 200 years ago.)

I. R. Prigogine failed to switch from linear to nonlinear TNS theory. It is obvious that now TNS may suffer the fate of the *I. Pavlov* reflex theory in physiology. All the sciences of living systems (or 3TS according to *W. Weaver*) require a non-linear approach. But what is the essence of such non-linearity? Two Nobel laureates tried to answer this question at the end of the 20th century (*I. R. Prigogine* and *M. Gell-Mane*.) They tried to introduce the concept of “complexity” for describing 3TS and living systems, but over these 35 years a strict definition of “complexity” was not proposed in all of world science.

J. Horgan, a renowned historian of science, has wryly stated on this subject [20] that *S. Lloyd* in the 1990s offered no less than 30 definitions of “complexity”, but there is no strict definition of the term till today. There is no understanding of what this term means (in DSA) since the dynamic Lorentz chaos has nothing to do with living systems (3TS) [3-6].

It is essential that it is *I. R. Prigogine* and *M. Gell-Mann* tried to describe 3TS-complexity using the Lorentz dynamical chaos theory, but their efforts were unsuccessful. In the new chaos-self-organization theory (CSO) we proved that Lorentz’s theory is inapplicable to living systems. However, the deterministic approach should not be written off. The compartmental-cluster theory of biosystems (CCTBS) was developed at the end of the 20th century [10–13]. The core of the CCTBS is a system of equations:

$$\frac{dx}{dt} = A(y)x - bx + ud, \quad (1)$$

$$y = C^T x, \quad (2)$$

where the biosystem state vector $x(t)=(x_1, x_2, \dots, x_m)^T$ can be in the stationary modes (SM) as $dx/dt \neq 0$. We emphasize that living systems cannot be in such stationary modes, so in CSO we introduce a completely different understanding of SM. Note that the systems (1) contain the dissipative term $-bx$ and external drivers, represented as ud . CCTBS describes dissipative biosystems away from equilibrium, but the equilibrium characteristics are not presented. In reality, living systems (systems of the third type according to *W. Weaver*) not only lack SM but also cannot demonstrate statistical robustness for consecutive samples x_i [14].

We proved (in CSO) that CCTBS is a transitional theory from DSA to CSO. However, CCTBS models can describe the statistical chaos of 3TS if we switch to equations with a discontinuous right-hand side (the theory was developed by *A. F. Filippov* and *V. A. Galkin* [21–22].) Statistical chaos can be deduced in CCTBS, which proves the *Eskov-Zinchenko* (EZE) effect [23]. Once again, we emphasize that the CCTBS is a transitional theory between the deterministic approach and the new CSO. The CSO proves uncertainties of the 1st and 2nd kind, which are not present in the DSA, but the first uncertainties related to the number of elements (and their behavior) in the compartment are already introduced in the CCTBS.

All living systems (LSS) can be characterized as max indeterminate systems that meet the main system principle: the behavior of a single element does not affect the evolution of the entire system. In CCTBS this is already strictly followed while constructing clusters and compartments, but the evolution of clusters and compartments are described by the system (1.) In system (1), the matrix function $A(y)$, where $y(t)$ is the 3TS-complexity output function, has certain (generic) constraints. In general, CCTBS was the beginning of the transition to the third paradigm of natural science [3, 11, 15] and to the CSO, where uncertainty is a key concept. Why are we now talking about the need to move to the third paradigm and CSO? To answer this question, let us consider some experimental evidence for the particular chaotic nature of the 3TS [23].

N. A. Bernstein Hypothesis and the Eskov-Zinchenko Effect

The hypothesis of “repetition without repetition” [24] was proposed by *N. A. Bernstein* in 1947, but we could prove it only 20-25 years ago [14]. Having said that, *W. Weaver* in 1948 [2] only suggested the hypothesis about special 3TSs. Still, there is no understanding of the special 3TS complexity in modern science. We work in biomedicine, psychology, environmental studies using functional analysis (determinism) and a stochastic approach. It is common for medical and biological cybernetics (without any prospects for

development.) About 25 years ago the N. A. Bernstein hypothesis was proved, and the concept of EZE was introduced, i.e. the concept of statistical sampling instability in biomechanics [3, 14].

EZE was discovered in biomechanics and then extended to other FSOs, such as the cardiovascular system (CVS) [8–11, 17]. Note that in biomechanics, EZE is the most pronounced, since the share of stochasticity is minimal (below 10%.) Let us consider EZE as applied to specific examples from biomechanics for tremorograms (TMG) and tappinggrams (TPG) as examples of involuntary (TMG) and arbitrary (TPG) movements [25]. Later EZE was also proved as applied to the physiology of the CPS and other properties of the human body.

Refer to Table 1 as an example. It presents the Wilcoxon p criteria in a matrix of pairwise comparisons of 15 tremorogram samples consequentially acquired from the same person in their unchanged physiological state. If $p \geq 0.05$, such a TMG pair would have one (total) parent population. It follows from Table 1 that k_1 (for $p \geq 0.05$) is extremely small ($k_1=3$) It means that there is no statistical robustness in the TMG samples. The samples with probability $\beta \geq 0.95$ are not statistically similar, and it proves the special properties of 3TS-complexity. Note that such statistical chaos has nothing in common with the Lorentz chaos so much praised by I. R. Prigogine [19], M. Gell-Mann and S. Lloyd.

Table 1

Pairwise comparison matrix of tremorogram samples for the same person (no-load, $n = 15$ repetitions).
Wilcoxon criterion is used (significance: $p < 0.05$, matches: $k_1 = 3$)

	1	2	3	4	5	6	7	8	9	10	11	12	13	14	15
1		0,00	0,00	0,00	0,00	0,00	0,00	0,00	0,00	0,00	0,00	0,00	0,00	0,00	0,00
2	0,00		0,00	0,00	0,00	0,00	0,00	0,00	0,00	0,00	0,00	0,00	0,00	0,00	0,00
3	0,00	0,00		0,00	0,00	0,00	0,00	0,00	0,00	0,00	0,00	0,00	0,00	0,00	0,00
4	0,00	0,00	0,00		0,00	0,00	0,00	0,00	0,00	0,00	0,00	0,00	0,00	0,00	0,00
5	0,00	0,00	0,00	0,00		0,00	0,00	0,00	0,00	0,00	0,00	0,00	0,00	0,00	0,00
6	0,00	0,00	0,00	0,00	0,00		0,00	0,00	0,00	0,00	0,00	0,00	0,00	0,00	0,00
7	0,00	0,00	0,00	0,00	0,00	0,00		0,00	0,01	0,00	0,00	0,00	0,00	0,00	0,00
8	0,00	0,00	0,00	0,00	0,00	0,00	0,00		0,00	0,00	0,00	0,00	0,00	0,00	0,00
9	0,00	0,00	0,00	0,00	0,00	0,00	0,01	0,00		0,00	0,00	0,00	0,00	0,00	0,00
10	0,00	0,00	0,00	0,00	0,00	0,00	0,00	0,00	0,00		0,51	0,00	0,00	0,01	0,70
11	0,00	0,00	0,00	0,00	0,00	0,00	0,00	0,00	0,00	0,00	0,51		0,00	0,00	1,00
12	0,00	0,00	0,00	0,00	0,00	0,00	0,00	0,00	0,00	0,00	0,00	0,00		0,00	0,00
13	0,00	0,00	0,00	0,00	0,00	0,00	0,00	0,00	0,00	0,00	0,00	0,00	0,00		0,00
14	0,00	0,00	0,00	0,00	0,00	0,00	0,00	0,00	0,00	0,01	0,00	0,00	0,00	0,00	
15	0,00	0,00	0,00	0,00	0,00	0,00	0,00	0,00	0,00	0,70	1,00	0,00	0,00	0,00	

Table 1 and hundreds of similar ones [3, 5, 22, 25] prove the N. A. Bernstein hypothesis about “repetition without repetition” [24]. The hypothesis is now expressed as the Eskov-Zinchenko effect (EZE), based on the statistical instability of not only biomechanical properties (refer to Table 1 for TMG), but also for many other body properties of any human being. Now let us consider the statistical chaos of electromyograms (EMG) (refer to Table 2, where $k_2=6$), and RR intervals (RRI) (refer to Table 3, where $k_3=10$) and many other properties of the human body.

Indeed, Table 2 is a pairwise comparisons matrix for EMG samples (at fixed tension $F_1=50 N$) and RRI samples (Table 3) also for the same person (in a relaxed state.) In any case, the share of stochasticity in such pairwise comparison matrices of TMG, EMG, and RRI samples is extremely small. For TMG $k_1 < 5\%$, for EMG $k_2 < 10\%$, while for RRI $k_3 < 20\%$. We built hundreds of such matrices both for individuals (for $n=15$ repetitions) and for groups with various 3TS-complexity properties.

In all the matrices for the different SSS, EEG, EMG, TMG, etc. values, the number of k pairs meeting Wilcoxon, Newman-Keuls, Kraskell-Wallis criteria $p \geq 0.05$ is extremely small. It is impossible to arbitrarily reproduce samples of any x_i , i.e. $x(t)$ samples of the human body state. We deal with processes that demonstrate “repetition without repetition” i.e., EZE. One wonders why for more than 70 years nobody working in the living system research tried to test the statistical robustness of $x(t)$ samples. For more

Table 2

Pairwise comparison matrix of electromyograms (EMG) for the same person, low muscle tension ($p = 50$ N). Wilcoxon criterion is used (significance: $p < 0.05$, matches: $k_2 = 6$)

	1	2	3	4	5	6	7	8	9	10	11	12	13	14	15
1		0,00	0,00	0,00	0,51	0,00	0,00	0,00	0,00	0,00	0,00	0,00	0,00	0,00	0,00
2	0,00		0,03	0,05	0,00	0,00	0,00	0,00	0,00	0,00	0,00	0,00	0,00	0,00	0,00
3	0,00	0,03		0,87	0,00	0,00	0,00	0,00	0,00	0,00	0,00	0,00	0,00	0,00	0,00
4	0,00	0,05	0,87		0,00	0,00	0,00	0,00	0,00	0,00	0,00	0,00	0,00	0,00	0,00
5	0,51	0,00	0,00	0,00		0,00	0,00	0,00	0,00	0,00	0,00	0,00	0,00	0,00	0,00
6	0,00	0,00	0,00	0,00	0,00		0,00	0,00	0,71	0,00	0,00	0,00	0,00	0,00	0,00
7	0,00	0,00	0,00	0,00	0,00	0,00		0,00	0,00	0,00	0,00	0,04	0,01	0,00	0,01
8	0,00	0,00	0,00	0,00	0,00	0,00	0,00		0,00	0,00	0,00	0,00	0,00	0,00	0,00
9	0,00	0,00	0,00	0,00	0,00	0,71	0,00	0,00		0,00	0,00	0,00	0,00	0,00	0,00
10	0,00	0,00	0,00	0,00	0,00	0,00	0,00	0,00	0,00		0,00	0,00	0,07	0,00	0,00
11	0,00	0,00	0,00	0,00	0,00	0,00	0,00	0,00	0,00	0,00		0,00	0,00	0,45	0,00
12	0,00	0,00	0,00	0,00	0,00	0,00	0,04	0,00	0,00	0,00	0,00		0,26	0,00	0,00
13	0,00	0,00	0,00	0,00	0,00	0,00	0,01	0,00	0,00	0,07	0,00	0,26		0,00	0,00
14	0,00	0,00	0,00	0,00	0,00	0,00	0,00	0,00	0,00	0,00	0,45	0,00	0,00		0,00
15	0,00	0,00	0,00	0,00	0,00	0,00	0,01	0,00	0,00	0,00	0,00	0,00	0,00	0,00	

Table 3

Pairwise comparison matrix of RR interval samples for the same person (no-load, $n = 15$ repetitions). Wilcoxon criterion is used (significance: $p < 0.05$, matches: $k_3 = 10$)

	1	2	3	4	5	6	7	8	9	10	11	12	13	14	15
1		0,02	0,00	0,00	0,00	0,00	0,00	0,00	0,00	0,00	0,56	0,00	0,00	0,00	0,00
2	0,02		0,00	0,00	0,00	0,00	0,00	0,09	0,00	0,05	0,24	0,00	0,00	0,00	0,04
3	0,00	0,00		0,00	0,00	0,00	0,00	0,00	0,00	0,00	0,00	0,00	0,00	0,00	0,00
4	0,00	0,00	0,00		0,89	0,00	0,00	0,00	0,00	0,00	0,00	0,00	0,00	0,00	0,00
5	0,00	0,00	0,00	0,89		0,00	0,00	0,00	0,00	0,00	0,00	0,00	0,00	0,00	0,00
6	0,00	0,00	0,00	0,00	0,00		0,16	0,00	0,00	0,00	0,00	0,00	0,00	0,00	0,00
7	0,00	0,00	0,00	0,00	0,00	0,16		0,00	0,00	0,00	0,00	0,00	0,00	0,00	0,00
8	0,00	0,09	0,00	0,00	0,00	0,00	0,00		0,00	0,72	0,00	0,00	0,00	0,00	0,80
9	0,00	0,00	0,00	0,00	0,00	0,00	0,00	0,00		0,00	0,00	0,00	0,40	0,02	0,00
10	0,00	0,05	0,00	0,00	0,00	0,00	0,00	0,72	0,00		0,00	0,00	0,00	0,00	0,66
11	0,56	0,24	0,00	0,00	0,00	0,00	0,00	0,00	0,00	0,00		0,00	0,00	0,00	0,00
12	0,00	0,00	0,00	0,00	0,00	0,00	0,00	0,00	0,00	0,00	0,00		0,00	0,00	0,00
13	0,00	0,00	0,00	0,00	0,00	0,00	0,00	0,00	0,40	0,00	0,00	0,00		0,92	0,00
14	0,00	0,00	0,00	0,00	0,00	0,00	0,00	0,00	0,02	0,00	0,00	0,00	0,92		0,00
15	0,00	0,04	0,00	0,00	0,00	0,00	0,00	0,80	0,00	0,66	0,00	0,00	0,00	0,00	

than 70 years since the publication of N. A. Bernstein [24] and W. Weaver [2] no one researcher checked the statistical robustness of samples of any human body properties. Over the past 150–200 years, science confidently operated with various statistical methods but had no insight into the statistical instability of x_i biosystem samples [11, 14–15, 19–23]. The modern science of living systems is under the illusion that human body property samples are statistically robust, although any such sample is unique (historical).

Uncertainties of the 1st and 2nd Kind in CSO: the Problem of Invariant Selection

With hundreds of matrices similar to Tables 1, 2, 3 we can apply the uncertainty of the 2nd kind to biology, psychology, medicine, environmental studies, and other “non-exact” sciences. We use the

term “non-exact” because any sample x_i of both one person (for repeated measurements) and a group (for repeated x_i measurements) is unique. The sample is arbitrarily unique from a stochastic point of view. In other words, it concerns not only statistical distribution functions $f(x)$ due to their mismatch, but also spectral signal densities (SSD), autocorrelations $A(t)$ and other statistical characteristics of any human body property [26-30].

In medical and biological cybernetics, there is a global problem with the identification and simulation of stationary modes (SM) in complex biosystems. It is impossible to come to a stationary mode within the framework of determinism (functional analysis), i.e. to obtain $dx/dt=0$ and $x_1=const$ for 3TS. However, from the EZE viewpoint and the uncertainty of the 2nd kind, it is impossible to maintain the statistical functions $f(x)$, SSD, $A(t)$ unchanged, and all stochasticity (as we prove) is unique. This means that the sample x_i obtained at the time interval Δt_1 cannot be arbitrarily reproduced at the next interval Δt_2 (at $\Delta t_1=\Delta t_2$.) Any sample is unique, it is historical and cannot be predicted in the future [24-25].

It is high time to stop using stochastic approaches to the study and simulation of any biosystem. If a biosystem is unchangeable (in the physiological, biological sense), its properties will be statistically unstable. There is the problem of choosing invariants to describe the stationary modes of 3TS-complexity. How can we register the changes in the biosystem if $dx/dt=0$ is continuous in the unchanged state, while $f(x)$, SSD, $A(t)$ are continuous and change chaotically?

Note that the Lorentz dynamical chaos (two Nobel laureates *I. R. Prigogine* [19] and *M. Gell-Mann* had great hopes for it) has nothing to do with the description of complex biosystems – 3TS, either [14]. In Lorentz attractors, we have invariants, i.e. we register a uniform distribution, and $f(x)$, SSD, $A(t)$ do not change. For 3TS, the situation is the opposite: everything changes continuously and chaotically. We need new invariants, new concepts of static and dynamical (evolution) states of 3TS-complexity, which could describe the uncertainty of the 2nd kind [14].

Now it is proved that uncertainties of the 1st kind exist in CSO, as stochasticity indicates that the samples of properties x_i do not change, while by other methods we record real changes (evolution) of the biosystem. Uncertainties of the 1st and 2nd kind exchange the concepts of statics (unchanged 3TS properties) and kinematics (3TS evolution.) What in stochasticity is considered unchanged (x_i samples), shows statistical instability in CSO. On the contrary, what can be considered unchanged in stochasticity (samples do not statistically vary for different physiological states), in CSO can be estimated as significant changes (evolution.)

There are significant contradictions between stochasticity and the real behavior of human body function properties. It is necessary to develop new biocybernetics that considers uncertainties of the 1st and 2nd kind. At the same time, it is necessary to develop new invariants and new models for describing 3TS-complexity. Now we are creating such a theory as CSO based on the new, third paradigm of natural science [3–5, 10–11]. These paradigms are deterministic (based on functional analysis), stochastic, and CSO-based [3–5, 10–11].

CSO-Based Biocybernetics Development Prospects

The core of the third paradigm and CSO is the concept of uncertainty. In the deterministic approach, everything is strictly defined: both the initial state $x(t_0)$ as the Cauchy problem, the entire process path in the phase state space (PSS), and the final state of the system $x(t_k)$. We can repeat the process many times and get to the point $x(t_k)$ in the PSS many times.

In stochasticity, we have a strict (repeating), definite $x(t_0)$, since the experience shall be repeatable, but getting to a finite point $x(t_k)$ is a nearly impossible task in PSS for a continuous random variable. However, we can obtain a sample $x_i(t_k)$ and repeat the statistical function $f(x)$, SSD, $A(t)$, etc. Under stochasticity, we have invariants if nothing happens to the system and if $x(t_0)$ is repeated many times.

The situation with 3TS is completely different. In CSO, we cannot arbitrarily reach $x(t_0)$, repeat the $x(t)$ path in PSS, or repeat samples $x(t_k)$. Everything changes constantly and chaotically. Therefore, we had to introduce new invariants for stationary modes of 3TS-complexity and define new concepts of statics and kinematics for the state vector of the biosystem $x(t)$ in the PSS. In CSO we introduced a concept similar to the Heisenberg uncertainty principle applied to errors (more precisely, to variation margins) for any variable x_{i1} and its change rate $x_{i2}=dx_{i1}/dt$.

In such a two-dimensional phase state space of the vector $xi=(x_{i1}, x_{i2})^T$, we can define properties

of some limited PSS region (as a pseudoattractor [PA] or Eskov quasiattractor), where the vector $x_i(t)$ moves continuously and chaotically. The area S of such a PA, its center coordinates are invariant for the given physiological state of the biosystem. We proved it in numerous studies of recorded TMG, tappinggrams (TPG), EMG, CVS properties, electroencephalograms (EEG), electroneurograms (ENG) and many other properties x_i of the human body [21–23, 26–30].

The introduction of new invariants as PA properties based on the uncertainty x_i made it possible to develop new simulation models of 3TS-complexity even within the deterministic approach. For this purpose, we used models from the compartmental-cluster theory of biosystems (CCTBS) with the addition [12–13] of discontinuous functions to the right side of the differential equations [21, 22]. It turned out that CCTBS produces matrices similar to Tables 1, 2, 3 and thousands of others (with low k_1, k_2, k_3 values.)

With PA estimation in psychology, medicine, environmental studies we could identify the real differences between various physiological states of both an individual and groups. These individuals can be in different states and we can detect the differences between using the uncertainty of the 2nd kind. Moreover, we used two main properties of 3TS (continuous reverberations, i.e., $dx/dt \neq 0$, and chaos $x(t)$) to run neural networks. Finally, we arrived at the modeling of heuristic brain activities [11]. Chaos and reverberations are the attributes of any living system. It is a foundation of CSO and the third paradigm [26–30].

Conclusion

Over the past 40–50 years there was some decline in research interest in cybernetics as a theory of system regulation (it divided into many areas) and in biomedical cybernetics in particular. However, the general problems of control in living and nonliving systems are still relevant today. In our opinion, it is now possible to revive such interest due to the discovery of the systems of the 3rd kind (3TS-complexity) and the proof of their special properties [26–27].

We are talking about the lack of statistical robustness of any human body (or a group of persons) properties x_i in an unchanged physiological state. As a result, the Eskov-Zinchenko effect (EZE) was proved, new invariants for the biosystem state vector (based on pseudoattractors) were introduced, uncertainties of the 1st and 2nd kind were presented, and the models of 3TS behavior were developed. The key novelty is the special uncertainty (and it is global) of any properties x_i of the biosystem [25, 26–30].

As a result, we came up with new models of heuristic human brain activity and new models used in personalized medicine. We think that there are new prospects for medical and biological cybernetics by studying uncertainties of the 1st and 2nd kind, building mathematical models with a discontinuous right part (CCTBS-based) in the area of personalized medicine, psychology, and environmental studies. At the same time, we propose some methods for system synthesis, i.e. finding order properties (key diagnostic features.) All this is a foundation for the development of new areas in biocybernetics and medicine and opens up new prospects for the development of cybernetics in general. The future of cybernetics is studying living systems, the principles of their organization, and the complexity of the systems of the 3rd kind.

REFERENCES

1. Anohin P. K. *Cybernetics of Functional Systems*. M.: Meditsina; 1998. 400 p. (In Russ.)
2. Weaver W. Science and Complexity. *American Scientist*. 1948;36:536–544.
3. Eskov V. M., Filatova O. E., Bashkatova Yu. V., Nuvaltseva Ya. N., Vedeneeva T. S. A New Understanding of Statics in Biomechanics and the Problem of Homeostasis Standards. *Complexity. Mind. Postnonclassic*. 2019;3:22–31. (In Russ.)
4. Eskov V. M., Arshinov V. I. State of Science in Modern Russia. *Complexity. Mind. Postnonclassic*. 2019;3:32–41. (In Russ.)
5. Popov Yu. M., Ivanova N. V., Beloshchenko D. V., Porosinin O. I., Ignatenko A. P. Chaos Hierarchy in Motion Control Systems. *Complexity. Mind. Postnonclassic*. 2018;4:24–33. (In Russ.)
6. Prokhorov S. A., Gumarova O. A., Monastyretskaya O. A., Khvostov D. Yu., Afanevich I. A. Unstable Systems: the Problem of Homogeneity of Groups. *Complexity. Mind. Postnonclassic*. 2019;1:62–72. (In Russ.)

7. Eskov V. M., Eskov V. V., Gavrilenko T. V., Zimin M. I. Uncertainty in the Quantum Mechanics and Biophysics of Complex Systems. *Moscow University Physics Bulletin*. 2014;69(5):406–411.
8. Eskov V. M. Evolution of the Emergent Properties of Three Types of Societies: The Basic Law of Human Development. *Emergence: Complexity and Organization*. 2014;16(2):107–115.
9. Eskov V. M., Eskov V. V., Gavrilenko T. V., Vochmina J. V. Biosystem Kinematics as Evolution: Stationary Modes and Movement Speed of Complex Systems: Complexity. *Moscow University Physics Bulletin*. 2015;70(2):140–152.
10. Eskov V. M., Eskov V. V., Vochmina J. V., Gavrilenko T. V. The Evolution of the Chaotic Dynamics of Collective Modes as a Method for the Behavioral Description of Living Systems. *Moscow University Physics Bulletin*. 2016;71(2):143–154.
11. Filatova O. E., Melnikova E. G., Gorbunov S. V., Nuvaltceva Ya. N. Peculiarities of Homeostatic Systems (Third Type). *Complexity. Mind. Postnonclassic*. 2019;2:28–39. (In Russ.)
12. Eskov V. M. Identification of Parameters of Linear Models of Transmitters. *Measurement Techniques*. 1993;36(4):365–368.
13. Eskov V. M., Filatova O. E. Respiratory Rhythm Generation in Rats: The Importance of Inhibition. *Neurophysiology*. 1993;25(6):348–353.
14. Filatova O. E., Gorbunov S. V., Shchipitsin K. P., Gumarova O. A., Korolev Yu. Yu. Concept of Uniformity for Experimental Groups in Biomechanics. *Complexity. Mind. Postnonclassic*. 2018;3:26–33. (In Russ.)
15. Popov Yu. M., Khvostov D. Yu., Muravyova A. N., Gumarova O. A. The Role of Paradigms and Methodology in the Development of Science. The Inevitability of the 3rd Paradigm. *Complexity. Mind. Postnonclassic*. 2018;4:34–43. (In Russ.)
16. Pyatin V. F., Galkin V. A., Eskov V. V., Ilyashenko L. K. Physical Bases of the Study and Modeling of the Brain Heuristic Activity. *Complexity. Mind. Postnonclassic*. 2018;4:59–67. (In Russ.)
17. Filatov M. A., Grigorieva S. V., Gorbunov D. V., Beloshenko D. V., Fadushina S. I. Heterogeneity of One-Time Samples of Parameters of Functional Systems of a Human Organism. *Complexity. Mind. Postnonclassic*. 2019;2:71–79. (In Russ.)
18. Haken H. Principles of Brain Functioning: a Synergetic Approach to Brain Activity, Behavior and Cognition. *Springer Series in Synergetics*. Springer; 1995. 349 p.
19. Prigogine I. R. The Philosophy of Instability. *Futures*. 1989;21(4):396–400.
20. Horgan J. *The End of Science. Facing the Limits of Knowledge in the Twilight of the Scientific Age*. Addison-Wesley, Helix; 1996.
21. Filippov A. F. Ordinary Differential Equations with Discontinuous Right-Hand Sides. *Math. Collection*. 1960;51(4):101–128. (In Russ.)
22. Galkin V. A. *Analysis of Mathematical Models: Systems of Conservation Laws, Boltzmann and Smoluchowski Equations*. M.: BINOM. Lab. znaniy; 2009. 408 p. (In Russ.)
23. Filatova O. E., Bazhenova A. E., Grigorieva S. V., Ilyashenko L. K. Estimation of the Parameters for Tremograms According to the Eskov–Zinchenko Effect. *Biophysics*. 2018;63(2):262–267.
24. Bernshtein N. A. *The coordination and regulation of movements*. Oxford, New York: Pergamon Press; 1967. 196 p.
25. Ilyashenko L. K., Bazhenova A. E., Berestin D. K., Grigorieva S. V. Chaotic Dynamics Parameters of the Tremograms at the Stress Exposure. *Russian Journal of Biomechanics*. 2018;22(1):62–71.
26. Shakirova L. S., Sinenko D. V., Voroshilova O. M., Ilyujkina I. V. The Application of Interattractor Distance Matrices to the Evaluation of Heart Rate Variability Spectral Power Distribution Parameters in School Students Travelling in the North-South Direction. *Complexity. Mind. Postnonclassic*. 2016;1:5–11. (In Russ.)
27. Nifontova O. L., Shakirova L. S., Nersisyan N. N., Rassadina Y. V. Dynamics of Spectral Power of Heart Rate Variability in Students the Latitudinal Movement. *Journal of New Medical Technologies, eEdition*. 2016;1:34–42. (In Russ.)
28. Shakirova L. S., Filatova D. Yu., Trusov M. V., Moroz O. A. Megafactory Matrix of Distances in the Assessment of Parameters of Cardiovascular System of Girls and Boys in Terms of Latitudinal Displacement. *Journal of New Medical Technologies, eEdition*. 2017;1:24–29. (In Russ.)

29. Filatov M. A., Filatova D. Yu., Himikova O. I., Romanova Yu. V. The Application of the Interattractor Distance Matrix Method to the Evaluation of Human Physiological Function Variables. *Complexity. Mind. Postnonclassic.* 2012;1:20–24. (In Russ.)
30. Eskov V. V., Filatov M. A., Filatova D. Yu., Prasolova A. A. The Boundaries of Determinism and Stochasticity as Applied to Biosystem Studies: Complexity. *Complexity. Mind. Postnonclassic.* 2016;1:83–91. (In Russ.)

DOI: 10.51790/2712-9942-2020-1-1-9

MATHEMATICAL MODEL AND SOFTWARE FOR AVALANCHE FORECASTING**Mikhail I. Zimin¹, Olga A. Kumukova², Mikhail M. Zimin¹**¹ 2554620 ONTARIO LTD., Toronto, Canada, zimin7@yandex.ru² High-Mountain Geophysical Institute, Nalchik, Russian Federation, kumukova@rambler.ru

Abstract: the study presents mathematical models and software for avalanche forecasting. They take into account the avalanche occurrence rate for specific slopes. The database is also presented.

Keywords: snow, avalanche, forecasting, danger, mathematical models and software.

Cite this article: Zimin M. I., Kumukova O. A., Zimin M. M. Mathematical Model and Software for Avalanche Forecasting. *Russian Journal of Cybernetics*. 2020;1(1):63–80. DOI: 10.51790/2712-9942-2020-1-1-9.

МАТЕМАТИЧЕСКОЕ И ПРОГРАММНОЕ ОБЕСПЕЧЕНИЕ ДЛЯ ПРОГНОЗИРОВАНИЯ ВОЗМОЖНОСТИ СХОДА СНЕЖНЫХ ЛАВИН**М. И. Зимин¹, О. А. Кумукова², М. М. Зимин¹**¹ 2554620 ONTARIO LTD., г. Торонто, Канада, zimin7@yandex.ru² Высогогорный геофизический институт, г. Нальчик, Российская Федерация, kumukova@rambler.ru

Аннотация: описано математическое и программное обеспечение для прогнозирования возможности схода снежных лавин. Учитываются данные о возникновении этих склоновых процессов с конкретных склонов. Описана база данных.

Ключевые слова: снег, лавина, прогноз, опасность, математическое и программное обеспечение.

Для цитирования: Зимин М. И., Кумукова О. А., Зимин М. М. Математическое и программное обеспечение для прогнозирования возможности схода снежных лавин. *Успехи кибернетики*. 2020;1(1):63–80. DOI: 10.51790/2712-9942-2020-1-1-9.

The paper is translated into English by the authors.

Introduction

RD 52.37.612-2000 Guideline [1] is currently used for avalanche danger forecasting in the Russian Federation. However, unexpected avalanches do occur, although rarely. Therefore, further improvement of the avalanche forecasting methods is of some interest.

The accuracy of avalanche forecasting can be improved by considering more extensive historical data. A separate database is created for each avalanche site. It complicates the forecasting center operations, but it certainly improves the quality of the risk estimation.

Avalanche Forecasting Algorithm

To simulate the local avalanche risk, we developed forecasting dependences. Their parameters were derived for the following conditions:

1. The number of unexpected avalanches does not exceed one in a thousand (in this case, a small slope process rarely results in human casualties, so the acceptable probability is relatively high.)
2. The number of correct forecasts should be as high as possible.

The forecasting dependence factors were estimated to the nearest hundredth.

The result was the following algorithm.

First, we check whether the avalanche danger is exceptionally high.

First, the following values are calculated [1, 2]:

$$p_{\alpha i} = [0.8 \exp(-|\alpha - 35.0|/7.2)]^{3.1 \{1 + \exp[9(\alpha - 90)] + \exp[9(14.0 - \alpha)]\}}, \quad (1)$$

$$p_{li} = \begin{cases} [(1.65/\pi)\text{arctg}(L/16)]^{2.9\{1.0+\exp[2.2(7.1-L)]\}} & \text{at } \alpha \leq 58^\circ \\ [(1.54/\pi)\text{arctg}(L/2,6)]^{3.1\{1.0+\exp[142(0.12-L)]\}} & \text{at } \alpha > 58^\circ \end{cases}, \quad (2)$$

$$p_{hi} = \left[\frac{1.71}{\pi} \text{arctg} \left(2.7h^{1.3} \right) \right]^{2.6\{1+\exp[3.6(51.0-100h)]\}}, \quad (3)$$

where $p_{\alpha i}$ accounts for the slope angle contribution to the exceptionally high avalanche danger occurrence; p_{li} accounts for the contribution of the avalanche nucleation zone length (hypotenuse) to the exceptionally high avalanche danger occurrence, p_{hi} accounts for the contribution of the slope snow layer thickness to the exceptionally high avalanche danger occurrence.

Then we estimate the comprehensive contribution of the slope angle, the avalanche nucleation area length (hypotenuse) and the slope snow layer thickness to the exceptionally high avalanche danger occurrence. For this purpose we estimated the parameters [1, 2]:

$$p_{\alpha i1} = p_{\alpha i}^{1-0.43p_{li}-0.47p_{hi}}, \quad (4)$$

$$p_{hi1} = p_{hi}^{1-0.49p_{\alpha i}-0.49p_{li}}, \quad (5)$$

$$p_{li1} = p_{li}^{1-0.13p_{\alpha i}-0.08p_{hi}}, \quad (6)$$

$$p_i = p_{\alpha i1}p_{li1}p_{hi1}, \quad (7)$$

where $\mathbf{p}_{\alpha i1}$ accounts for the slope angle contribution to the exceptionally high avalanche danger occurrence also taking into account the values of p_{hi} and \mathbf{p}_{li} ; \mathbf{p}_{hi1} accounts for the slope snow thickness contribution to the exceptionally high avalanche danger occurrence also taking into account the values of $\mathbf{p}_{\alpha i}$ and \mathbf{p}_{li} ; \mathbf{p}_{li1} accounts for the contribution of the avalanche nucleation area length (hypotenuse) to the exceptionally high avalanche danger occurrence taking into account the values of $\mathbf{p}_{\alpha i}$ and p_{hi} ; p_i accounts for the comprehensive contribution of the slope angle, the avalanche nucleation area length (hypotenuse) and the slope snow layer thickness to the exceptionally high avalanche danger occurrence.

The following values are calculated [1, 2]:

$$p_{qi} = \left[\frac{2}{\pi} \text{arctg}(0.52q) \right]^{1-0.17p_i}, \quad (8)$$

$$d_{qi} = \begin{cases} 0.161q, & \text{if } q \leq 46 \\ 2.8q - 121.4, & \text{if } q > 46, \end{cases} \quad (9)$$

where $p_{\alpha i}$ accounts for the total precipitation contribution to the exceptionally high avalanche danger occurrence; \mathbf{q} is the total precipitation for the last day, \mathbf{d}_{qi} accounts for the $\mathbf{p}_{qi}(\mathbf{q})$ curve shape contribution to the exceptionally high avalanche danger occurrence.

$$p_{oi} = \left[\frac{1.97}{\pi} \text{arctg} \left(o^{0.63} \right) \right]^{1-0.15p_i}, \quad (10)$$

where \mathbf{p}_{oi} accounts for the precipitation rate contribution to the exceptionally high avalanche danger occurrence; \mathbf{o} is the average precipitation rate for the last 3 hours, mm/h

$$p_{vi} = \left[\frac{1.6}{\pi} \text{arctg}(0.8v) \right]^{1-0.2p_i}, \quad (11)$$

where \mathbf{p}_{vi} accounts for the wind speed contribution to the exceptionally high avalanche danger occurrence, \mathbf{v} is the wind speed, m/sec

$$p_{t10i} = \begin{cases} \left[\frac{2}{\pi} \text{arctg}(1.5g_{rt10}) \right]^{1-0.05p_i} & \text{at } t_{10} \leq -0.3 \\ \frac{2}{\pi} \text{arctg}[11.7(g_{rt10} + 2.3)] & \text{at } t_{10} > -0.3 \end{cases}, \quad (12)$$

$$d_{t10i} = \begin{cases} 0.12g_{rt10} & \text{at } t_{10} \leq -0.3 \\ 2.2(1.8 + g_{rt10}) & \text{at } t > -0.3 \end{cases}, \quad (13)$$

$$g_{rt10} = \frac{|t_{10}|}{h_{10}}, \quad (14)$$

where p_{t10i} accounts for the 10-day average snow temperature gradient contribution to the exceptionally high avalanche danger occurrence; g_{rt10} is the 10-day average snow temperature gradient; d_{t10i} accounts for the $p_{t10i}(t_{10})$ curve shape contribution to the exceptionally high avalanche danger occurrence.

$$g_{rt10} = \frac{2|t|}{h + h_0}, \quad (15)$$

g_{rt10} is the average snow layer temperature gradient for the entire snow-on-slope period, °C/m

$$p_{ti} = \begin{cases} \frac{2}{\pi} \arctg(g_{rt} - 13.2) & \text{at } t \leq -0.3 \\ \frac{2}{\pi} \arctg(g_{rt} + 11.2) & \text{at } t > -0.3 \end{cases}, \quad (16)$$

$$d_{ti} = \begin{cases} \frac{2}{\pi} \arctg(0.06\tau) & \text{at } t \leq -0.3 \\ \frac{2}{\pi} \arctg\tau & \text{at } t > -0.3 \end{cases}, \quad (17)$$

where p_{ti} accounts for the temperature gradient contribution to the exceptionally high avalanche danger occurrence; d_{ti} accounts for the $p_u(t)$ curve shape contribution to the exceptionally high avalanche danger occurrence.

The snow condition grade in terms of affecting the exceptionally high avalanche danger occurrence is [1, 2]:

$$q_i = p_i^{1 - \frac{2}{\pi} \arctg(0.4p_{oi} + d_{qi}p_{qi} + p_{vi} + d_{ti}p_{ti} + d_{t10i}p_{t10i})}. \quad (18)$$

If $q_i \geq 0.9$, we assume that an exceptionally high avalanche danger exists [1, 2]. Otherwise, we check whether we should expect a mass-scale, high-volume avalanching when from 10 to 50% of the avalanche catchment area is affected by the avalanche.

An “exceptionally high avalanche danger” forecast covers only the next day [1, 2]. For the next second and third days in this case the forecast is “unstable snow cover, large avalanches expected covering 10 to 50% of the avalanche catchment area” [1, 2].

A multi-step process is used to identify possible mass-scale, high-volume avalanching event.

First, the values [1, 2] are calculated:

$$p_{\alpha d} = p_{\alpha i}, \quad (19)$$

$$p_{l d} = p_{l i}, \quad (20)$$

$$p_{hd} = \left[\frac{1.71}{\pi} \arctg(2.7h^{1,3}) \right]^{2.6[1 + e^{3.2(38 - 100h)}]}, \quad (21)$$

where $p_{\alpha d}$ accounts for the slope angle contribution to the mass-scale, high-volume avalanching probability; $p_{l d}$ accounts for the contribution of the avalanche nucleation zone length (hypotenuse) to the mass-scale, high-volume avalanching probability; p_{hd} accounts for the contribution of the slope snow layer thickness to the mass-scale, high-volume avalanching probability.

Then we estimate the comprehensive contribution of the slope angle, the avalanche nucleation area length (hypotenuse) and the slope snow layer thickness to the mass-scale, high-volume avalanching probability. For this purpose we estimated the parameters [1, 2]:

$$p_{\alpha d1} = p_{\alpha d}^{1 - 0.43p_d - 0.47p_d}, \quad (22)$$

$$p_{hd1} = p_{hd}^{1 - 0.49p_{\alpha d} - 0.49p_{l d}}, \quad (23)$$

$$p_{li1} = p_{li}^{1-0.13p_{\alpha i}-0.08p_{hd}}, \quad (24)$$

$$p_d = p_{\alpha d} p_{ld} p_{hd}, \quad (25)$$

where $p_{\alpha d}$ accounts for the slope angle contribution to the mass-scale, high-volume avalanching probability accounting for p_{hd} and p_{ld} values; p_{hd} accounts for the contribution of the slope snow layer thickness to the mass-scale, high-volume avalanching probability accounting for $p_{\alpha d}$ and p_{ld} values; p_{ld} accounts for the avalanche nucleation zone length (hypotenuse) to the mass-scale, high-volume avalanching probability accounting for $p_{\alpha d}$ and p_{hd} ; p_d accounts for the comprehensive contribution of the slope angle, the avalanche nucleation area length (hypotenuse) and the slope snow layer thickness to the mass-scale, high-volume avalanching probability.

The following values are calculated [1, 2]:

$$p_{qd} = \left[\frac{2}{\pi} \arctg(0.8q) \right]^{1.0-0.9p_d}, \quad (26)$$

$$d_{qd} = \begin{cases} 0.71q, & \text{if } q \leq 10 \\ 1.65q - 15.79, & \text{if } q > 10, \end{cases} \quad (27)$$

where p_{qd} accounts for the total precipitation contribution to the mass-scale, high-volume avalanching probability; d_{qd} accounts for the $p_{qd}(q)$ curve shape contribution to the mass-scale, high-volume avalanching probability.

$$p_{od} = \left[(1.97/\pi) \arctg(o^{1.3}) \right]^{1-0.05p_d}, \quad (28)$$

where p_{od} accounts for the last 3 h precipitation rate contribution to the mass-scale, high-volume avalanching probability

$$p_{vd} = [(1.4/\pi) \arctg v]^{1-0.17p_d}, \quad (29)$$

where p_{vd} accounts for the wind speed contribution to the mass-scale, high-volume avalanching probability

$$d_{t10d} = \begin{cases} 0.62g_{rt10} & \text{at } t_{10} \leq -0.3 \\ 0.38g_{rt10} & \text{at } -0.3 < t_{10} \leq 13 \\ 1.26g_{rt10} & \text{at } t_{10} \leq -0.3 \\ 0.38g_{rt10} & \text{at } t_{10} > 13 \\ 2.2(g_{rt10} + 1.8) & \text{at } t_{10} > -0.3 \end{cases}, \quad (30)$$

$$p_{t10d} = \begin{cases} [(2.0/\pi) \arctg(2.2g_{rt10})]^{1-0.17p_d} & \text{at } t_{10} \leq -0.3 \text{ and } g_{rt10} \leq 13 \\ [(2.0/\pi) \arctg(2.9g_{rt10})]^{1-0.22p_d} & \text{at } t_{10} \leq -0.3 \text{ and } g_{rt10} > 13 \\ (2.0/\pi) \arctg[11.7(g_{rt10} + 2.3)] & \text{at } t_{10} > -0.3 \end{cases}, \quad (31)$$

where d_{t10d} accounts for the $p_{t10d}(g_{rt10})$ curve shape contribution to the mass-scale, high-volume avalanching probability; p_{t10d} accounts for the 10-day average snow temperature gradient contribution to the mass-scale, high-volume avalanching probability

$$p_{td} = \begin{cases} (2.0/\pi) \arctg(g_{rt} - 9.2) & \text{at } t \leq -0.3 \\ (2.0/\pi) \arctg(g_{rt} + 13.8) & \text{at } t > -0.3 \end{cases}, \quad (32)$$

where p_{td} accounts for the contribution of the snow temperature gradient over the entire snow-on-slope period to the mass-scale, high-volume avalanching probability

$$p_{h0d} = \left[(1.95/\pi) \arctg(h_0^{3.4}) \right]^{1-0.07p_d}, \quad (33)$$

where p_{h0d} accounts for the contribution of the initial snow layer thickness to the mass-scale, high-volume avalanching probability

$$d_{td} = \begin{cases} (2,0/\pi)\arctg(0,17\tau) & \text{at } t \leq -0,3 \\ (2,0/\pi)\arctg(2,44\tau) & \text{at } t > -0,3 \end{cases}, \quad (34)$$

where \mathbf{d}_{td} accounts for the contribution of the snow-on-slope period to the mass-scale, high-volume avalanching probability; τ is the snow-on-slope period.

The snow condition grade in terms of affecting the mass-scale, the high-volume avalanching probability is [1, 2]:

$$q_d = p_d^{[1 - \frac{1,99}{\pi} \arctg(0,4p_{od} + d_{qd}p_{qd} + p_{vd} + d_{td}p_{td} + 0,7p_{h0d} + d_{t10d}p_{t10d})]}, \quad (35)$$

where \mathbf{q}_d is the snow condition grade in terms of affecting the mass-scale, high-volume avalanching probability.

If $\mathbf{q}_d \geq 0.9$, then the forecast is “mass-scale, high-volume avalanching is expected covering 10 to 50% of the avalanche catchment area” [1, 2]. For the second day, the forecast is “unstable snow cover, large-scale avalanches expected covering 10 to 50% of the avalanche catchment area” [1, 2]. For the third day, the forecast is “unstable snow cover, small avalanching is expected covering up to 10% of the avalanche catchment area” [1, 2].

If $\mathbf{q}_d < 0.9$, we should check if the snow layer is unstable (avalanches are not guaranteed in this case.)

Possible snow cover instability is estimated as follows.

First, the values [1, 2] are calculated:

$$p_\alpha = p_{\alpha i}, \quad (36)$$

$$p_l = p_{li}, \quad (37)$$

$$p_h = \left[(2/\pi)\arctg(4.8h^{1.8}) \right]^{2.3 [1 + 3.2(22.0 - 100h)]}, \quad (38)$$

where p_α accounts for the slope angle contribution to the snow cover instability; p_l accounts for the contribution of the avalanche nucleation zone length (hypotenuse) to the snow cover instability; p_h accounts for the contribution of the slope length (hypotenuse) to the probability of snow cover instability.

Then we estimate the comprehensive contribution of the slope angle, the avalanche nucleation area length (hypotenuse) and the slope snow layer thickness to the probability of snow cover instability. For this purpose the values are calculated [1, 2]:

$$p_{\alpha 1} = p_\alpha^{1 - 0.43p_l - 0.47p_h}, \quad (39)$$

$$p_{h1} = p_h^{1 - 0.49p_\alpha - 0.49p_l}, \quad (40)$$

$$p_{l1} = p_l^{1 - 0.13p_\alpha - 0.08p_h}, \quad (41)$$

$$p = p_{\alpha 1}p_{l1}p_{h1}, \quad (42)$$

where $\mathbf{p}_{\alpha 1}$ accounts for the slope angle contribution to the probability of snow cover instability also taking into account the values of p_l and p_h ; \mathbf{p}_{h1} accounts for the slope snow thickness contribution to the probability of snow cover instability also taking into account the values of p_α and p_l ; \mathbf{p}_{l1} accounts for the contribution of the avalanche nucleation area length (hypotenuse) to the probability of snow cover instability taking into account the values of p_α and p_h ; \mathbf{p} accounts for the comprehensive contribution of the slope angle, the avalanche nucleation area length (hypotenuse) and the slope snow layer thickness to the probability of snow cover instability.

The following parameters are then determined:

$$p_q = \begin{cases} (2,0/\pi)\arctg(0,12q) & \text{at } q \leq 11 \\ [(2,0/\pi)\arctg(q - 10,968)]^{1 - 0,08p} & \text{at } q > 11 \end{cases}, \quad (43)$$

$$d_q = \begin{cases} (2.0/\pi) \operatorname{actg}(q/14, 0) & \text{at } q \leq 11 \\ 14.6 & \text{at } q > 11 \end{cases}, \quad (44)$$

where \mathbf{p}_q accounts for the total precipitation contribution to the probability of snow cover instability; \mathbf{d}_q accounts for the $\mathbf{p}_q(\mathbf{q})$ curve shape contribution to the probability of snow cover instability.

$$p_o = \left[(1.97/\pi) \operatorname{arctg} \left(o^{1.3} \right) \right]^{1-0.05p}, \quad (45)$$

where \mathbf{p}_o accounts for the last 3 h precipitation rate contribution to the probability of snow cover instability

$$p_{vv} = [0.96 + 18.36(2.0/\pi) \operatorname{arctg}(1100d_h)] \operatorname{arctg}[(v/3.2)^{1.7}], \quad (46)$$

$$p_v = 0.95^{1+e^{12(5.6-v)}} p_{vv}, \quad (47)$$

where \mathbf{p}_v accounts for the contribution of the last day wind speed and snow layer thickness variation to the probability of snow cover instability; \mathbf{d}_h is the snow layer thickness variation for the last day, m.

$$p_{h0} = \left[(1.95/\pi) \operatorname{arctg} \left(h_0^{3.4} \right) \right]^{1-0.07p}, \quad (48)$$

where \mathbf{p}_{h0} accounts for the contribution of the initial snow layer thickness to the probability of snow cover instability

$$p_{t10} = \begin{cases} \{(1.98/\pi) \operatorname{arctg}[4.2(g_{rt10} - 16.3)]\}^{1-0.11p} & \text{at } t_{10} < -0.3 \text{ and } g_{rt10} > 16.3 \\ 0.074(1.98/\pi) \operatorname{arctg}[1.4(g_{rt10} - 16.3)] & \text{at } t_{10} < -0.3 \text{ and } g_{rt10} \leq 16.3 \\ \{(2.0/\pi) \operatorname{arctg}[4.8(g_{rt10} + 13)]\}^{1-0.08p} & \text{at } t_{10} \geq -0.3 \end{cases}, \quad (49)$$

where \mathbf{p}_{t10} accounts for the last 10 day-average temperature gradient contribution to the probability of snow cover instability

$$d_t = \begin{cases} 16.0 \frac{2}{\pi} \operatorname{arctg}(0.0017\tau) & \text{at } t < -0.3 \text{ and } g_{rt} > 9.6 \\ 0.9 \frac{2}{\pi} \operatorname{arctg}(0.0006\tau) & \text{at } t < -0.3 \text{ and } g_{rt} \leq 9.6 \\ 9.0 \frac{2}{\pi} \operatorname{arctg}(\tau) & \text{at } t \geq -0.3 \end{cases}, \quad (50)$$

where \mathbf{d}_t accounts for the contribution of the initial snow-on-slope period to the probability of snow cover instability

$$p_t = \begin{cases} \frac{2}{\pi} \{\operatorname{arctg}[4.6(g_{rt} - 8.6)]\}^{1.0-0.05p}, & \text{if } g_{rt} > 9.6 \text{ and } t < -0.3 \\ \frac{0.17}{\pi} \operatorname{arctg}[1.1(g_{rt} - 9.6)], & \text{if } g_{rt} \leq 9.6 \text{ and } t < -0.3 \\ \frac{2}{\pi} \operatorname{arctg}[3.8(g_{rt} + 6.0)], & \text{if } t \geq -0.3 \end{cases}, \quad (51)$$

where \mathbf{p}_t accounts for the contribution of the snow temperature gradient to the probability of snow cover instability [1, 2].

The snow condition grade in terms of affecting the probability of snow cover instability is

$$q_p = p^{1-\frac{2}{\pi} \operatorname{arctg}(0.4p_o + d_q p_q + p_v + d_t p_t + 0.7p_{h0} + 12.3p_{t10})}. \quad (52)$$

where \mathbf{q}_d is the snow condition grade in terms of affecting the probability of snow cover instability.

Then the avalanche danger is evaluated based on the experimental data. Pattern recognition methods are used. The basic training sample is:

```

6 49
1 1 26.0 0.9 16.3 0.5 120.0 11.0
2 0 11.0 0.3 2.9 0.5 70.0 0.0
3 1 15.0 0.4 0.3 0.0 32.0 1.0
4 1 16.0 0.5 1.0 0.2 96.0 2.0
5 0 10.0 0.2 2.3 0.4 40.0 0.0
6 0 38.0 2.0 14.1 0.1 90.0 10.0
7 1 42.0 2.2 1.8 1.1 101.0 7.0
8 0 9.0 0.3 2.0 0.4 54.0 1.0
9 0 13.0 0.2 0.0 0.0 120.0 0.0
10 1 42.0 1.8 7.9 0.6 37.0 12.0
11 1 35.0 1.8 7.3 0.8 54.0 3.0
12 0 13.0 0.2 0.9 0.1 80.0 1.0
13 1 14.0 0.3 1.1 0.0 25.0 2.0
14 0 14.0 0.4 2.9 0.6 160.0 1.0
15 1 38.0 0.2 1.3 0.2 80.0 5.0
16 1 14.0 0.3 0.7 0.0 50.0 0.0
17 0 10.0 0.2 0.8 0.0 130.0 0.0
18 1 25.0 1.5 9.3 1.9 80.0 8.0
19 1 17.0 0.3 0.6 0.0 85.0 1.0
20 0 11.0 0.1 0.7 0.0 120.0 1.0
21 1 32.0 1.4 24.1 0.2 70.0 4.0
22 0 11.0 0.3 2.9 0.5 40.0 0.0
23 1 14.0 0.3 2.1 0.3 70.0 0.0
24 0 19.0 0.3 2.3 0.5 65.0 1.0
25 1 42.0 1.7 14.3 1.5 115.0 9.0
26 1 15.0 0.4 0.8 0.0 50.0 0.0
27 0 11.0 0.1 2.8 0.0 57.0 1.0
28 1 38.0 2.1 16.5 1.6 76.0 5.0
29 0 10.0 0.2 1.4 0.0 25.0 2.0
30 0 17.0 0.2 1.1 0.3 130.0 0.0
31 0 19.0 0.1 0.0 0.0 133.0 3.0
32 1 40.0 2.1 8.1 0.2 70.0 11.0
33 0 11.0 0.1 1.0 0.0 130.0 0.0
34 1 14.0 0.3 1.0 0.0 90.0 1.0
35 0 17.0 0.3 0.2 0.0 150.0 1.0
36 1 53.0 1.3 7.4 0.6 137.0 1.0
37 1 15.0 0.2 2.8 0.2 23.0 2.0
38 0 12.0 0.3 0.4 0.0 60.0 12.0
39 0 9.0 0.3 2.6 0.6 30.0 1.0
40 0 15.0 0.2 2.9 0.0 60.0 0.0
41 1 31.0 2.2 19.5 0.0 87.0 14.0
42 0 9.0 0.2 2.0 0.5 29.0 0.0
43 0 42.0 2.1 6.4 0.6 115.0 13.0
44 1 26.0 2.0 4.4 0.4 86.0 4.0
45 1 14.0 0.3 2.9 0.6 58.0 1.0
46 0 11.0 0.1 0.0 0.0 95.0 2.0
47 0 40.0 2.0 13.4 0.1 98.0 9.0
48 0 11.0 0.3 0.4 0.0 63.0 0.0
49 1 36.0 2.2 10.2 1.2 49.0 6.0

```

The first line contains the number of points and the number of variables. Each subsequent line contains point number, the situation code (0: no avalanche, 1: avalanche), slope angle (degrees), slope snow

thickness (m), total precipitation over the last 24 h (mm), precipitation rate over the last 3 h (mm/h), slope length (hypotenuse), (m), wind speed (m/s.)

The sample can be supplemented with experimental data for a specific area.

Two pattern recognition algorithms were used [3]. In the first one, the separating surface passes through the midpoint of the line connecting the centers of scattering perpendicular to it. The second select selects the closest point.

p_a values are estimated to reduce the fuzziness:

$$p_a = q_p \frac{1+1.05u_1+1.05u_2}{1+1.05w_1+1.05w_2}, \quad (53)$$

and

$$p_a^* = p_a^{(1-p_a)/1.1}. \quad (54)$$

When the first algorithm identifies avalanche danger, then $u_1 = 0$ and $w_1 = 0.5$. When the first algorithm identifies no avalanche danger, then $u_1 = 0.5$ and $w_1 = 0$; when the second algorithm identifies avalanche danger, then $u_2 = 0$ and $w_2 = 0.5$, when the second algorithm identifies no avalanche danger, then $u_2 = 0.5$ and $w_2 = 0$.

If $p_a \geq 0.32$, then the snow is unstable. Otherwise, there is no avalanche danger.

If $p_a \geq 0.32$ and $p_a^* < 0.9$, the next day forecast is “unstable snow cover, small avalanching is expected covering up to 10% of the avalanche catchment area”. If $p_a \geq 0.32$ and $p_a^* \geq 0.9$, the next day forecast should be “unstable snow cover, large-scale avalanching is expected covering 10 to 50% of the avalanche catchment area”, and for the second day the forecast should be “unstable snow cover, small avalanching is expected covering up to 10% of the avalanche catchment area”.

If the day-average temperature exceeds 0.4°C , and the snow thickness exceeds 0.52 m, i.e. $65^\circ \geq \alpha > 15^\circ$ and $l > 60$ m, the next day forecast is “unstable snow cover, large-scale avalanches expected covering 10 to 50% of the avalanche catchment area”. For the second day, the forecast is “unstable snow cover, small avalanching is expected covering up to 10% of the avalanche catchment area”.

If the day-average temperature exceeds -0.2°C , $0.52 \text{ m} \geq h > 0.22$ m, $65^\circ \geq \alpha > 15^\circ$ and $l > 6$ m, the next day forecast is “unstable snow cover, small avalanches expected covering up to 10% of the avalanche catchment area”.

The snow layer thickness used shall be reduced by the thickness of the top layer with its snow density exceeding 430 kg/m^3 .

The seismic load is accounted as follows [2]. As the simulation shows, the avalanche danger during an earthquake does not change, if we use the following values instead of h and q :

$$h_s = k_s [h - (1 - p_{eI} k_\rho k_e) h_{430}], \quad (55)$$

$$q_s = q + p_{eI} q_e, \quad (56)$$

where h_{430} is the snow layer thickness starting at the Earth surface with its density exceeding 430 kg/m^3 , p_{eI} is the probability of I points (MSK-81 scale) earthquake

$$k_\rho = \frac{2}{\pi} \text{arctg} \left\{ 0.0000149 \cdot \left[I \cdot \left(\frac{910}{\rho_{430}} \right) \right]^{6.906} \right\}, \quad (57)$$

$$k_e = \frac{2}{\pi} \text{arctg}(3.972 \cdot 10^{-9} \cdot I^{9.438}), \quad (58)$$

$$k_s = \begin{cases} 1 & \text{at } I < 5 \\ 1 + 0.2p_{eI}(I - 5) & \text{at } 5 \leq I < 8 \\ 1 + 0.32p_{eI}(I - 5) & \text{at } I \geq 8 \end{cases}, \quad (59)$$

$$q_e = \begin{cases} 0 & \text{at } I < 5 \\ 4.4(I - 5) & \text{at } 5 \leq I < 8 \\ 16.2(I - 5) & \text{at } I \geq 8 \end{cases}, \quad (60)$$

where I is the earthquake intensity at the Earth surface (MSK-81 scale), ρ_{430} is the average density of the snow layer starting at the Earth surface with its density $> 430 \text{ kg/m}^3$.

To further refine the avalanche forecasting, historical data are also used. Snow thickness, total precipitation, precipitation intensity, wind speed (max gust) and air temperature for the last 24 hours are considered. Since the presence of slope snow is required for an avalanche, similar to the almost significant confidence probability [4], the current value is matched against the past value of 0.95. For the other parameters, a value of 0.9 is used. It corresponds to a confidence level value of 0.9, which is feasible in real life [5].

A decision whether a particular situation is similar to one of the avalanche dangers that occurred in the past is based on the balance of probabilities standard [6]. It means that the fact is proved if, with the evidence presented, it can be concluded that the fact rather occurred than not. Therefore, to identify the slope snow condition as similar to one of the past avalanche dangers, the snow thickness and any other two parameters are required to match it.

Table 1

Avalanche Danger in the Trans-Kam Area in November 1998

Date	τ, h	q, mm	$o, \text{mm/h}$	$v, \text{m/s}$	q_f, mm	h, m	$t_{24}, [^\circ\text{C}]$	Avalanching
10.11.1998	24	3	0	1	0	0.03	-6.0	-
11.11.1998	48	0.4	0	4	0	0.07	-6.0	-
12.11.1998	72	0	0	2	0	0.05	-3.1	-
13.11.1998	0	0	0	2	0	0.03	0.4	-
14.11.1998					0	0	3.6	-
15.11.1998					0	0	3.2	-
16.11.1998					0	0	2.4	-
17.11.1998					0	0	2.1	-
18.11.1998	24	21.8	1	1	0	0.01	2.1	-
19.11.1998	48	14.2	2	2	0	0.02	1.1	-
20.11.1998					0	0	-0.3	-
21.11.1998					0	0	-0.1	-
22.11.1998					0	0	0.3	-
23.11.1998					0	0	-0.5	-
24.11.1998					0	0	-1.1	-
25.11.1998					0	0	-0.2	-
26.11.1998					0	0	3.3	-
27.11.1998					0	0	1.4	-
28.11.1998	24	12.1	0	2	0	0.02	0.1	-
29.11.1998	48	0	0	3	0	0.02	-0.3	-
30.11.1998	72	25.5	0	1	20.0	0.26	-0.5	-

An individual database shall be compiled for each avalanche catchment area. Excel was used for this purpose. The software can connect to code written, for example, in C++. In this way, the computation routine and the data storage system are combined, to take full advantage of both C++ Builder and Excel. Moreover, Excel is quite effective for creating simple databases and has a range of data visualization tools. Finally, it is easy to use. The general avalanche danger forecasting method can be further adapted to specific conditions. In some cases, the forecasting can be significantly refined, because it considers various local

features not taken into account in the generic algorithm. Some abnormal cases which sometimes occur in highly unusual circumstances are also considered.

Avalanche Danger Trend Forecasting Algorithm

The snow instability grade, mass-scale, large-volume avalanching, or exceptionally high avalanche danger situations may change in time. As the equations show, any of these functions can asymptotically tend to one, asymptotically tend to zero, be constant, or oscillate. Accordingly, special functions are required to approximate their time dependences.

We should also note that it is possible to obtain only a very limited raw data sample, so the dependency generation method should match the amount of data and the complexity of the resulting function.

In this case, the most appropriate one is the structural risk minimization method providing such a capability. Besides, [7] describes the use of complex functions in this method as required for estimating the avalanche danger trend.

Avalanche danger often remains unchanged for a long time. For example, the “no avalanche danger” situation persisted in the Trans-Kam region in November 1998 for three weeks, as shown in Table 1. In the table, q_f is the expected total precipitation for the next day.

Another example is an almost constant avalanche risk level “unstable snow cover, small avalanching is expected covering up to 10% of the avalanche catchment area” in January 1999. The data are shown in Table 2.

Table 2

Avalanche Danger in the Trans-Cam Area in January 1999

Date	τ , h	q , mm	o , mm/h	v , m/s	q_f mm	h [m]	t_{24} [°C]	Forecast for this day	Avalanching
01.01 1999	840	0.8	0.27	3	0	0.50	-15.3	Unstable snow cover, small avalanching is expected covering up to 10% of the avalanche catchment area (as of 31.12.1998)	-
02.01 1999	864	0	0	1	0	0.45	-9.7	Unstable snow cover. Large avalanching is expected covering from 10% to 50% of the avalanche catchment area (as of 01.01.1999)	-
03.01 1999	888	0	0	3	0	0.40	-7.5	Unstable snow cover, small avalanching is expected covering up to 10% of the avalanche catchment area (as of 02.01.1999)	-
04.01 1999	912	0	0	1	0	0.40	-5.6	Unstable snow cover, small avalanching is expected covering up to 10% of the avalanche catchment area (as of 03.01.1999)	-
05.01 1999	936	0	0	1	0	0.40	-3.4	Unstable snow cover, small avalanching is expected covering up to 10% of the avalanche catchment area (as of 04.01.1999)	Mass avalanching from the point.
06.01 1999	960	0	0	1	0	0.39	-5.2	Unstable snow cover, small avalanching is expected covering up to 10% of the avalanche catchment area (as of 05.01.1999)	Mass avalanching from the point
07.01 1999	984	0	0	1	0	0.38	-7.1	Unstable snow cover, small avalanching is expected covering up to 10% of the avalanche catchment area (as of 06.01.1999)	50 m ³ snow lenticle Stopped in the transit zone

Date	τ , h	q, mm	o, mm/h	v, m/s	q _f mm	h [m]	t ₂₄ [°C]	Forecast for this day	Avalanching
08.01 1999	1008	0	0	2	0	0.38	-5.4	Unstable snow cover, small avalanching is expected covering up to 10% of the avalanche catchment area (as of 07.01.1999)	100 m ³ snow lenticle, catchment area No. 91 Mass avalanching from the point
09.01 1999	1032	0	0	1	0	0.37	-4.9	Unstable snow cover, small avalanching is expected covering up to 10% of the avalanche catchment area (as of 08.01.1999)	-
10.01 1999	1056	0	0	3	7.0	0.37	-4.6	Unstable snow cover, small avalanching is expected covering up to 10% of the avalanche catchment area (as of 09.01.1999)	-
11.01 1999	1080	3.2	0.36	2	0	0.42	-2.4	Unstable snow cover, small avalanching is expected covering up to 10% of the avalanche catchment area (as of 10.01.1999)	Mass avalanching from the point
12.01 1999	1104	0	0	3	0	0.40	-8.9	Unstable snow cover, small avalanching is expected covering up to 10% of the avalanche catchment area (as of 11.01.1999)	Mass avalanching from the point
13.01 1999	1128	0	0	1	0	0.40	-6.6	Unstable snow cover, small avalanching is expected covering up to 10% of the avalanche catchment area (as of 12.01.1999)	-
14.01 1999	1152	0	0	2	0	0.38	-4.9	Unstable snow cover, small avalanching is expected covering up to 10% of the avalanche catchment area (as of 13.01.1999)	-
15.01 1999	1176	0	0	1	0	0.38	-3.7	Unstable snow cover, small avalanching is expected covering up to 10% of the avalanche catchment area (as of 14.01.1999)	-
16.01 1999	1200	0	0	2	0	0.38	-5.2	Unstable snow cover, small avalanching is expected covering up to 10% of the avalanche catchment area (as of 15.01.1999)	-
17.01 1999	1224	0	0	1	0	0.37	-4.8	Unstable snow cover, small avalanching is expected covering up to 10% of the avalanche catchment area (as of 16.01.1999)	-
18.01 1999	1248	0	0	2	0	0.35	-4.9	Unstable snow cover, small avalanching is expected covering up to 10% of the avalanche catchment area (as of 17.01.1999)	-
19.01 1999	1272	0	0	3	0	0.35	-5.2	Unstable snow cover, small avalanching is expected covering up to 10% of the avalanche catchment area (as of 18.01.1999)	-

Date	τ , h	q, mm	o, mm/h	v, m/s	q _f mm	h [m]	t ₂₄ [°C]	Forecast for this day	Avalanching
20.01 1999	1296	0	0	2	1	0.34	-5.9	Unstable snow cover, small avalanching is expected covering up to 10% of the avalanche catchment area (as of 19.01.1999)	-
21.01 1999	1320	0	0	2	0	0.34	-6.0	Unstable snow cover, small avalanching is expected covering up to 10% of the avalanche catchment area (as of 20.01.1999)	-
22.01 1999	1344	0	0	3	0	0.34	-6.1	Unstable snow cover, small avalanching is expected covering up to 10% of the avalanche catchment area (as of 21.01.1999)	-
23.01 1999	1368	0	0	3	0	0.34	-6.1	Unstable snow cover, small avalanching is expected covering up to 10% of the avalanche catchment area (as of 22.01.1999)	-
24.01 1999	1392	0	0	2	1	0.33	-8.7	Unstable snow cover, small avalanching is expected covering up to 10% of the avalanche catchment area (as of 23.01.1999)	-
25.01 1999	1416	0	0	2	0	0.33	-8.7	Unstable snow cover, small avalanching is expected covering up to 10% of the avalanche catchment area (as of 24.01.1999)	Two shells were fired. One avalanche was triggered
26.01 1999	1440	0	0	2	0	0.33	-9.4	Unstable snow cover, small avalanching is expected covering up to 10% of the avalanche catchment area (as of 25.01.1999)	-
27.01 1999	1464	0	0	4	0	0.33	-4.9	Unstable snow cover, small avalanching is expected covering up to 10% of the avalanche catchment area (as of 26.01.1999)	-
28.01 1999	1488	0	0	3	0	0.33	-8.4	Unstable snow cover, small avalanching is expected covering up to 10% of the avalanche catchment area (as of 27.01.1999)	-
29.01 1999	1512	0	0	3	0	0.33	-6.9	Unstable snow cover, small avalanching is expected covering up to 10% of the avalanche catchment area (as of 28.01.1999)	-

The fact that the snow was unstable is confirmed by the avalanches on 5.01-8.01, 11.01-12.01 and the slope process initiation after the shelling of the avalanche catchment area on 25.01.

The risk of avalanches can increase quickly and then decrease. This is shown in Table 3.

Table 3

Avalanche danger in the Trans-Cam area in February 1999

Date	τ , h	q, mm	o, mm/h	v, m/s	q _f mm	h [m]	t ₂₄ [°C]	Forecast for this day	Avalanching
16.02 1999	1944	2.3	2.3	4	2	0.57	-2.2	Unstable snow cover, small avalanching is expected covering up to 10% of the avalanche catchment area (as of 15.02.1999)	-

Date	τ , h	q, mm	o, mm/h	v, m/s	q _f mm	h [m]	t ₂₄ [°C]	Forecast for this day	Avalanching
17.02 1999	1968	12.3	0.83	4	15	0.67	-3.6	Unstable snow cover, small avalanching is expected covering up to 10% of the avalanche catchment area (as of 16.02.1999)	-
18.02 1999	1992	29.4	1.0	2	1	0.89	-2.6	Avalanche danger. Large avalanching is expected covering 10 to 50% of the avalanche catchment area (as of 17.02.1999). The forecast is simulated	Catchment areas (CA) 43, 49, 75 ^a , 83, 87, 91' generated 100 m ³ avalanches; AA 41, 55, 56, 57, 80, 82, 93, 50, 39, 40, 60, 69, 71, 84, 88: 200 m ³ ; CA 65, 81: 300 m ³ ; CA 28, 46: 500 m ³ ; CA 37, 72, 73, 74,91: 1,000 m ³ ; CA 102, 103: 2,000 m ³ ; CA 35, 67, 70: 5,000 m ³ ; CA74 ^a : 50,000 m ³
19.02 1999	2016	5.5	1.4	4	30	0.64	-4.3	Unstable snow cover. Large avalanching is expected covering 10% to 50% of the avalanche catchment area (as of 17.02.1999)	CA 205 ^a generated 15,000 m ³ avalanches; CA No. 3: 5,000 m ³ , CA No. 5: 200 m ³ , CA No. 4: 100 m ³ . 8 shells were fired, 8 avalanches triggered
20.02 1999	2040	31.7	1.32	8	2	1.27	-5.7	Unstable snow cover. Large avalanching is expected covering 10% to 50% of the avalanche catchment area (as of 19.02.1999)	CA No. 91 generated an avalanche exceeding 1,000 m ³ . The avalanche blocked the river and the road
21.02 1999	2064	0	0	4	2	1.15	-11.2	Avalanche danger. Large avalanching is expected covering 10 to 50% of the avalanche catchment area (as of 20.02.1999)	Twelve shells were fired. Six avalanches were triggered
22.02 1999	2088	0	0	2	0	1.05	-7.2	Unstable snow cover. Large avalanching is expected covering 10% to 50% of the avalanche catchment area (as of 20.02.1999)	-
23.02 1999	2112	0	0	1	0	0.92	-4.4	Unstable snow cover, small avalanching is expected covering up to 10% of the avalanche catchment area (as of 20.02.1999)	CA No. 74 ^a generated a 2,000 m ³ avalanche; CA No. 103: 500 m ³ ; CA No. 102: 200 m ³

Date	τ , h	q, mm	o, mm/h	v, m/s	q _f mm	h [m]	t ₂₄ [°C]	Forecast for this day	Avalanching
24.02 1999	2136	0	0	2	8	0.95	-2.1	Unstable snow cover, small avalanching is expected covering from 10% to 50% of the avalanche catchment area (as of 23.02.1999)	-
25.02 1999	2160	0.13	0.13	2	0	0.94	-3.0	Unstable snow cover, small avalanching is expected covering from 10% to 50% of the avalanche catchment area (as of 24.02.1999)	-
26.02 1999	2184	0.3	0.3	2	3	0.94	-7.6	Unstable snow cover, small avalanching is expected covering up to 10% of the avalanche catchment area (as of 25.02.1999)	-

On 18.02 and 21.02 there was a sharp avalanche danger increase which quickly decreased. The forecasting is confirmed by both the mass avalanches and a successful avalanche triggering.

In particular, the Chebyshev polynomials can be used to describe a constant, increasing, and first increasing, then decreasing avalanche danger. This is particularly efficient when we should determine whether the risk of avalanches remains constant.

The Chebyshev polynomials are as follows [8]:

$$Q_0 = 1, \quad (61)$$

$$Q_1 = x, \quad (62)$$

$$Q_2 = 2x^2 - 1, \quad (63)$$

$$Q_3 = 4x^3 - 3x. \quad (64)$$

The application of complex functions to the structural risk minimization method is presented in [9]. First, the values of $\mathbf{z}_i = \mathbf{f}(\mathbf{x}_i)$ are estimated, and then $\mathbf{y}(\mathbf{z})$ relation is fitted. We can reasonably choose a special function to describe the avalanche danger trend.

The snow condition grade in terms of affecting the avalanche danger occurrence can also increase or decrease asymptotically. The following functions are suitable for describing the dependencies

$$y(x) = \frac{2}{\pi} \operatorname{arctg}(ax), \quad (65)$$

where \mathbf{a} is an unknown coefficient

$$y(x) = th(ax). \quad (66)$$

To describe an oscillatory process we can use a function as follows

$$y(x) = \sin(ax + b), \quad (67)$$

where \mathbf{a} , \mathbf{b} are unknown coefficients.

As an example, we can analyze the trend of snow condition grade in terms of affecting the exceptionally high avalanche danger occurrence from the initial data listed in Table 4. The plot is shown in Fig. 1.

The estimations showed that it is best approximated by function (66). The fitted relation is $\mathbf{q}_1(\mathbf{t}) = 0.309\mathbf{t} + 0.299\mathbf{th}(\mathbf{t}/15)$. Its limit value is less than 0.9, so reaching the exceptionally high avalanche danger is not expected.

Avalanche Danger Forecasting Software

The **asf-3** software can be used to assess avalanche danger. Its initial window is shown in Fig. 2.

Table 4

Exceptionally high avalanche danger occurrence vs. time (t: time)

t, hours	0	3	6	9	12	15	18	21	24	27	30	33
q_i	0.322	0.356	0.397	0.445	0.501	0.534	0.562	0.573	0.584	0.595	0.602	0.607

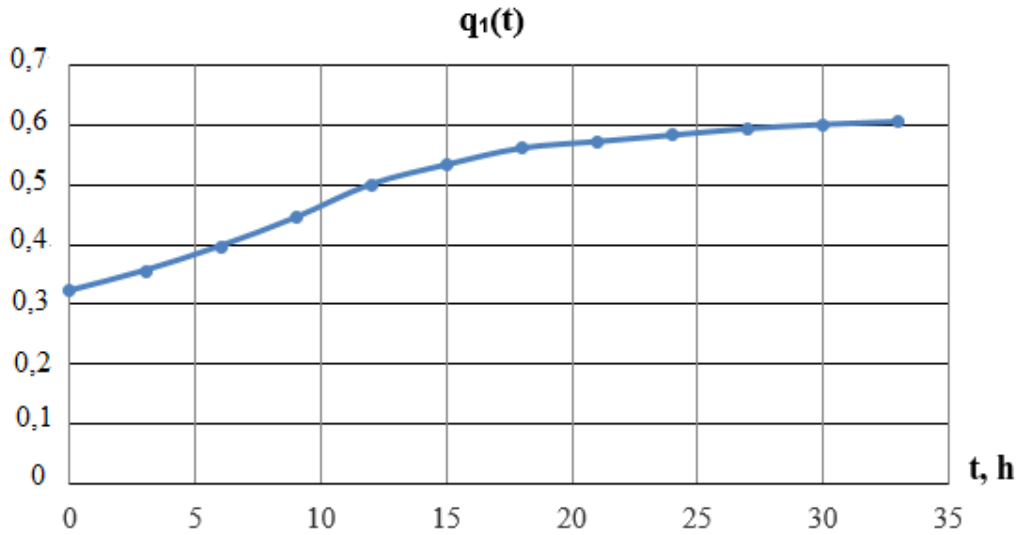


Figure 1. Initial dependence for the exceptionally high avalanche danger occurrence

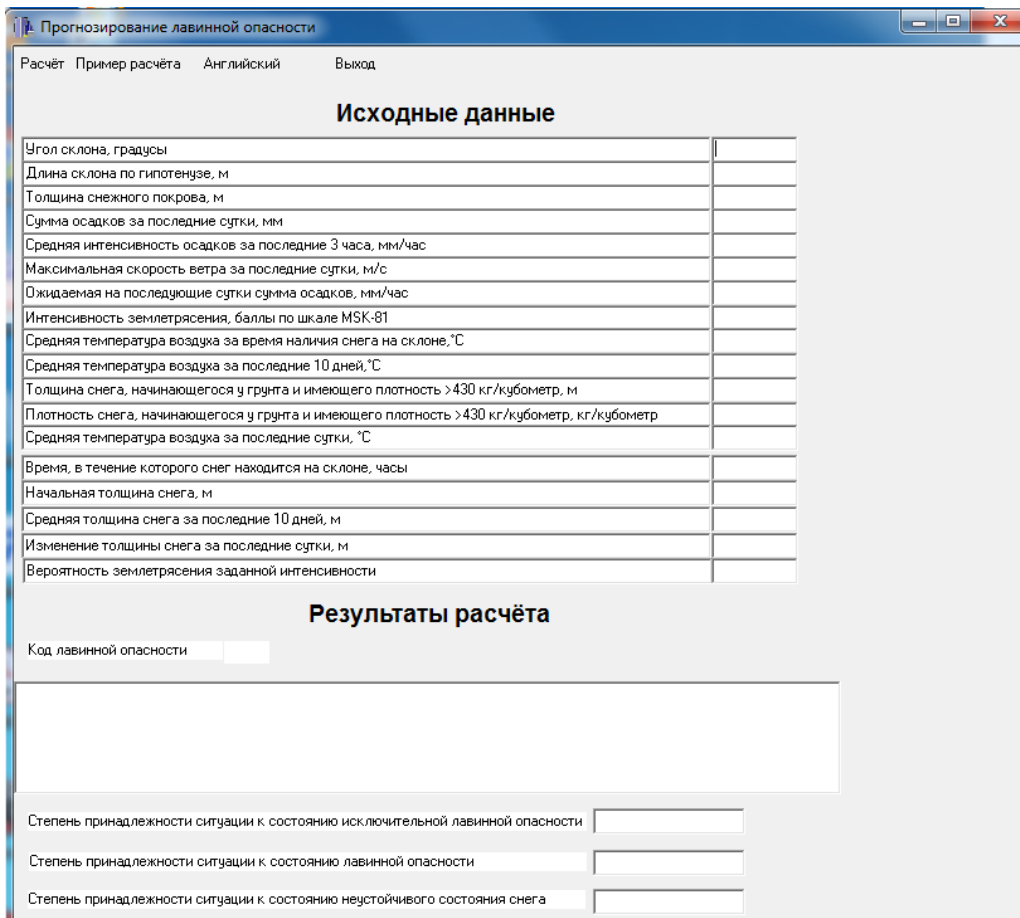


Figure 2. The asf-3 software initial window

The software can not only assess the current situation, but assess unstable snow grade, avalanche danger, and exceptionally high avalanche danger occurrence at different points in time.

To estimate the optimal complex function coefficients, it is generally required to solve a system of transcendental equations. A modified method described in [2] is used for this purpose. Let us define the function $\mathbf{F}(\mathbf{x}_1, \mathbf{x}_2, \dots, \mathbf{x}_n)$. First, random coordinate values are selected: $\mathbf{x}_1 = \mathbf{x}_{11}$, $\mathbf{x}_2 = \mathbf{x}_{21}$, ..., $\mathbf{x}_n = \mathbf{x}_{n1}$. Then the values $\mathbf{x}_2, \mathbf{x}_3, \dots, \mathbf{x}_n$ are fixed, while \mathbf{x}_1 is changed randomly. After that, the target function vs. \mathbf{x}_1 relation is found in the specified one-dimensional section with the structural risk minimization method [10, 11] using a class of Chebyshev polynomials [8]. Then its extremum is identified and the variable value is fixed. After that, in contrast to the algorithm described in [2], near the point of extremum an interval is defined. Its start and end points are estimated as

$$x_{1N} = x_{1\min} + 0.62(x_{1E1} - x_{1\min}), \quad (68)$$

$$x_{2N} = x_{1E1} + 0.38(x_{1\max} - x_{1E1}), \quad (69)$$

where \mathbf{x}_{1E1} is the \mathbf{x}_1 coordinate of the found extremum point, $\mathbf{x}_{1\min}$ is the start point of the \mathbf{x}_1 range; $\mathbf{x}_{1\max}$ is the end point of the \mathbf{x}_1 range, \mathbf{x}_{1N} is the new start point of the \mathbf{x}_1 range; \mathbf{x}_{2N} is the new end point of the \mathbf{x}_1 range. It is the golden ratio extensively used in various fields [7]. Then the extremum search is repeated in a new interval, and the value of \mathbf{x}_1 at the new point is fixed.

The procedure is then applied to all the variables using the previously found optimal values of the preceding variables. The more starting points, the less chance of missing the global extremum [4].

The choice of a structural risk minimization method is governed by the following. Solving the system of transcendental equations is rather time-consuming, so the number of experimental points in one-dimensional sections is limited. Besides, as the initial data are fuzzy, the solutions contain some interference. The problems with developing dependencies from small samples are quite different from the classical problems of reconstructing dependencies from large samples. The difference is that for a limited sample size it is required to balance the dependence complexity with the amount of available empirical data.

It is advisable to apply the structural risk minimization method [10, 11]. Its essence is as follows. If we define a structure within an admissible set of solutions, i.e., a system of nested sets, each of them containing more and more complex solutions, then along with empirical risk minimization for its elements there is an opportunity to optimize the estimation quality by structure elements. This makes it possible to find a solution that gives a better guaranteed average risk minimum compared to a solution that produces an empirical risk minimum across the entire admissible set.

The structural risk minimization method applications for a given amount of information enables us to find the optimal number of members of the series that approximates the dependence. An arbitrary choice of this parameter can lead to a paradox. Suppose we need to reconstruct the dependence $\mathbf{y}=\mathbf{f}(\mathbf{x})$ from ten experimental points. In this case, the empirical risk is zero when using the 9th-degree polynomial. However, the optimal degree of polynomial \mathbf{n} can be 1.

With the structural risk minimization method, the regression fitting problem is reduced to minimizing the following value [10]:

$$J(k) = I_E(k)\Omega, \quad (70)$$

where $\mathbf{J}(\mathbf{k})$ is the average risk, $\mathbf{I}_e(\mathbf{k})$ is the empirical risk, \mathbf{k} identifies a particular function of a certain class, Ω is a variable.

As the sample volume increases, the Ω value always tends to one [10], although it differs in each specific case, if the sample is small, it may deviate significantly from 1. Then a function that produces a small empirical risk may not yield a small average risk.

There are different classes of basis functions. Chebyshev polynomials are easy to compute and enable to solve a wide range of dependence reconstruction problems. Besides, their use minimizes the max error. It is important when there are large errors in the raw data.

Then $\mathbf{y}(\mathbf{x})$ is presented as a series

$$y(x) = \sum_{i=0}^k \alpha_i Q_i(x), \quad (71)$$

where α_i is the i th expansion factor, $\mathbf{Q}_i(\mathbf{x})$ is a Chebyshev polynomial of the i th power.

With such a representation, the empirical risk functional is [10]:

$$I_E = \frac{1}{l} \sum_{j=1}^l \left[y_j - \sum_{i=0}^k \alpha_i Q_i(x_j) \right]^2, \quad (72)$$

where l is the sample volume.

At a fixed maximum polynomial degree, the α_i coefficients when the empirical risk is at its minimum are calculated by solving a system of linear algebraic equations [10]:

$$\Phi^T \Phi[\alpha] = \Phi^T [y]^T, \quad (73)$$

where Φ is a matrix of Chebyshev polynomial values at the points of interest, $[y]$ is a row matrix of the y values at the points of interest, $[\alpha]$ is a column matrix of the α_i factors.

The estimated approximation quality valid for any random sample with the probability $1-\eta$ is expressed as [10]:

$$J(k) = \frac{I_M}{1 - \sqrt{\frac{(k+1) \left[\ln \left(\frac{l}{k+1} \right) + 1 \right] - \ln \eta}{l}}}, \quad (74)$$

where $1-\eta$ is the probability of the estimate (2.2.11) being valid, $\mathbf{J}(\mathbf{k})$ is the average risk.

(74) depends on the degree of the polynomial \mathbf{k} . The degree at which $\mathbf{J}(\mathbf{k})$ is the smallest is the optimal degree of polynomial approximation. The regression function itself is approximated by a polynomial of this degree

minimizing the empirical risk functional.

Since Chebyshev polynomials are orthogonal on the interval $[-1, 1]$, if the independent variable values are not specified within this range, they shall be reduced to it as follows [10]:

$$x_i = \frac{(x_{gi} - c_1)}{c_2},$$

where x_i is the independent variable values reduced to $[-1, 1]$, x_{gi} are the initial independent variable values

$$c_1 = \frac{(x_{g \max} + x_{g \min})}{2},$$

$$c_2 = \frac{(x_{g \max} - x_{g \min})}{2},$$

where $x_{g \min}$ is the min independent variable value, $x_{g \max}$ is the max independent variable value.

It is possible to implement the algorithm with Excel. In the same system, one can create databases and plot graphs. It should be noted C++ programs can connect to Excel files.

Conclusion

The mathematical model and software for avalanche forecasting based on RD 52.37.612-2000 Guidelines, historical avalanche databases, and avalanche danger trend evaluation ensure acceptable safety in avalanche-affected areas. They can be used for the planning and implementation of various preventive measures.

REFERENCES

1. Zimin M. I. *Avalanche Forecasting*. St. Petersburg: Gidrometeoizdat; 2000. 16 p. (In Russ.)
2. Eskov V. M., Gavrilenko T. V., Zimin M. I., Zimina S. A. *Neural Network-Based Identification and Studying Chaotic Dynamics Systems*. Tula: Izdatel'stvo TuLGU; 2016. 398 p. (In Russ.)
3. Kuzin L. T. *Fundamentals of Cybernetics*. V. 2. M.: Ehnergiya; 1979. 584 p. (In Russ.)
4. Sobol' I. M. *Monte-Karlo Numerical Methods*. M.: Nauka; 1973. 312 p. (In Russ.)
5. Blokhin A. V. *The Theory of Experiment*. Part 1. Minsk: Ehlektronnaya kniga BGU; 2002. 69 p. (In Russ.)

6. Budylin S. L. Judicial Activism or the Balance of Probabilities. The Russian and International Standards of Proof. *The Russian Federation Higher Arbitrazh Court Proceedings*. 2014;3:25–57. (In Russ.)
7. Kovalev F. V. *The Golden Ratio in Painting*. Kiev: Vyshcha shkola; 1989. 143 p. (In Russ.)
8. Korn G., Korn T. *Mathematics Handbook for Engineers and Researchers*. M.: Nauka; 1984. 832 p. (In Russ.)
9. Zimin M. M. The Application of Complex Functions to the Structural Risk Minimization Method. *Natural and Technical Sciences*. 2019;6:234–237. (In Russ.)
10. *Data Fitting Algorithms and Codes* / Ed. V. N. Vapnik. M.: Nauka; 1984. 816 p. (In Russ.)
11. Vapnik V. *Estimation of Dependences Based on Empirical Data*. New York: Springer-Verlag New York; 2006. 505 p.

Digital edition. Full paper texts are published on the official web site: jcyb.ru.

Founder and publisher address:

Federal State Institution “Scientific Research Institute for System Analysis of the Russian
Academy of Sciences”,
Russian Federation 117218 Moscow Nakhimovsky Prosp., d. 36, korp. 1.
Tel.: +7 (495) 718-2110.

Date of issue: 31.03.2020.

Paper size: 60 × 84/8.

Free of charge.